MEASUREMENT OF THE ENERGY SPECTRA OF

PRIMARY COSMIC RAY PROTONS AND ALPHA PARTICLES

A THESIS

submitted by

GEOFFREY MARTIN COURTIER

for the degree of

DOCTOR OF PHILOSOPHY

in the

UNIVERSITY OF LONDON

ABSTRACT.

Most of the measurements on the primary differential spectra of protons and α-particles up to 1960 suggested that they were similar throughout the solar cycle on a rigidity scale, although information on the lower rigidity particles was rather sparse. In order to obtain further experimental data on these particles in a region where their velocity β is considerably less than unity, balloon flights have been made with a modified Scintillator-Cerenkov telescope, with a view to determining whether the 11 year solar modulation of galactic cosmic rays is of a convective or static nature. The flights were made from Kiruna, N. Sweden (65° geomagnetic latitude) and Bedford, England (50° geomagnetic latitude) in 1961 and 1962, the data being obtained by telemetry.

The integral fluxes of protons and α-particles which were obtained are in general agreement with the values expected at this stage of the solar cycle.

		26.8.61	21.7.62		20.5.62
protons*	>1.0 Gv.	1380 ± 160	2060 ± 175	>2.5 Gv.	1300 ± 165
α-particles†	>1.0 Gv.	199 ± 16	253 ± 12	>2.5 Gv.	155 ± 10

* statistical and extrapolation errors.

† statistical and resolution errors.

The differential spectrum of protons has been measured

from 0.6 to 2.0 Gv. and suggests that in this region it is fairly

flat and different from the shape of the α-particle spectrum.

Investigation of the changes in intensity at low rigidity suggests

a solar source of protons up to 0.9 Gv. even during recognised

quiet times, three years after the solar maximum of 1958.

The modulation of the proton rigidity interval 1.0 to 1.5 Gv.

indicates that the galactic spectrum below 2.0 Gv. is probably

better represented by the solar minimum spectrum than a continuation

of the exponential form applicable to higher rigidities.

The following fluxes were obtained for the rigidity

interval 1.0 to 1.5 Gv.

	26.8.61	21.7.62
protons	115 ± 20	190 ± 20
α-particles	12 ± 4	23 ± 6

Errors include statistics and interval uncertainties.

These measurements together with the few others available provide

evidence that the modulation of the galactic flux is not purely

rigidity dependent, moreover they show reasonable agreement with

the type of variation to be expected for a convective solar wind

modulation.

CONTENTS

CHAPTER 1

INTRODUCTION

1.1   General introduction.

The study of cosmic rays has made much progress in recent
years as a result of observations made with balloons, rockets and
satellites. Not only do these measurements add to the significance
of investigations made at lower depths in the atmosphere by
enabling response functions to be determined over the latitude
sensitive region, but detailed measurements of the primary cosmic
ray components and their energies can be made that are not
possible at sea level. In particular, the nucleonic composition
can be measured directly, whereas at sea level the degradation of
primary particles on passing through the atmosphere causes the
effects of the proton flux to obscure those due to the less
numerous components with charge $Z > 1$. Low energy particles are
rapidly absorbed, and even at high latitudes where they are free
from the influence of the geomagnetic field they produce very
little response at sea level. They must therefore be measured
above the atmosphere directly or by electromagnetic sounding
techniques.

The great sensitivity of slow particles to the environment
through which they pass renders them particularly suitable as a

means of indicating conditions within that environment. With sufficient knowledge about the earth's atmosphere and magnetic field, their filtering effect on the primary cosmic rays can be used to measure the cosmic ray energy spectra. In turn, these data are a valuable source of information on the extra-terrestial environment as well as on the origin of the particles themselves. For instance, the characteristics of the interplanetary field are reflected in such effects as the anisotropy of both solar and galactic cosmic rays, the 27 day variation, Forbush decreases after large solar flares, and the 11 year cycle of intensity. Some important aspects of these time variations of cosmic rays have not yet been very thoroughly investigated, particularly at the low energy end of the spectrum. This is largely due to the extra difficulties involved in their measurement.

It is particularly interesting to study the α-particle and proton components of cosmic rays since, apart from being the most abundant, they have a widely differing charge to mass ratio, giving a value of Energy per nucleon : Rigidity which for α-particles is exactly half that for protons of the same velocity. This fundamental difference can affect their relative motion under certain circumstances. For instance, whereas in a static magnetic field the motion of a collision-free particle will be governed by its rigidity only, which defines the radius of curvature of its path, in a convective field the motion of a particle will also

PARTICLE VELOCITY AGAINST RIGIDITY

Legend:
1 — H_1
2 — He_3
3 — H_2 He_4 C N O
4 — Li_7
5 — H_3

VELOCITY β

RIGIDITY GV.

FIGURE 1.1

- 9 -
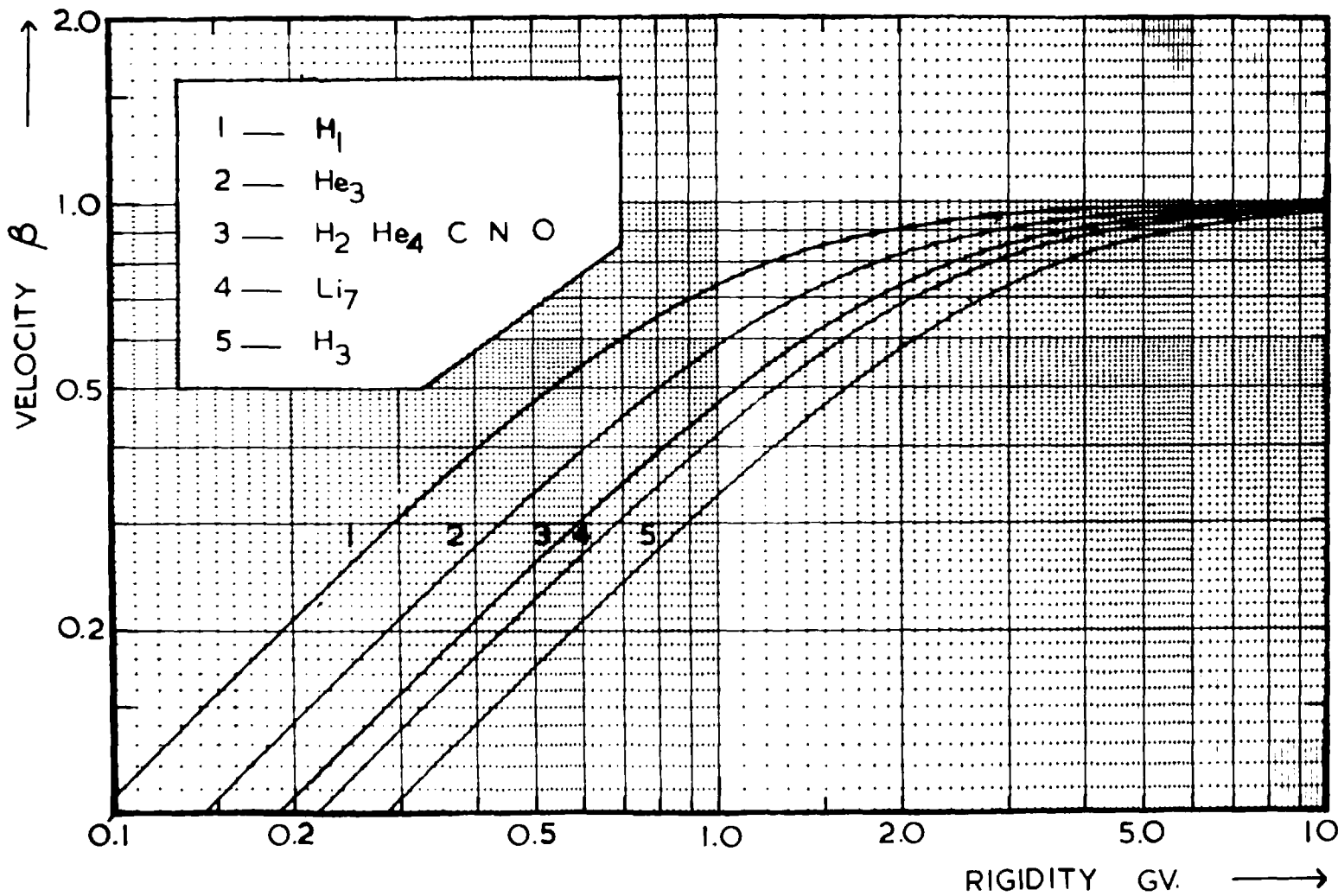
depend on its velocity. Qualitatively a proton and α-particle of

the same magnetic curvature will spend different times in any

region of the field and therefore if the environment is moving or

changing with time their trajectories are affected differently.

It has been stressed by Elliot (1962) that a critical evaluation

of the simultaneous changes in intensity of α-particles and

protons, over the 11 year solar modulation cycle, can provide a

crucial verification or otherwise of the extent to which this

modulation is dependent on particle energy or velocity β, apart

from the measured rigidity dependence, and hence whether or not

the gross features of the interplanetary field are convective, as

is suggested by certain theories e.g. Parker (1958), and Singer

(1958). Such measurements imply investigation at the low energy

end of the primary spectrum as can be seen from the rigidity-

velocity relations for different particles shown in Figure 1.1,

the optimum suitability of the α-particles and protons is obvious

from their divergent values of β and since the various other

isotopes are rare.

At the lower energies the means of measuring the energy

spectra are divided broadly into two categories by whether or not

they are dependent on geomagnetic theory. A good knowledge of the

cosmic ray threshold rigidities over the earth can give measurements

of the spectra between 2 and 15 Gv. rigidity, but more direct

methods are applicable at low rigidities by determining the energy

loss and range of individual particles. This can be carried out
by either emulsion or counter techniques, preferably as high as
possible above the atmosphere, each method having its particular
merit. Emulsion measurements, when carefully carried out, provide
a slightly more definitive value for the primary particle energies
in view of the possibility of counter-checking the range, track
density and scattering for each particle and knowing the zenith
angle of arrival. On the other hand, although a counter detector
payload is necessarily more complex, time variations are more
easily observed, the data can be interpreted much more rapidly and
include the possibility of automatic processing and reduction so
thereby a far greater amount can be handled. A counter balloon
flight of 100 cm^2. steradian hrs. will generally provide adequate
statistics on protons and α-particles to give an energy and charge
resolution equal to that obtainable from emulsions.

Recent measurements of these particles have been largely
concentrated on the spectra of solar produced particles at the
times of flares, and are therefore more relevant to a knowledge
of their production and acceleration mechanisms, and the field
configurations between the sun and earth. A number of such
measurements have been made by various experimenters using
different techniques which are well summarized by Frier (1963) and
Frier and Webber (1963). They conclude that the spectra of solar
flare particles can be described by the form $J = J_o \, e^{-P/P_o}$ where

J_o and P_o are intensity and rigidity parameters characteristic of the flare. The spectrum is the same function of rigidity for both α-particles and protons but with different J_o. At quiet times, in the absence of solar disturbances, the influence of the large scale interplanetary field is open to observation by its effect on the spectra of galactic cosmic rays at distances beyond the earth's orbit. It is with such measurements that the present thesis is largely concerned.

Before proceeding with a discussion of the experiment in relation to previous work, a few of the parameters that will be referred to are defined here.

Energy, unless otherwise mentioned, will be used to describe Kinetic Energy per Nucleon, T.

$$T = m_o c^2 (\gamma - 1) \quad eV.$$

where $m_o c^2$ is the rest mass of a nucleon and $\gamma = (1 - \beta^2)^{-\frac{1}{2}}$.

Rigidity, P is related to the particle radius of gyration, ρ such that:

$$P = Am_o \beta c^2 \gamma / Ze = 300B\rho \quad volts$$

where Ze is the total charge on the particle, A is the atomic number of the particle and B gauss is the field strength.

Particle flux, J will refer to the omni-directional flux in units of particles / metre^2 second steradian.

From these definitions it follows that the relation between the differential energy and rigidity spectra is:

$$dJ/dP = dJ/dT \cdot (\beta Z/A) \qquad \ldots\ldots\ldots 1.1$$

For large velocities when $\beta \sim 1$ the two forms of describing the spectra are indistinguishable.

1.2   Historical background.

Early evidence for solar modulation of the galactic cosmic ray intensity was provided when Forbush (1954) demonstrated that the variations in intensity, as measured with ion chambers at ground level during the period 1937 to 1952, were closely correlated with the average sunspot numbers. Since then, this correlation has been open to a more detailed investigation due to the installation, prior to the International Geophysical Year, of the standard neutron monitor network (Simpson, 1955) and the standard meson telescope (Elliot, 1958). These monitors provide a large amount of continuous data of high statistical accuracy from which, when corrected for meteorological effects, it is possible to study the latitude effect of the many short and long term variations of intensity with time, including the 11 year variation. Such measurements can only be related quantitatively to changes in the primary particle spectrum from a knowledge of the threshold rigidities over the earth (Quenby and Webber, 1959; Quenby and Wenk, 1962; Sauer, 1963.) and the specific yield functions (Webber and Quenby, 1959; Webber, 1962a). These

latter again rely on a knowledge of the differential primary intensities which must be obtained at the top of the atmosphere.

Preceding and during the last solar minimum, surveys at high altitude with various detectors made it clear that the 11 year solar modulation process has a far greater influence on low rigidity particles. A large amount of this evidence came from ionization chambers flown with balloons at different latitudes, (Neher, 1956) and aircraft latitude surveys of the nucleonic component, (Meyer and Simpson, 1957) although it was difficult to deduce absolute particle spectra from these results. The main problem in making primary particle measurements, even with balloons, is in the extrapolation of the measured flux over the last few millibars and in this connection it is first essential to discriminate between the protons and α-particles.

This has been done in a number of experiments since the discovery of heavy nuclei in the primary cosmic radiation (Frier et al., 1948; Bradt and Peters, 1948), and recent estimates for the relative intensities are not significantly different from an early value for the ratio protons/α-particles of 7 quoted by Ney and Thon (1951). The apparent constancy of this ratio, which is independent of the latitude of measurement, is consistent with identical rigidity spectra for these two components throughout the solar cycle. Furthermore, direct simultaneous determinations of the differential spectra, together with integral measurements from

1955 to 1959 by McDonald and Webber (1959), suggested that the

range over which the spectra are similar could be extended from

17 Gv. down to 1.0 Gv. In addition these investigators found that

the data for medium nuclei $(6 \leq Z \leq 9)$ were fitted by the

differential spectrum for α-particles for various stages of the

solar cycle (McDonald and Webber, 1962a), and also that the

integral flux measurements above 2 Gv. followed the same form of

long term variation as the α-particles. These findings on the

heavier elements are in agreement with those of other experimenters

e.g. (Aizu et al., 1961; Biswas et al., 1960; Evans, 1960;

Fichtel, 1961.) and are consistent with similar unmodulated spectra

for these particles, irrespective of the modulating mechanism, in

view of the near equal charge to mass ratios for particles with

$Z \geqslant 2$.

In the case of α-particles and protons there appears to be

no evidence at present to contradict the similarity of their

rigidity spectra above 1.5 Gv. although, except for α-particles in

the range 1.5 to 3 Gv., these results rely on integral flux

measurements which are not sufficiently accurate to be sensitive

to slight differences in the differential spectra. Below these

values however the conclusions can only be tentative as the data

available are rather sparse. Simultaneous measurements of these

two components have been lacking and some of the later results

are conflicting, particularly those regarding the shape of the

low energy proton spectrum. A comparison with α-particles has

been very difficult up to now as there have been virtually no

measurements of primary α-particles below 1.0 Gv. The only

occasion near solar minimum on which simultaneous differential

fluxes of protons and α-particles were obtained was at Minneapolis

in 1956, and the over-lapping rigidity range was between 1.2 and

1.4 Gv. (McDonald and Webber, 1962b). There is possibly some

doubt whether, in this region, these results are completely free

from geomagnetic effects which, although not changing the

differential rigidity intensities of various nuclei relative to

one another, would distort the shape of the galactic spectra.

There have been many occasions when the geomagnetic

threshold rigidity at Minneapolis has been apparently lowered

at the times of geomagnetic storms (Bhavsar, 1962; Earl, 1962;

Frier, 1962). In these instances the cut-off has not been sharp

but has introduced a smooth but definite bending over of the

spectrum. A similar effect on α-particles due to the threshold

rigidity at Moberly was measured under quiet conditions by

simultaneous balloon flights at two different latitudes

(Friedlander and Spring, 1962); the measured threshold of 2.1 Gv.

was in good agreement with the theoretical value. By comparison

with these effects, the theoretical threshold at Minneapolis,

1.34 Gv. (Quenby and Wenk, 1962) and 1.38 Gv. (Sauer, 1963) for

undisturbed times, if operating on a spectrum extending below

these values, would modify it to a form not unlike that found by McDonald and Webber at Minneapolis in 1956. It is therefore difficult to separate the solar and geomagnetic influences with confidence in this instance and, in order to allow for similar uncertainties arising from incomplete knowledge of threshold rigidities, it is essential for measurements of the solar modulated galactic spectrum at low rigidities to be made at very high geomagnetic latitudes.

The high latitude surveys of Neher (1956) and Winkler and Anderson (1957) with ionization chambers provided evidence for the existence of low rigidity particles in 1955 which is apparently in conflict with the conclusions of McDonald based on measurements at a similar time. Also, results published by Webber (1962) for a balloon flight made in 1956 from International Falls (geomagnetic latitude 59°N.) showed a higher flux of low rigidity protons than at Minneapolis (geomagnetic latitude 55°N.).

By comparison, an α-particle spectrum measurement made at high latitude (61°N.) and at solar minimum by Frier et al. (1959) appears to be in reasonable agreement with McDonald and Webber (1962 b) concerning these particles, (1962b) that the spectrum falls off rapidly around 1.0 Gv. However the air cut-off for this flight prevented detection of particles below this rigidity if they were arriving at the top of the atmosphere.

Most of the available data on the differential spectra of

low rigidity α-particles for quiet solar conditions are shown in
Figure 1.2 for which the relevant flight details are given in
Table 1.1 . In these results, which have been divided into
different periods during the solar cycle, the modulation can be
clearly seen, and in spite of the flattening in the region of 1.5
to 3 Gv. at solar maximum the lower rigidities are depressed even
further. The proton data seem to behave contrary to this.

Some results of recent direct investigations of the
differential primary proton spectrum, which have been free from
geomagnetic effects, are shown in Figure 1.3. Most of these have
been obtained using counters which utilize a combination of either
or both range and energy loss technique. The main reason for
divergence of the very low rigidity results, if they are not a
true reflection of the intensities at different times, possibly
depends more on the difficult interpretation of the raw data in
terms of a true primary flux than on the actual measurements.
For comparison the mean differential spectra of α-particles,
scaled up by a factor of 7.0 for three phases of the solar cycle,
are also shown. The proton measurements which have been made
since solar maximum clearly indicate an enhanced flux below 1.0 Gv.
compared to the tendency of the 1956 and 1958 proton results
which, as discussed, are probably not independent of the
geomagnetic field. The shape of the spectrum is quite different
from that of α-particles if they are extrapolated into this region

below 1.0 Gv. In order to determine how much these effects are
due to the presence of solar produced protons or ionization losses,
which are greater for α-particles, between the source and the earth,
and whether the spectral differences are produced by the
interplanetary field, more data are obviously required on
α-particles below 1.0 Gv. together with more extensive differential
proton flux measurements. With the aim of providing such
information on these particles a new form of Scintillator-Cerenkov
detector was developed and flown in a number of balloon flights.
This will now be described in the following chapter.

TABLE 1.1

Key to Figure 1.2: Differential spectra of α-particles.

June 1954 – Sept. 1956	⊙ 18.6.54	Frier et al. (1959)
	♠ 7.7.55	McDonald and Webber (1962b)
	♦ 2.8.56	McDonald and Webber (1962b)
	♦ 18.9.56	Duke (grain density and range) (1960)
	♠ 18.9.56	Duke (multiple scattering) (1960)
May 1957 – Aug. 1957	◈ 17.5.57	Frier et al. (1959)
	◈ 30.7.57	Frier et al. (1959)
	♦ (4.10.50)	Fowler et al. (1957)
Sept. 1957 – Aug. 1959	◈ 11.9.57	Aizu et al. (1961)
	♠ 16.2.58	McDonald and Webber (1962b)
	♠ 2.7.58	McDonald and Webber (1962b)
	◈ 3.8.58	Engler et al. (1961b)
	◈ 29.7.59	Stephenson and Waddington (1961)

Key to Figure 1.3: Differential spectra of protons.

July 1955 – July 1958 (Minneapolis)	♠ 7.7.55	McDonald and Webber (1962b)
	♠ 22.8.56	McDonald and Webber (1962b)
	♦ 16.2.58	McDonald and Webber (1962b)
	♦ 2.7.58	McDonald and Webber (1962b)
Sept. 1960 – Sept. 1962	◈ 22.8.60	Vogt (1962)
	◈ 15.9.60	Vogt (1962)
	◈ 8.8.61	Meyer and Vogt (1963)
	♦ 15 – 28 8.61	Bryant et al. (1962)
♦ 7.7.61	♦ 28.7.62	Fichtel et al. (1963)
	♦ 5.9.62	Brunstein (1963)

JUNE 1954 - SEPT. 1956   MAY 1957 - AUG. 1957   SEPT. 1957 - AUG. 1958

FIGURE 1.2

DIFFERENTIAL INTENSITY OF α-PARTICLES. PARTICLES / M² SEC. STERADIAN MV.

RIGIDITY GV.

(See Table 1.1 for references)

Differential Proton Spectrum.
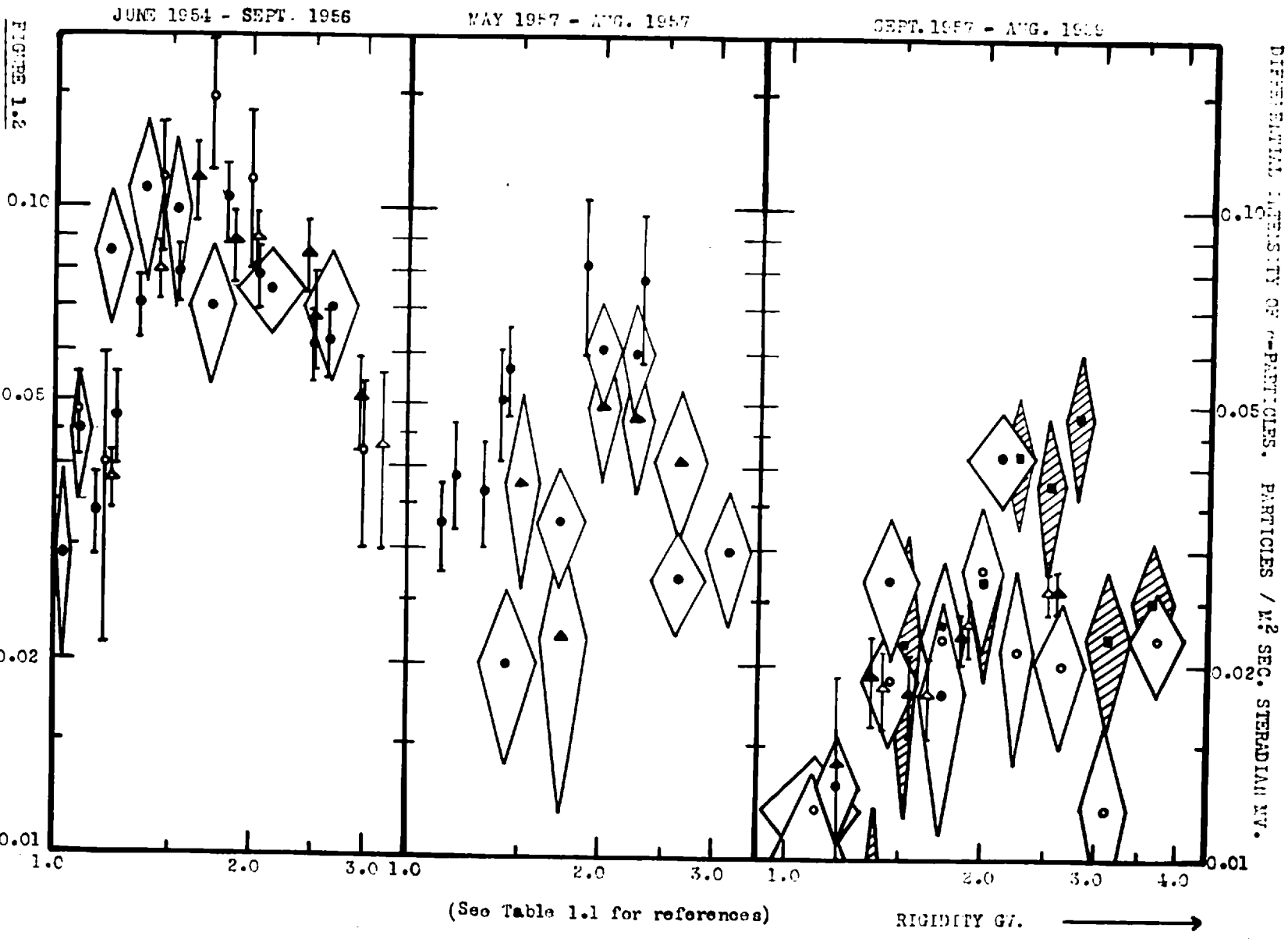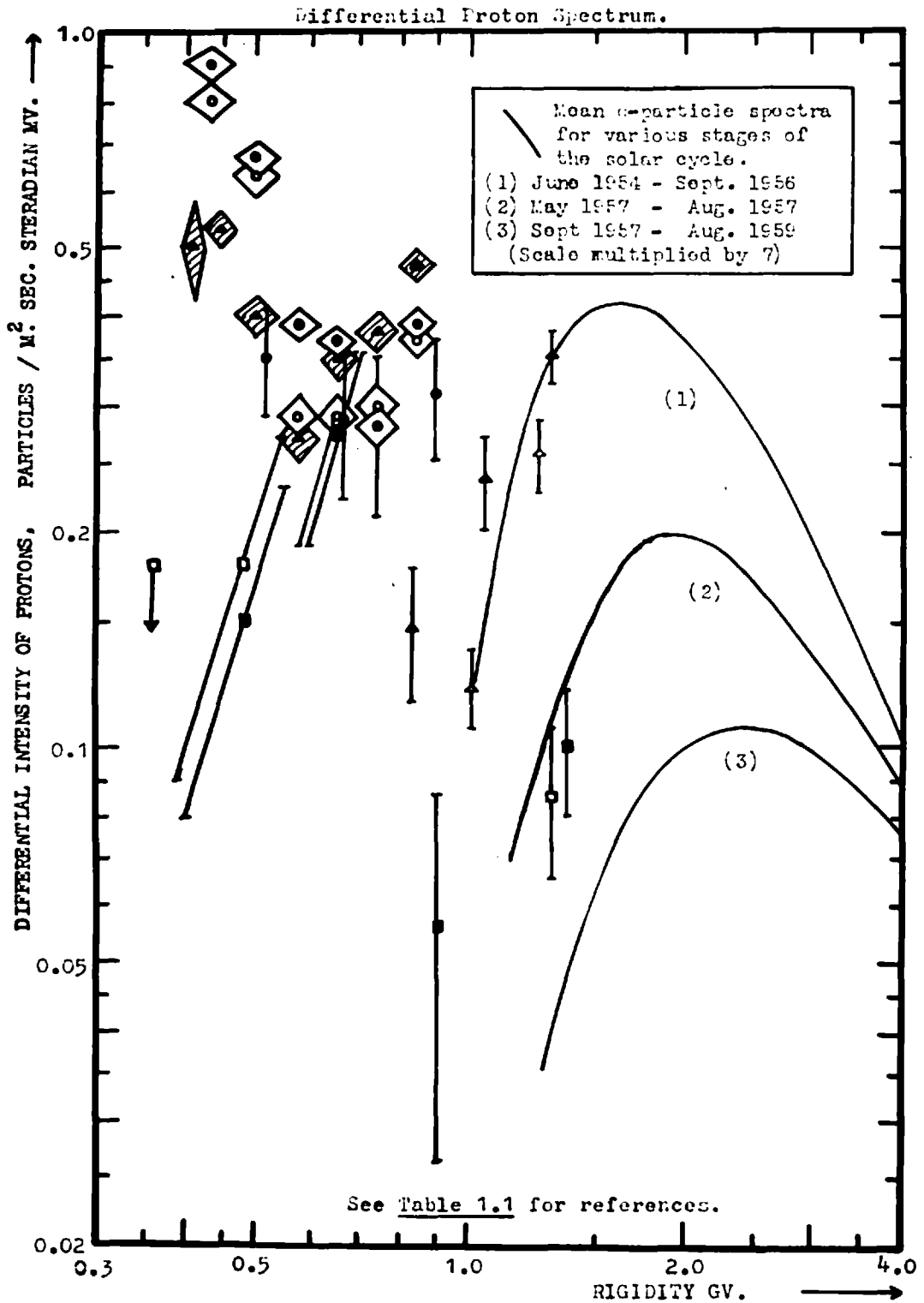
FIGURE 1.3

CHAPTER 2

THE MODIFIED CERENKOV SCINTILLATOR DETECTOR.

2.1   The energy response of a mixed detector.

The detection of particles by a Scintillation-Cerenkov coincidence device is limited to those with a velocity above the Cerenkov threshold, $\beta = 1/n$. For a typical solid radiator such as perspex, for which the refractive index 'n' is about 1.5, this threshold corresponds to a particle energy of 350 Mev./nucleon (proton rigidity 0.83 Gv.). In the present experiment it was desired to extend the response to lower proton energies and for this purpose a Cerenkov radiator which displayed a significant residual scintillation was considered.

The differential number of photons radiated at a given wavelength per unit path length of a charged particle passing through a material is given by the classical relation which was first derived by Frank and Tamm (1937).

$$\frac{d^2N}{d\ell\,d\lambda} = \frac{2\pi z^2}{137}\left[1 - \frac{1}{\beta^2 n^2(\lambda)}\right]\frac{1}{\lambda^2} \qquad \cdots\cdots\cdots\; 2.1$$

where ℓ (cms) is the path length of the particle, with charge Ze.

β is the particle velocity in units of c ~~cms./sec.~~

$n(\lambda)$ is the refractive index of the material.

λ (cms) is the wavelength of the Cerenkov radiation.

With a radiator having a finite transmission window for which n varies by only 1 → 2% over the range of wavelength, dispersion may be neglected, and the integral light intensity as a function of particle rigidity is obtained as in Figure 2.1 for S/C = 0 and taking n = 1.58. Since the form of the emission spectrum is independent of β, a relative response similar to Figure 2.1 is expected when the light from particles traversing a constant thickness of radiator is measured with a photomultiplier. The results of a number of workers have confirmed the theoretical relation in this way within the accuracy of their experiments. In particular Winkler et al. (1955) have made measurements over a range of β ≤ 0.85 using $\pi^{\pm}$ mesons from the Chicago synchrocyclotron and Millar and Hinks (1957) have tested the light output saturation at higher relativistic velocities. The dependence on Z^2 is also well established from numerous balloon flights that have been made to investigate the charge composition of the primary cosmic radiation. (Linsley, 1955; Horwitz, 1955; Webber, 1956; McDonald and Webber, 1955.)

Figure 2.1 (S/C = ∞) also shows the most probable energy loss by ionization for a charged particle passing through material and calculated from the expression:

$$E_o - E_p = \frac{2Cm_e c^2 x}{\beta^2} \cdot Log\left[\frac{4Cm_e^2 c^4 x Z_1^2}{(1 - \beta^2)I_2^2} - \beta^2 + j \right] \text{ .. 2.2}$$

FIGURE 2.1

RELATIVE RESPONSE.

RIGIDITY GV.
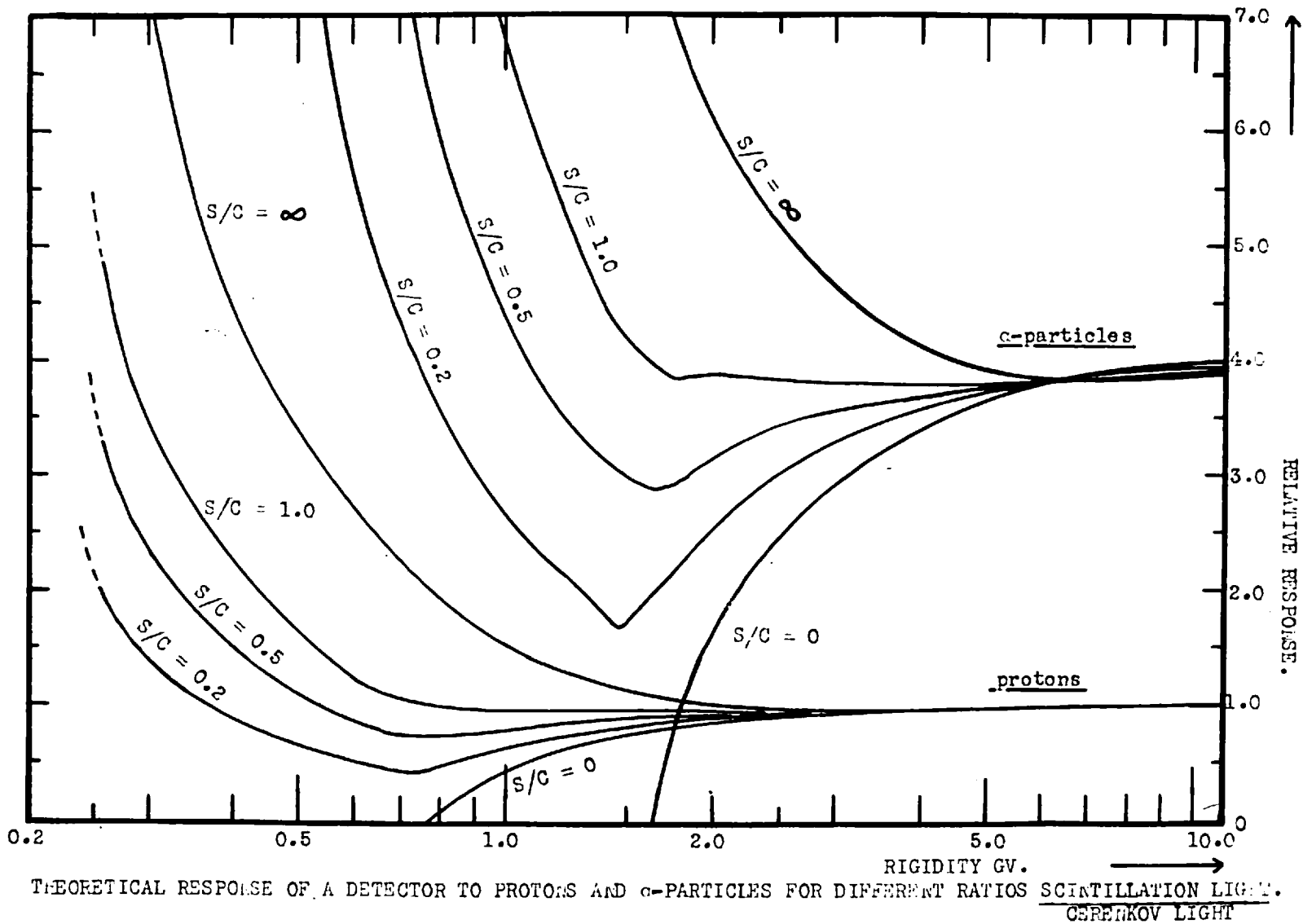
THEORETICAL RESPONSE OF A DETECTOR TO PROTONS AND α-PARTICLES FOR DIFFERENT RATIOS SCINTILLATION LIGHT.
CERENKOV LIGHT

S/C = ∞

S/C = ∞

S/C = 1.0

S/C = 0.5

S/C = 0.2

α-particles

S/C = 1.0

S/C = 0.5

S/C = 0.2

S/C = 0

protons

S/C = 0

FIGURE 2.2

α-particle rigidity

4.0   2.8   2.0 Gv.

Minimum ionizing α-particles

Theoretical two dimensional response;

○ Experimental two dimensional response; for protons and α-particles of different rigidity.

OUTPUT OF CERENKOV DETECTOR

Minimum ionizing protons

proton rigidity

2.0   1.0   0.8   0.7   0.6   0.5   0.45   0.4 Gv.
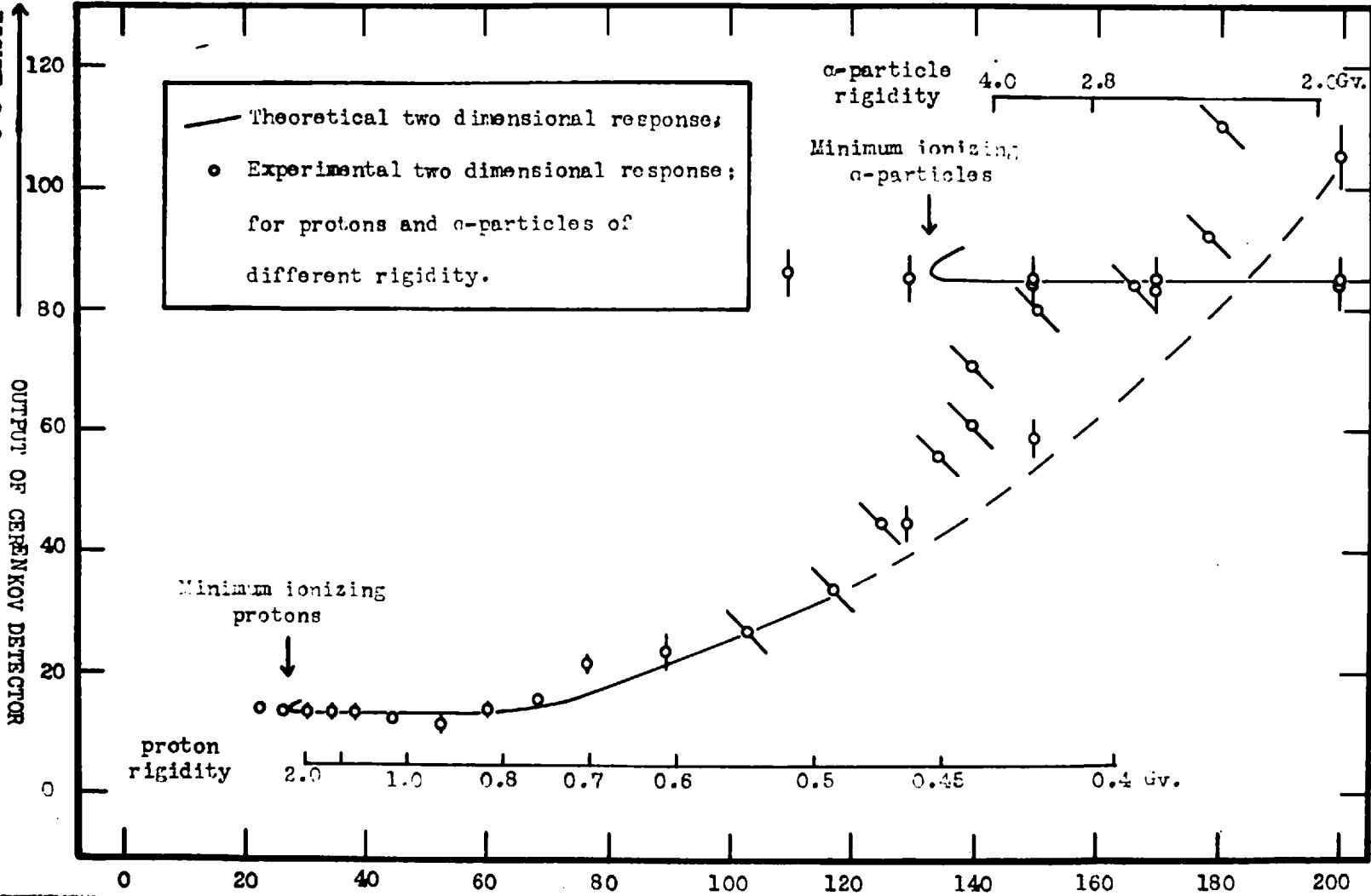
Two dimensional pulse height distribution (loci of the most probable response in both detectors).

OUTPUT OF SCINTILLATOR DETECTOR ⟶

E_o (Mev.) = Initial energy of the incident particle.

E_p (Mev.) = The most probable energy of the particle after
traversal of a thickness x gms./cm. of absorber.

C cm^2/gm. = $0.150 Z_2/A_2$; this is a measure of the electron collision
cross section of the absorber with atomic mass A_2 and
charge Z_2.

$m_e c^2$(Mev.)= Rest mass of an electron.

β = Velocity of the particle in units of the velocity of
light, c cms./sec.

Z_1 = Charge of the incident particle.

I_2 (Mev.) = Average ionization potential of the absorbing material.

x gm/cm^2 = Thickness of absorber traversed, taken as 1.32 for
Figure 2.1.

j = A universal dimensionless correction term which is a
function of β.

This formula was first derived for fast singly charged
particles by Landau (1944) using the basic theory on the mean
collision loss of energy of particles passing through matter which
has been extensively investigated and is well covered by Bethe (1930)
and Williams (1931). The form of the distribution in energy loss
about the most probable value given in the above formula, together
with the values for the parameter j have been computed by
Symon (1948) as functions of the incident particle velocity β and
the absorbing thickness x. Equation 2.2 is only valid for energy
losses less than 10% of the initial energy of the incident
particle which, for a radiator thickness of approximately 1.5 gms/cm^2.,
requires a proton rigidity of greater than 0.45 Gv. At the higher

energy losses however, the most probable loss approaches the mean energy loss and for rigidities less than 0.45 Gv. they are indistinguishable. The curves in Figure 2.1 have therefore been calculated at the low rigidity end using the computed range-energy figures given by Sternheimer (1959).

The relation between the light output in a scintillator to the energy lost by a particle passing through it is in general non-linear. One of the empirical forms of the relation which has been derived by Wright (1953) is given as:

$$dL/dx = A \, Log(1 + B \, dE/dx) \qquad \ldots\ldots\ldots\ldots \quad 2.3$$

Here dL/dx is the specific response of the scintillator as a function of the specific energy loss dE/dx (Mev. $gm.^{-1}$ cm^2.) where A and B are constants which depend on the scintillator considered. This mathematical form is derived theoretically on the idea of the excited column of molecules in the absorber transfering energy between themselves and partially quenching the available visible radiation energy. It can be seen that the relation becomes increasingly non-linear at larger values of dE/dx. The formula has been fitted to the experimental data over a range of dE/dx from 1.0 to $1 \cdot 10^3$ Mev. $gm.^{-1}$ cm^2. These data were obtained from artificially accelerated electrons, protons and α-particles passing through anthracene for which the value of the constant B was taken as 20 (mg. cm^{-2}. Mev^{-1}.), (Brooks, 1956).

Protons were used up to an energy 17 Mev. having values of dE/dx
of around 25 Mev. gm^{-1}. cm^2., and above these losses the specific
response is certainly not linear.

More recently Gooding and Pugh (1960) have made
measurements using NE 102 plastic scintillator which confirm the
form of this equation 2.3 for protons up to 150 Mev. (dE/dx down
to 4.5 Mev. gm^{-1}. cm^2.) and requiring B = 25 cm^2. mgm^{-1}. Since this
type of relation is valid for electrons down to their minimum
ionization loss it is reasonable that the equation can be extended
to cover minimum ionizing protons for which dE/dx is of the order
1.5 Mev. gm^{-1}. cm^2. Using the value of B for NE 102 it can be
shown that for protons of rigidity greater than 0.5 Gv. the
specific response of the scintillator relative to the minimum
ionizing response will be linearly proportional to the specific
energy loss within 5.0%. The linearity will be increasingly
better for particle rigidities approaching minimum ionization.
From these considerations the form of the most probable energy
loss curve S/C = ∞ in Figure 2.1 is a good representation of the
relative light output response of a scintillator as a function of
particle rigidity down to 0.1 Gv. This has been verified to the
order of precision of the present experiment as will be shown in
Section 2.5 .

The response of a mixed Cerenkov-Scintillation radiator
viewed with a single photomultiplier will depend on the proportion

of these two components. The curves in Figure 2.1 show the

rigidity responses of such a combined detector for different ratios

of Scintillation / Cerenkov light output S/C at β = 0.996 .

Curve S/C = ∞ is ^(for) a pure scintillator and curve S/C = 0 ^(for) a pure

Cerenkov detector, the effects of light saturation have been

ignored here. Also **drawn** are the responses for α-particles taken

to be 4 times the proton response at the same velocity β. It can

be seen from these curves that for a single detector of given

ratio S/C the response for α-particles becomes indistinguishable

from that for protons below a certain rigidity P . For a pure

scintillator this occurs at P = 0.45 Gv. but is reduced to less

than 0.3 Gv. for values of S/C between 0.1 and 1.0 . Such values

of S/C provide a better discrimination between protons and

α-particles than a pure scintillator and yet enable detection of

particles below the normal Cerenkov threshold as seen in curves

where S/C = 0. The use of such a mixed detector C + S' operating

in coincidence below a thin scintillation detector S will give a

two dimensional response distribution which will in principle

separate and resolve the rigidities of the proton and α-particle

components in the absence of protons below about 0.3 Gv. rigidity.

This can be arranged by observation at a suitable latitude and

altitude. In view of the Cerenkov component the response of this

detector will be directional to an extent depending on the ratio

S/C and also on the value of β for the particle being measured.

The theoretical response of the detector used in the present experiment is given in Figure 2.2 for different incident proton and α-particle rigidities and is described in Section 2.5 . In practice a statistical spread in response will be observed for any given rigidity and will be discussed in Section 2.4 .

2.2   The gondola electronics, telemetry and recording.

The requirements of the gondola electronics reduce to measuring and telemetering the individual pulse sizes from each photomultiplier for every particle passing through both detecting elements. A schematic block diagram of the system adopted is shown in Figure 2.3 .

The light outputs from the scintillator and Cerenkov radiators are amplified with the photomultipliers to produce voltage pulses of 1.2 μ secs duration. The pulses in each channel are then integrated and amplified and gated by the coincidence circuit for 10 μ secs so that they pass to the pulse'height to time' converter. This 10 μ sec. gating pulse is, however, inhibited during the dead time occupied by the transmission of each pulse, thus preventing overlap of information in the'height to time' converter. This latter produces a rectangular gating pulse of duration proportional to the voltage amplitude. The time duration of this pulse is then digitised by using it to switch
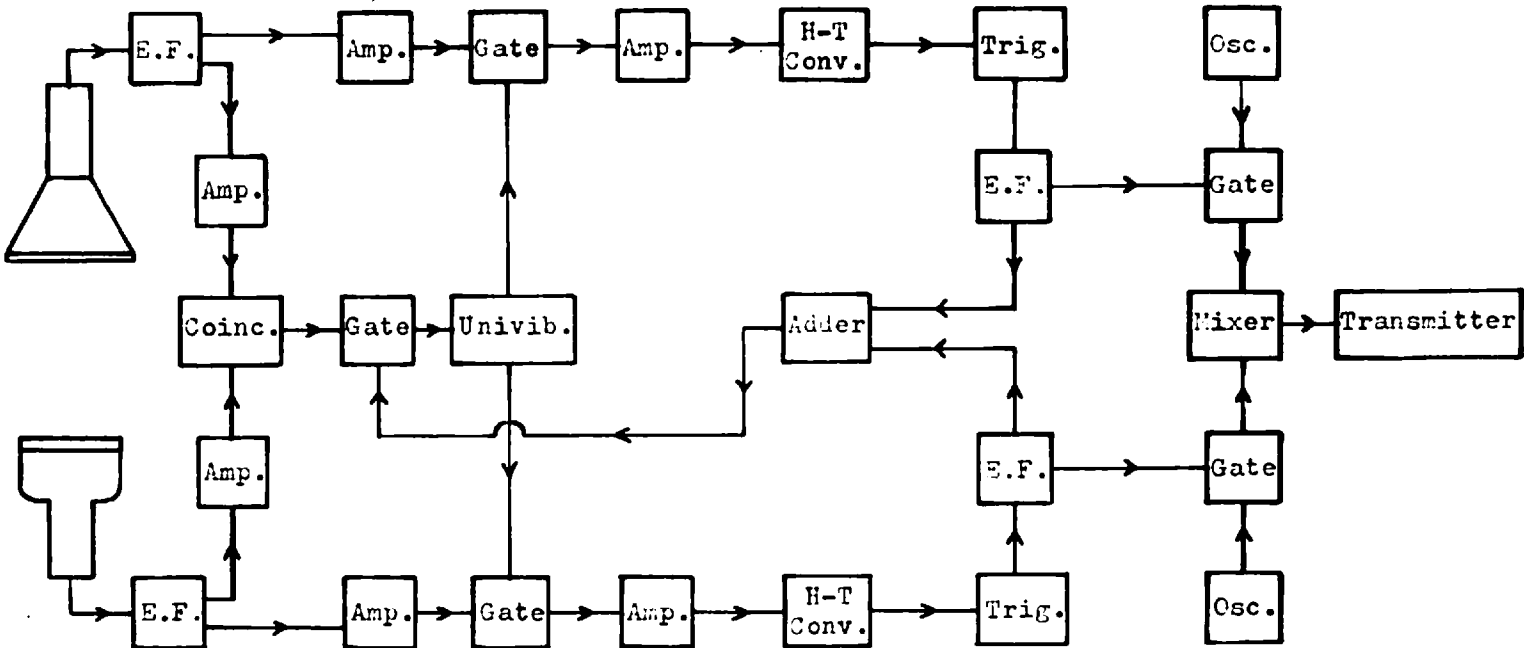
FIGURE 2.3   Block diagram of the teloscope electronics.

on a fixed-frequency continuously-running oscillator, and two oscillators, one for each channel, are then transmitted as subcarriers. The range of the 'height to time' converter is shown in the calibration in Figure 2.9b where the pulse size units correspond to the number of cycles of a 6 kc./sec. oscillator. The time scale is largely determined by the degree of accuracy to which the pulse heights are required. Fast times requiring high frequency oscillators are not possible using available commercial tape recorders and are also limited by the bandwidth of the telemetry, whereas the longer times introduce an increase in the electronics dead time during which the detector system is effectively insensitive. A subcarrier frequency of 6 kc./sec. was used as the best compromise which implies an accuracy of 10% for a 1.7 m. sec. pulse comprising 10 digits. In order to separate two subcarriers with a rejection ratio 1 : 10 and yet have a sufficiently low Q factor in the filters so that the transients do not smooth out more than one cycle, the other subcarrier was taken at a frequency of 34 kc./sec.

Two other narrower band subcarriers were used in order to transmit pressure and temperature conditions. A continuously running 400 c./sec. oscillator was switched on and off in a morse coded sequence determined by the air pressure and temperature inside the gondola. The Olland cycle system producing this code is shown diagrammatically in Figure 2.4a[*].

FIGURE 2.4a

Marker   Pressure code   Temperature code

FIGURE 2.4b

180
m s.

1   2   3   4   5   6   7

For discussion of tape playback see Section 2.2
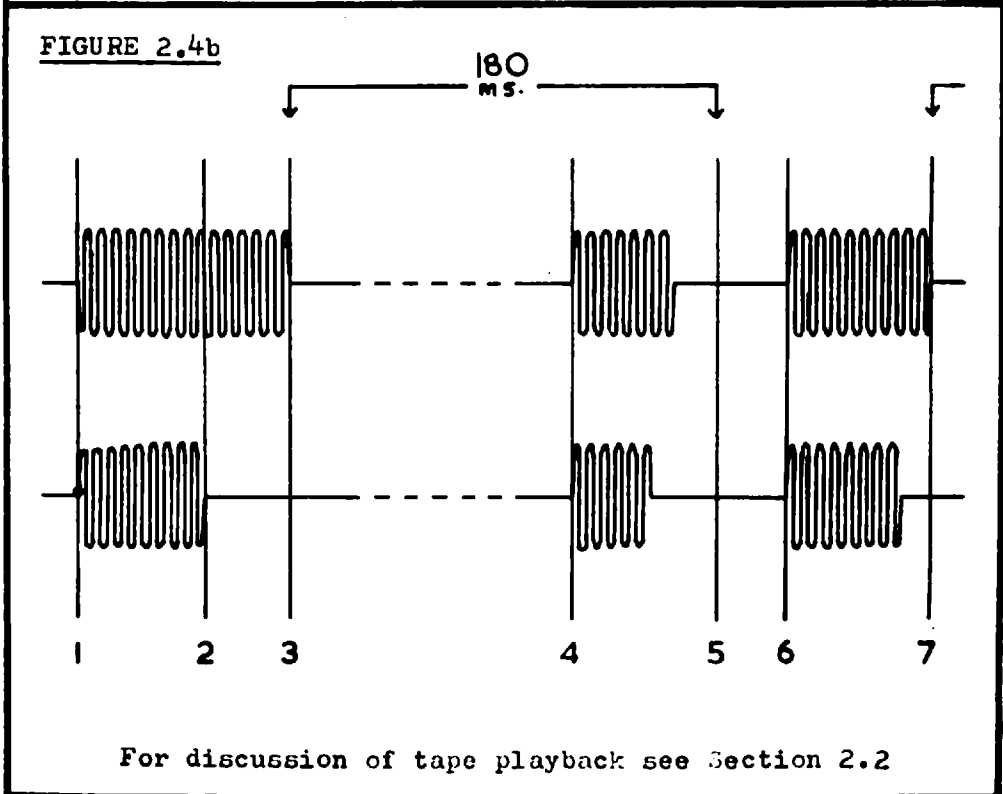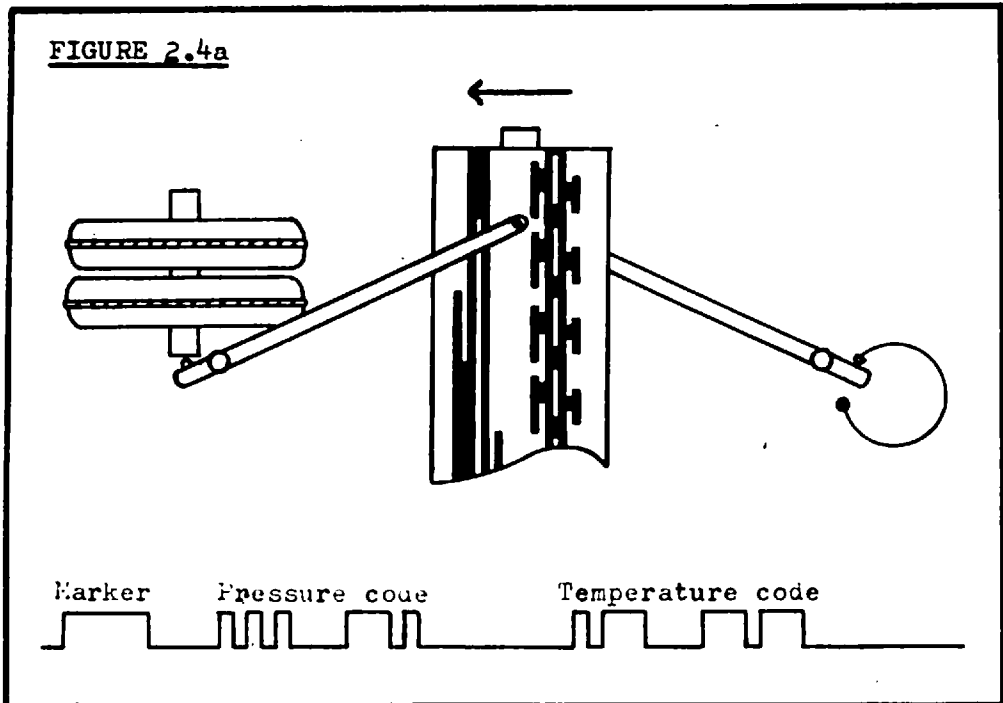
FIGURE 2.4a   Olland cycle and morse gating sequence.

FIGURE 2.4b   Pulse height data as recorded on two channel tape.

A temperature sensitive variable frequency oscillator was also
used to monitor the temperature of the batteries and to obtain
some measure of the thermal time-constants of the gondola insulation.

A single-valve frequency modulated transmitter and a receiver
system has been developed by Hedgecock (1962) for the requirements
of the present experiment. The transmitter radiates approximately
0.5 watts operating at 130 volts and has a transmitting frequency
of 153 mc./sec. An Eddystone 770R receiver was used which
required an antenna gain of approximately +18 db. in order to
extend the limit of useful range of the transmitter to the optical
horizon of approximately 280 miles. A low noise preamplifier
together with an 8 element yagi receiver antenna were employed
and both ground plane and turnstile radiators were used in the
gondola on different flights. The former was found to be more
free from fluctuations in signal strength caused by rotation when
the elements were not quite matched, but suffered in signal to
noise ratio on occasions when the balloon floated above the
receiving station. The latter, as expected from the polar
diagram, gave much better reception under these conditions.

The layout of the receiving and recording system is shown
in Figure 2.5 . Pressure and temperature readings on the 400c./sec.

* The device is one which has been developed by the Max Plank
Institut and is manufactured by the Albin Sprenger Co., W. Germany.

FIGURE 2.5
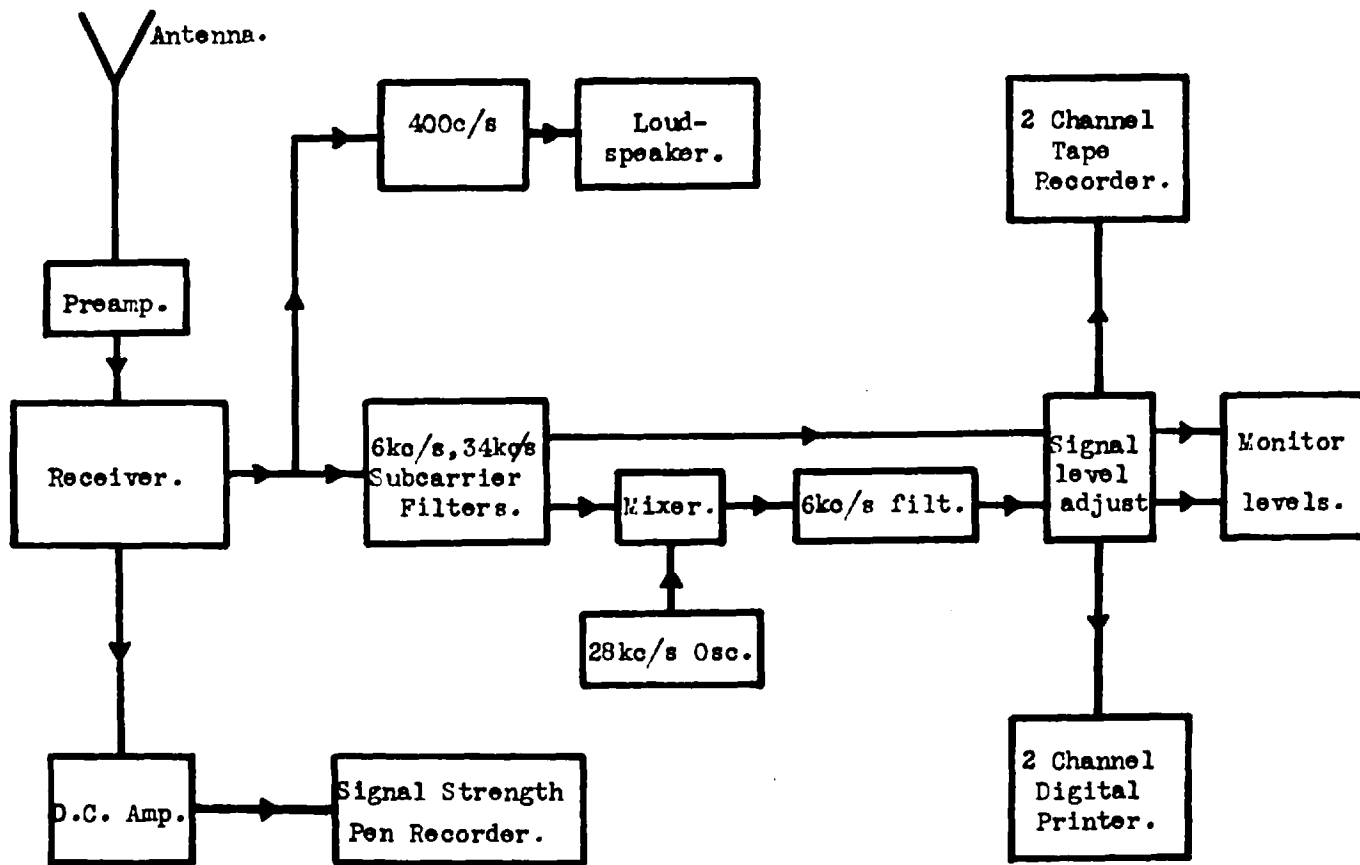
FIGURE 2.5   Block diagram of the telemetry receiving layout.

are interpreted and taken manually during the balloon flights although the level recorded on the tape, -34 db. w.r.t. the telescope channels, is sufficiently high to be replayed and heard with a tuned amplifier. The telescope subcarriers are separated, the higher 34 kc./sec. frequency then being mixed with a 28 kc./sec. crystal oscillator to obtain the 6 kc./sec. beat frequency which is then filtered out. Both channels are then recorded at the same frquency of 6 kc./sec. A typical record of the two telescope channels is shown together with the pressure and temperature code in Figures 2.4. Continuous monitoring of the signal strength facilitates adjustment of the receiver and steering of the antenna and also gives an indication of the drift and range of the balloon.

An automatic system for recovering the data from the tape was developed and is shown in Figure 2.6 . This was designed to print the number of recorded digits in the two channels which represent a measure of the response of the two telescope detector elements for each individual particle. A Hewlett-Packard digital printer type H 42-565A was used having a print time of 180 m. sec. (Maximum print rate 5/sec.) In order that the fraction of information lost due to the finite print time could be made small, a commercial tape deck was modified to give replay speeds of 1/6, 1/12, 1/24, and 1/48 of 3 3/4 inches per second which was the original recording speed. The percentage

FIGURE 2.6
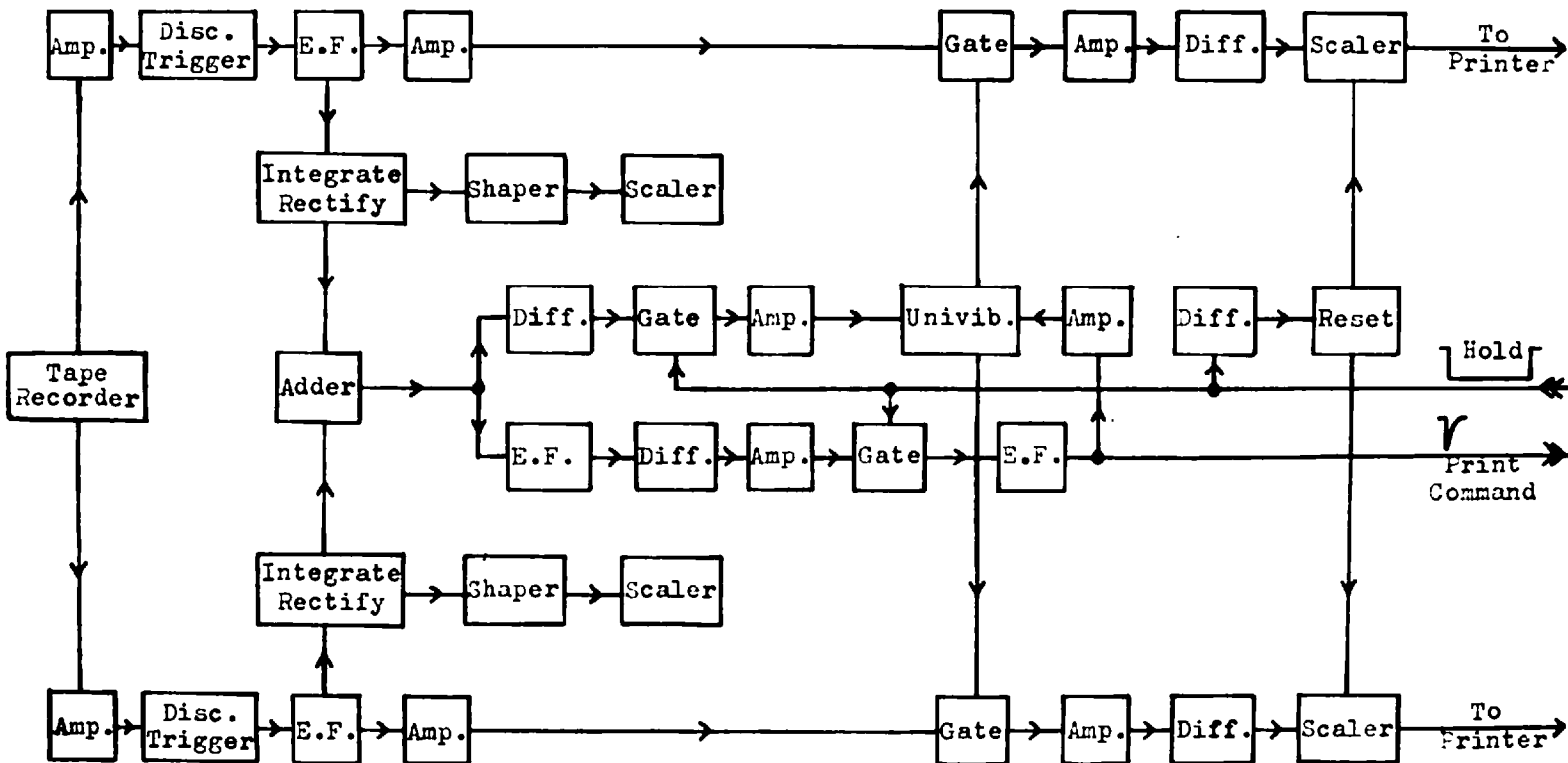
FIGURE 2.6   Block diagram of the automatic printout electronics.

of the data lost as a function of the tape slowing factor for
typical counting rates at altitude gave an optimum playback speed
of 1/12 when about 10% of the data were lost. This method of
recording in digital form has the advantage of being independent
of tape speed variations. From the tape playback a discriminator
rejects background noise below 50% of the full signal amplitude.
The time sequence of the automatic printout is illustrated by
Figure 2.4b which shows a typical record of the digitised data as
they appear on the tape playback. With reference to the figure:

1) Start of a pulse train initiated by a coincident particle.
The leading edge opens a gate which allows the number of cycles
to be counted by scalers which are coupled to the digital printer
by 10-line outputs produced from a diode matrix.

2) End of the shorter pulse train.

3) End of the longer pulse train. Scaler gate is closed and
printout cycle is initiated lasting 180 m. sec. during which the
scaler gate is held closed.

4) A further coincident particle arrives within the printer
dead time and is omitted.

5) End of print cycle, scalers are reset to zero and system
is ready to accept the next pulse train.

6) Scaler gate opens.

7) Print cycle commences as at 3).

A second set of scalers is used to count the total number

of particles in order to correct for the number which are omitted
by the printout. These are read visually.

2.3   The gondola telescope - environmental tests and calibrations.

The relatively lower abundance of α-particles compared to
protons requires a fairly large geometry if good statistics are
to be obtained from a balloon flight lasting a few hours. In
addition because of the low specific photon yield from a Cerenkov
detector it is desirable to couple the radiator directly to the
viewing photomultiplier tube. The configuration used utilized
a $\frac{1}{2}$" by $4\frac{1}{2}$" diameter disk of polyvinyltoluene coupled to a 5"
diameter photomultiplier tube (E.M.I. 9530) as a mixed C + S'
detector, and a 1/4" by 6" diameter disk of N.E. 102 scintillator
viewed centrally by a 2" diameter photomultiplier (E.M.I. 6970)
using a conical darvic reflector. These two elements give an
isotropic geometry factor of approximately 25 cm^2. steradian when
separated by 10". The calculation of the geometry of a
non-cylindrical telescope is treated in the Appendix A. To
provide a protective shield, both electrical and physical, the
tubes were encased in light-tight brass sheet cans, and in order
to leave a minimum of material above the scintillator the
electronics and battery supplies were attached beneath the
detector. The pressure measuring device and transmitter were

mounted below the battery box. A photograph of the detector is shown in Figure 2.10 .

The electronics were tested under the pressure and temperature conditions to be expected during a flight at altitude. Since the gondola was not pressurized, araldite was used for potting the E.H.T. dynode chain and the 1200 volt batteries were sealed in paraffin wax. Later flights have utilized an E.H.T. voltage converter. Each unit was tested for absence of corona down to pressures of 1 gm./cm^2. The combined detector and electronics system was tested for changes in gain with temperature using μ-mesons in the laboratory and they were found to be stable within 5% over the range 10° C. to 40° C., the gain dropping off to an increasing extent beyond these limits. It was necessary therefore to control the gondola temperature to lie within these limits and an expanded polystyrene cover together with a polythene bag were used to reduce convective cooling. In addition it was found that blackening 60% to 70% of the surface produced an equilibrium temperature at altitude of between 10° C. and 20° C. during the day for the air inside the gondola. In order to compensate for a 20° C. drop in gondola air temperature during the ascent the equipment was warmed to between 30° C. and 35° C. prior to the launching. With these precautions the battery temperature was maintained between 15° C. and 25° C. during the day due to their larger heat capacity and small amount of heat

generated within. This ~~degree~~ control of battery temperature was

important for satisfactory life times of the mercury cells used.

In all the flights reaching altitude the temperature was kept

within the operational limits but dropped quite considerably when

the balloons sank to denser air regions.

The pressure and temperature Olland cycles were calibrated

in the respective environmental enclosures since the pressure

coefficient of the temperature device is negligible, and the

pressure device calibration does not change by a detectable amount

over the range of temperature used. The sensitivity of the

pressure measurement varied from 0.5 Mb. at 200 Mb. to 0.3 Mb.

at 0 Mb. although on occasions the absolute calibration was

subject to an error $\pm$ 1 Mb. due to mechanical hysteresis. In

later flights an additional aneroid bellows was included so that

the range 1000 Mb. to 200Mb. was also measured to within 3 Mb.

Temperature measurement was to an accuracy of 1° C. which was

more than adequate.

The electronics circuitry was calibrated using

photomultiplier type pulses from a mercury relay millimicrosecond

pulse generator by measuring the digital output from the complete

system for a range of pulse amplitudes at the emitter follower

input. A typical example of the calibration for one of the

telescope channels is shown in Figure 2.9b which, although

obtained at altitude from the particles of different charge,

is of the same form if 20 units $\underset{\wedge}{\text{of }z^2}$ are taken as 5.0 volts. By

selecting the photomultiplier voltage the gain was adjusted so

that the most probable response from a fast meson produced an

output in the region of 20 to 30 units. The outputs due to

protons and α-particles therefore lay on the linear part of the

overall response calibration. The existence of a small threshold

voltage merely entailed adding a constant number of cycles to the

final output in order for it to represent the detector response.

2.4 Statistical fluctuations in response.

Pulse height distributions were obtained using μ-mesons

in order to test the degree of resolution of each detector. The

results of the scintillator detector response for three of the

telescopes is shown in Figure 2.7, these have been normalized for

convenience of comparison. It can be seen that within the

statistical errors they can be fitted by a single distribution

with a full width at half height of 40%.

In general the fluctuations in response from particles of

any given rigidity are due to a combination of the following

effects in a photomultiplier-radiator system:

   a) Statistical fluctuations in the ionization energy loss.

   b) Fluctuations in particle path length - (geometry effect).

   c) Non-uniform light collection from all areas of the radiator.

Normalized pulse height distributions for μ-mesons at sea level in the scintillator detector for the three gondolas from which primary particle data were obtained.

FIGURE 2.7

Statistical errors

Multiply ordinate by 250 for number of counts.

Gondola # 1B ●
Gondola # 2B ▲
Gondola # 2A ○

FIGURE 2.7

PULSE HEIGHT (ARBITRARY UNITS) ⟶
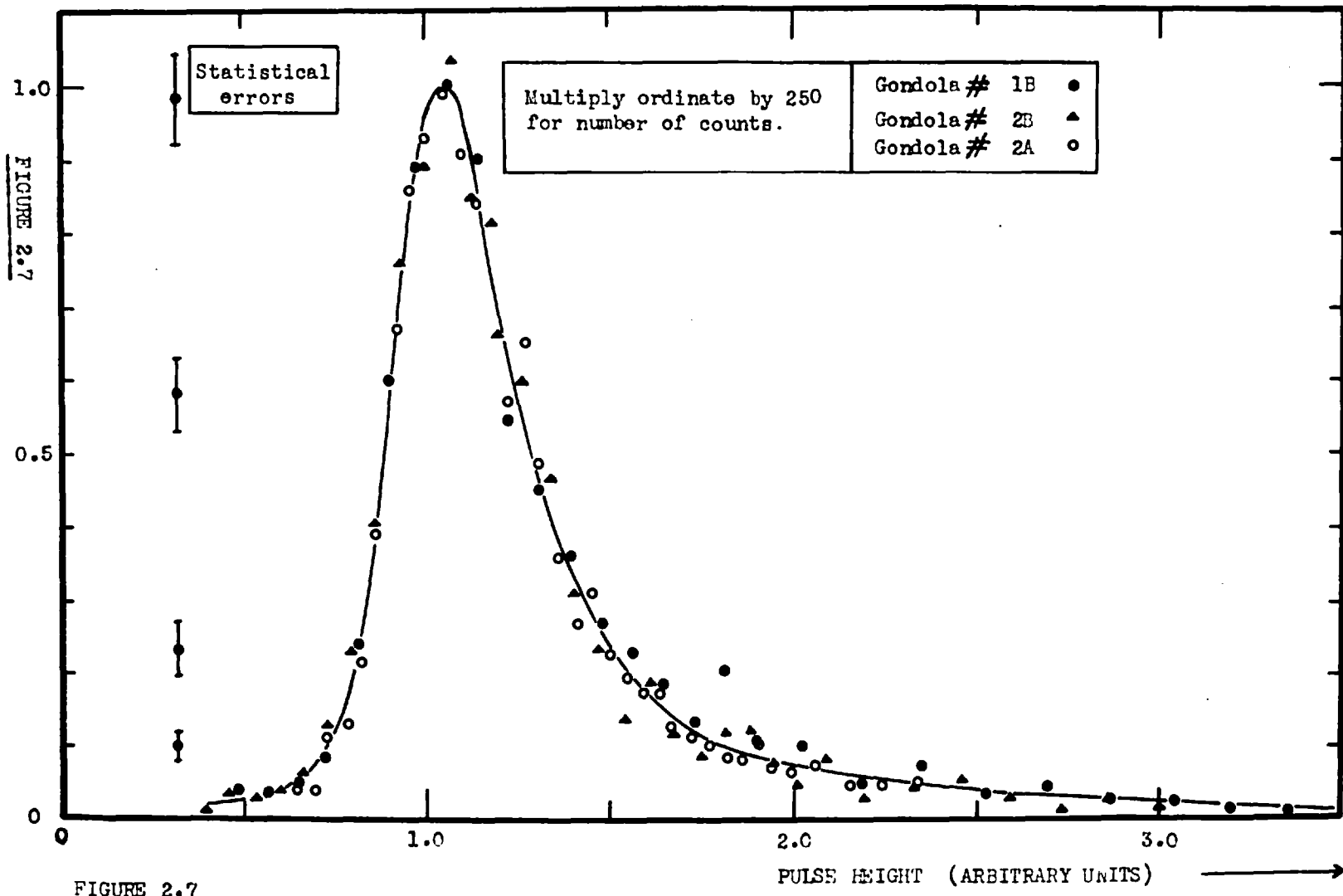
d) Non-uniform conversion efficiency over the photocathode
of the photomultiplier, and collection at the first dynode.

e) Statistical fluctuations in the number of photoelectrons.

f) Multiple particle events such as stars or accidental
coincidence.

g) Thermal noise and dark current in the photomultiplier.

The first two instances are fairly strongly asymmetric and
the other variations will be gaussian to a first approximation
with the exception of f) which is irregular. The predominant
effects for a scintillator detector are a), b), c) and e).
Calculation gives an average of about 4500 photons from 1/4" of
N.E. 102 for a minimum ionizing μ-meson. Taking a quantum
conversion efficiency of 15% and an estimated light collection
efficiency of 50% as an upper limit leaves 330 available
photoelectrons. These will contribute 12% half-width. The
relative contributions of the various factors are estimated to be
as follows in the detector employed. a) 26%, b) 8%, c) unknown
but small, d) $\sim$10%, e) 12%, f) negligible, g) small. These
effects are independent and combined must give an overall half-
width of 40% which suggests that some of the factors have probably
been underestimated. It has been found since however that a small
spread in final output is obtained for identical photomultiplier
pulse amplitudes photographed from an oscilloscope, although the
output for a certain test input pulse is stable. Unless this is

due to statistical errors in measurement, it is possible, ~~that~~ in view of the large factor of integration by the 'height to time' converter, that a slight variation in pulse shape for a certain anode charge due to dark current and thermal noise would lead to a small variation in output.

The mixed C + S' detector was blackened on the upper surface for the flights in order to obtain a better indication of the fast splash albedo. Under these conditions the number of available photons in the C + S' detector is about 500 for fast sea level μ-mesons. The contributions of the various factors are estimated to be as follows in terms of half widths.

a) 13%, b) 8%, c) + d) + e) 40%→50%, f) negligible, g) small.

2.5 Particle and charge resolution.

The response of the mixed detector was investigated for upward and downward moving particles by inverting the telescope. This was carried out with a clear disk of P.V.T. and then with the surface farthest from the tube blackened, the disk being coupled directly with a thin film of vaseline to the 5" tube. Figure 2.8 shows distributions obtained in this way, normalized to the same number of particles. The degree of separation for the two cases can be seen to be improved by blackening although there is some loss of pulse height due to the diminished reflected

FIGURE 2.8 Pulse height distributions in the mixed detector for sea level μ-mesons.

Surface of P.V.T. clear, A.

Surface of P.V.T. blackened, B.

(1)   (2)

NUMBER OF COUNTS (ARBITRARY UNITS)

PULSE HEIGHT (ARBITRARY UNITS)
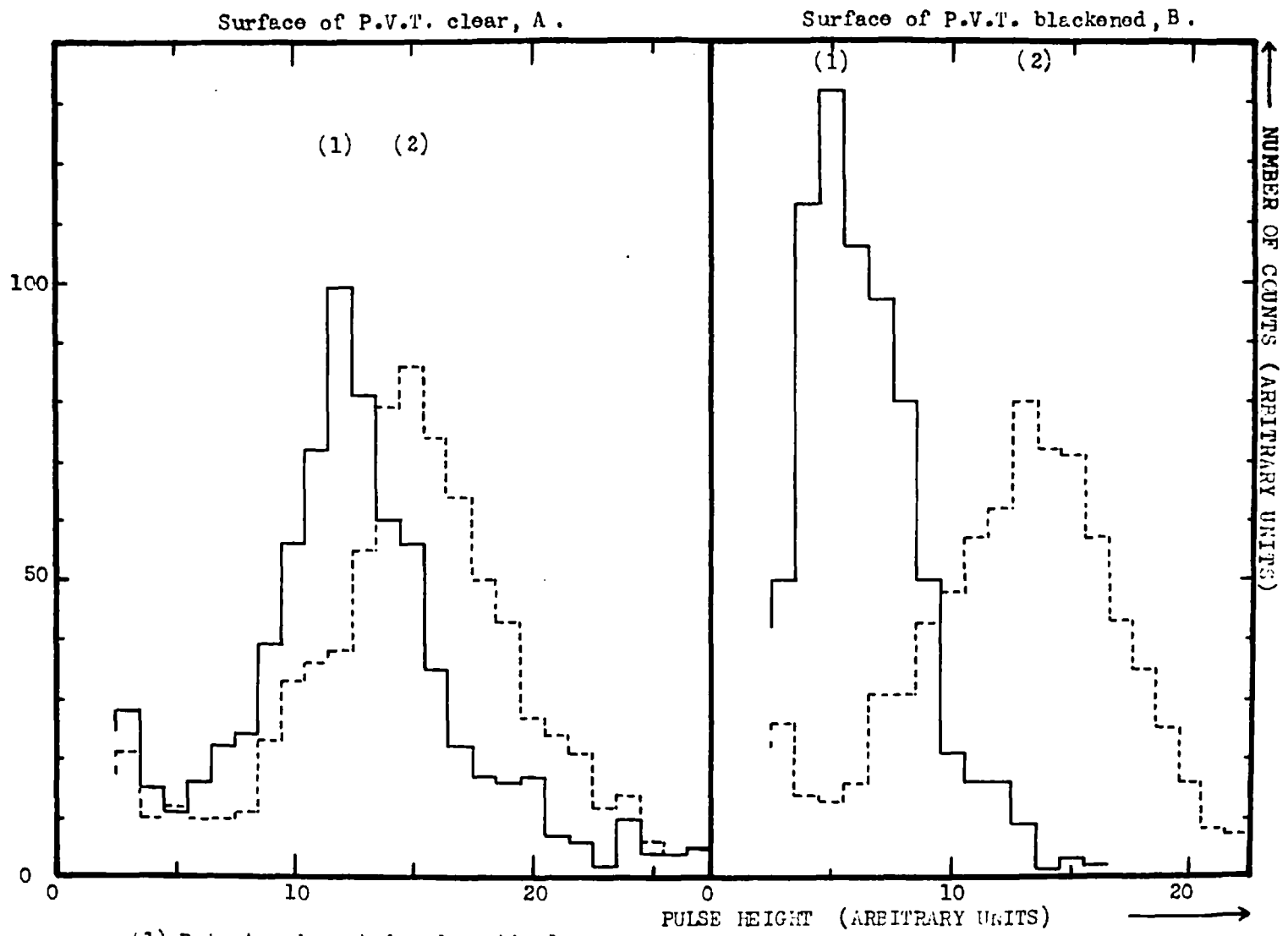
(1) Detector inverted and vertical.

(2) Detector upright and vertical.

scintillator component when upright. The asymmetry of the case
when blackened and inverted is significant in that the blackening
has also considerably diminished the reflected Cerenkov component.
The distribution is entirely due to direct residual scintillation.
(See Equation 2.6 below). An analysis of the most probable pulse
sizes for the four cases can give a measure of the Scintillation
to Cerenkov ratio and the fraction of light reflected from the
clear face.

Let the contributions to the most probable pulse size for
μ-mesons be C for the Cerenkov and Ck for the scintillator
components emitted in the direction of the tube face. Introducing
the average reflection factors for light emitted away from the
tube face r_c, r_c' and r_s, r_s' for the two components C and S where
the primes refer to the blackened condition, then:

$$1)A \qquad C(r_c + k(1+r_s)) \approx 2.45 \pm 0.05 \qquad \ldots\ldots 2.4$$

$$2)A \qquad C(1 + k(1+r_s)) = 3.05 \pm 0.05 \qquad \ldots\ldots 2.5$$

$$1)B \qquad C(r_c'+ k(1+r_s')) = 1.20 \pm 0.05 \sim Ck = S \qquad \ldots\ldots 2.6$$

$$2)B \qquad C(1 + k(1+r_s')) = 2.60 \pm 0.05 \sim C + S \qquad \ldots\ldots 2.7$$

Taking r_c' and r_s' to be small(≤ 0.1,) to reduce the
number of variables, and solving, gives S/C = 0.86 $\pm$ 0.10, and values
of $r_s = 0.40 \pm 0.20$, $r_c = 0.60 \pm 0.20$. This value of S/C can be
compared to the value 0.9 for relativistic protons which is

obtained from data on the two dimensional pulse height distributions
at altitude. A value S/C = 0.9 ± 0.05 for P.V.T. alone has been
measured by Pringle (1961). It must be noted that the response
of the detector includes light produced in the glass face of the
photomultiplier whereas this was negligible in the measurements
of Pringle. There is evidence, however, from experiments with
pyrex glass, that the ratio S/C for pyrex alone lies between 0.5
and 1.0, and this has been confirmed by some tests communicated
by D.R. Nicoll (1963). The presence of the tube face in these
circumstances does not therefore appreciably affect the ratio S/C,
although its thickness must be taken into account when determining
the response from very slow protons which are nearly stopped.

It is essential to be able to calibrate the response of
the detector in terms of the particle energy or rigidity. By
using two detectors with different characteristic responses as in
the present experiment, provided the responses are known, a
calibration is obtained by plotting one response against the other
on a two dimensional grid. The scintillator response can be
confidently expected to follow the ionization energy loss from
the considerations discussed in Section 2.1 . The mixed detector
consisting of a relatively weak radiator which is sealed to the
glass face of the photomultiplier consists essentially of four
elements since the light contribution from the glass is appreciable

especially for highly ionizing particles. In order to measure the light contribution from this glass a series of pulse height distributions were obtained using μ-mesons and different thicknesses of perspex radiator and glass. Peaks were obtained in the pulse height distribution for μ-mesons passing normally through the 6 mm. face of the photomultiplier and corresponded to a residual scintillation output in the glass in addition to Čerenkov light which was of the same order as that in the P.V.T. for equal thicknesses. The mixed detector response can therefore be calculated although it becomes rather complicated for slow particles which are near the end of their range.

The theoretical two dimensional response of the detector for protons and α-particles is shown in Figure 2.2 together with the observed pulse height distribution peaks. These have been obtained by taking pulse height distributions in the mixed detector C + S' for fixed intervals of scintillator response, and also from diagonal distributions which correspond to intervals where the sum of the scintillator and mixed detector outputs are constant. the agreement between the theoretical locus and experimental points is very good except for very slow protons near the α-particle region. This is probably due to both highly ionizing knock-on electrons with small range produced in the lower detector and the statistical weight of the fast α-particle distribution. The range of pulse heights shown does not accomodate the heavier particles
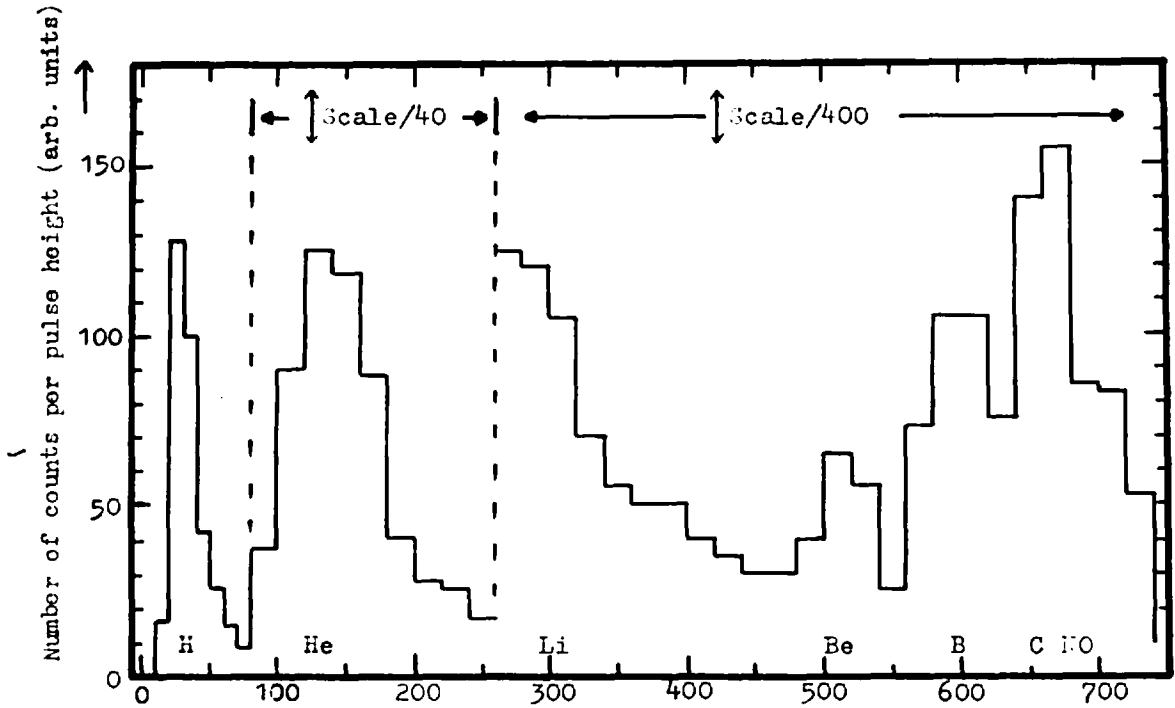
FIGURE 2.9a   Pulse height distribution in scintillator after charge discrimination in the mixed detector.
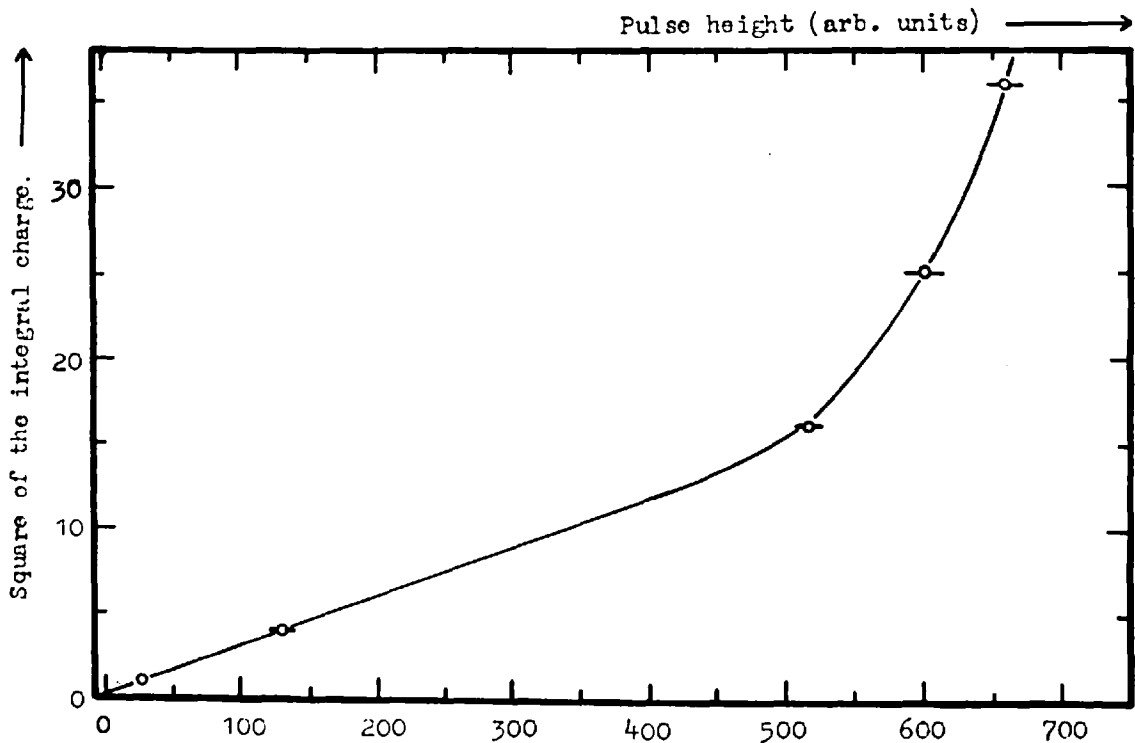
FIGURE 2.9b   Square of the integral charges plotted against the peaks in the pulse height distribution.
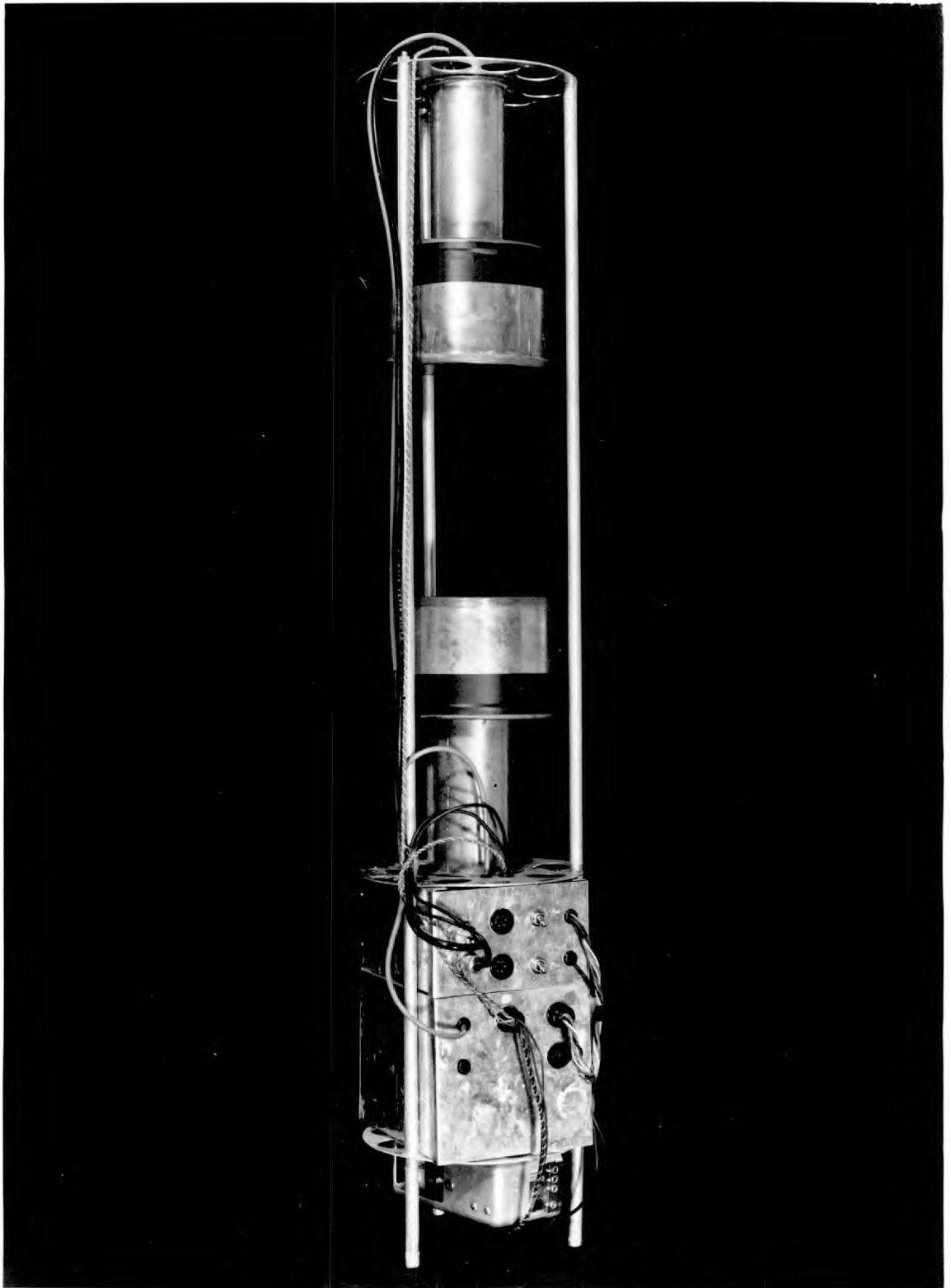
FIGURE 2.10 The gondola telescope structure.

some of which still lie within the dynamic range of the electronics
before amplifier saturation. An indication of the degree of
resolution of heavier particles is shown in Figure 2.9a. For
similar energy spectra the nuclei will produce peaks in the
response distribution which increase approximately as the square
of the nuclear charge. In Figure 2.9b the peak outputs have been
plotted against the square of the integral charges so that it is
possible to identify the nuclei. The position of the beryllium
point verifies that the response is linear over the proton and
α-particle region although the boron and carbon peaks lie in the
non-linear region of the 'height to time' converter. The electronics
saturate for all particles heavier than carbon and it is not
possible to resolve lithium from the slow α-particles and
background. The data for the particles with Z > 2 are derived
from a pressure range 10 to 30 gm./cm^2 here to give all available
statistics. Isotopes of hydrogen and helium in principle produce
distinguishable responses when β is less than about 0.7, however
they could not be separated with the degree of resolution of the
present detectors and in the analysis they are included with the
commonest isotope.

The detection of other radiation must be considered, as
some γ rays, mesons and electrons are capable of producing a
response of the same order as that from protons. The low γ ray
flux (Charkhchyan, 1961; Kidd, 1963) together with the low

probability of producing a fast electron pair in the counters, which are about 5% of a radiation length, is expected to produce a negligible contribution to the altitude counting rate. Fast mesons will produce responses identical to protons of the same velocity and there is no means of distinguishing these with the detector. From the results of Clark (1952) typical fluxes of mesons relative to protons are 7% at 20 gms/cm^2. and 12% at 50 gms/cm^2. increasing rapidly with atmospheric depth. However by extrapolating the observed intensities of fast particles to 0 gms/cm^2., where the meson flux is effectively zero, their contribution can be elZiminated; such an extrapolation will also include the rare fast downward moving secondary electrons. Recently results of Earl (1961) and Meyer and Vogt (1961), obtained with balloon flights at periods of quiet solar activity, have suggested the presence of a non-negligible flux of primary electrons below 2.0 Gv. rigidity. From their figures it is estimated that for the higher latitude flights made at a threshold rigidity of 0.5 Gv. the primary electron flux will amount to 2% ± 1% of the intensity of protons greater than 2 Gv.

In general the fluxes of particles other than nuclei can therefore be neglected. The corrections for secondary nuclei will be discussed in Section 3.2c together with interactions in the telescope and the albedo particles.

CHAPTER 3

ANALYSIS OF THE RESULTS FROM THE BALLOON FLIGHTS

3.1   The balloon flights.

Neoprene expansible rubber balloons were used to lift the apparatus to altitude. In order that they would float at a constant pressure and to prevent bursting they were fitted with a hinged valve over the neck of the balloon which was controlled by a fixed length of tape running diametrically through the balloon so that its diameter was limited. Laby et al. (1957) have calculated the floating altitude to be reached by such a constant volume balloon to be given by the following formula:

$$P_2 = \frac{L_2}{d_a - d_h} \cdot \frac{T_1}{T_g} \cdot \frac{P_g}{V_h} - \frac{L_2}{L_1} \cdot P_e \qquad \dots\dots\dots 3.1$$

P_2 (gm./cm^2.) is the pressure at the floating altitude.

P_e (gm./cm^2.) is the excess pressure inside the balloon taken as 0.4 .

Pg (gm./cm^2.) is the pressure at S.T.P. taken as 1015.

d_a and d_h (gm./cm^3.) are the densities of air and hydrogen respectively at S.T.P. : $1.22 \cdot 10^{-3}$, $8.5 \cdot 10^{-5}$.

L_2 (gms) is the balloon weight + payload.

L_1 (gms) is the gross lift = freelift + L_2.

T_1 and T_g ($^{\circ}$K) are the external air temperature at altitude

(T_1 = 233° K), and the temperature at the ground on inflation (T_g = 270° K).

V_h (cm³.) is the maximum volume of the balloon assumed spherical.

Curves of pressure altitude P_2 against payload have been constructed on the basis of this formula, assuming the above figures for the variables, in Figure 3.1 . The balloon weight was 6.75 Kgm. These curves show that, for light payloads, high altitudes can be achieved which are actually higher than is attainable with the equivalent volume of polyethylene balloon. This is due to the generally larger volume to weight ratio of neoprene balloons when they are fully extended at altitude. Polyethylene balloons can however be made much larger and are obviously superior with heavy payloads. The payload in the present experiment was approximately 11 Kgm. and the actual altitudes achieved in some of the flights are shown with the respective tape length in Figure 3.1 . In general they fell below the theoretical altitude and for a few flights (not shown) the valves did not operate satisfactorily and caused hydrogen leakage at a considerably lower altitude. Pressure altitude versus local time profiles are shown in Figure 3.2 for the three flights which provided most data. In these flights the balloons were filled with sufficient hydrogen to give a free-lift of 10% - 15% of the gross lift which produced an ascent rate of nearly 1000 feet per minute, and the diameters were taped to 45 feet.

The balloons did not drift appreciably in geomagnetic
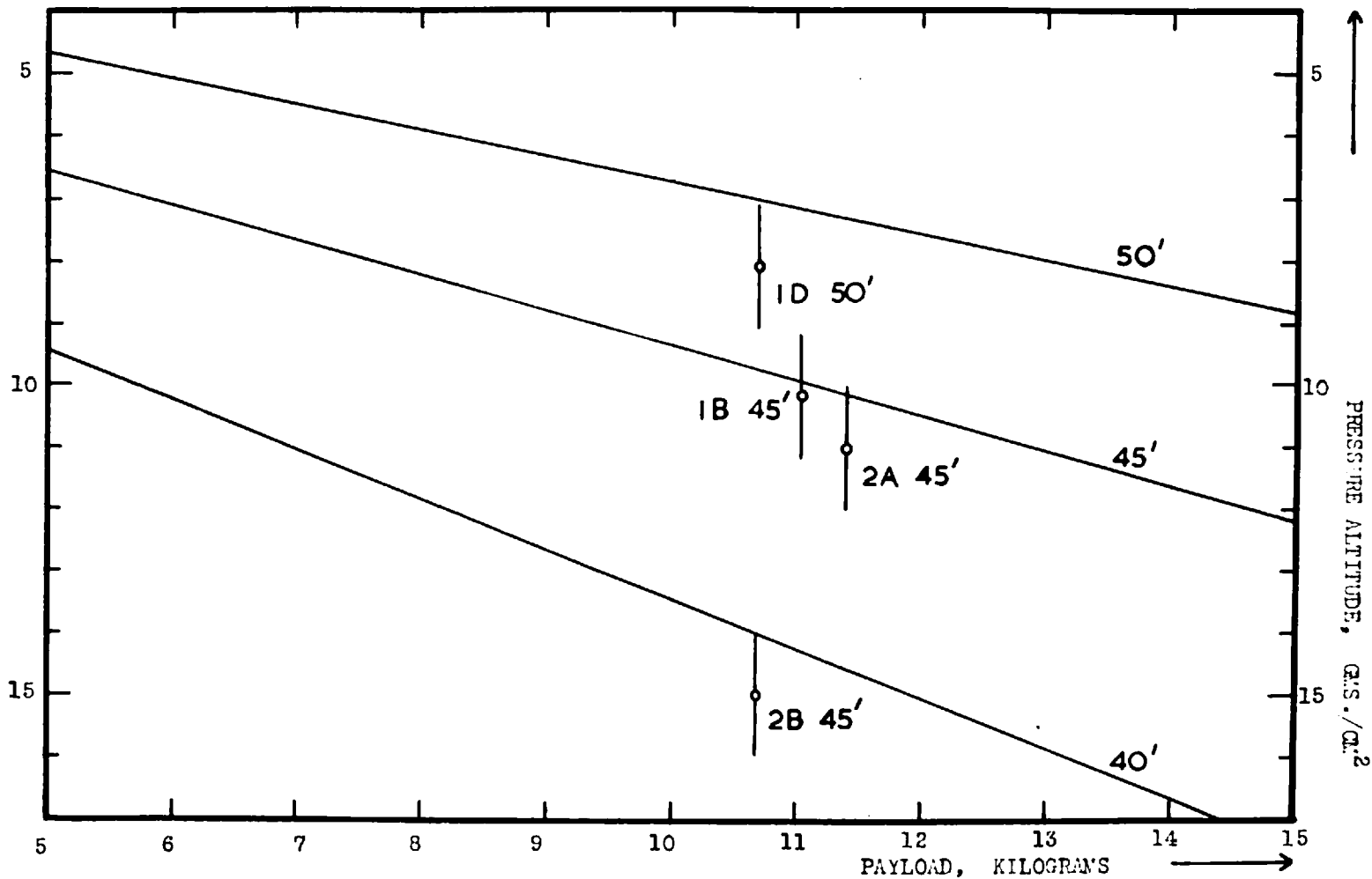
FIGURE 3.1   Theoretical altitude against payload for 6.75 Kg. valved neoprene balloon together with altitude attained for those flights reaching above 50gms./cm^2. as a function of tape length.
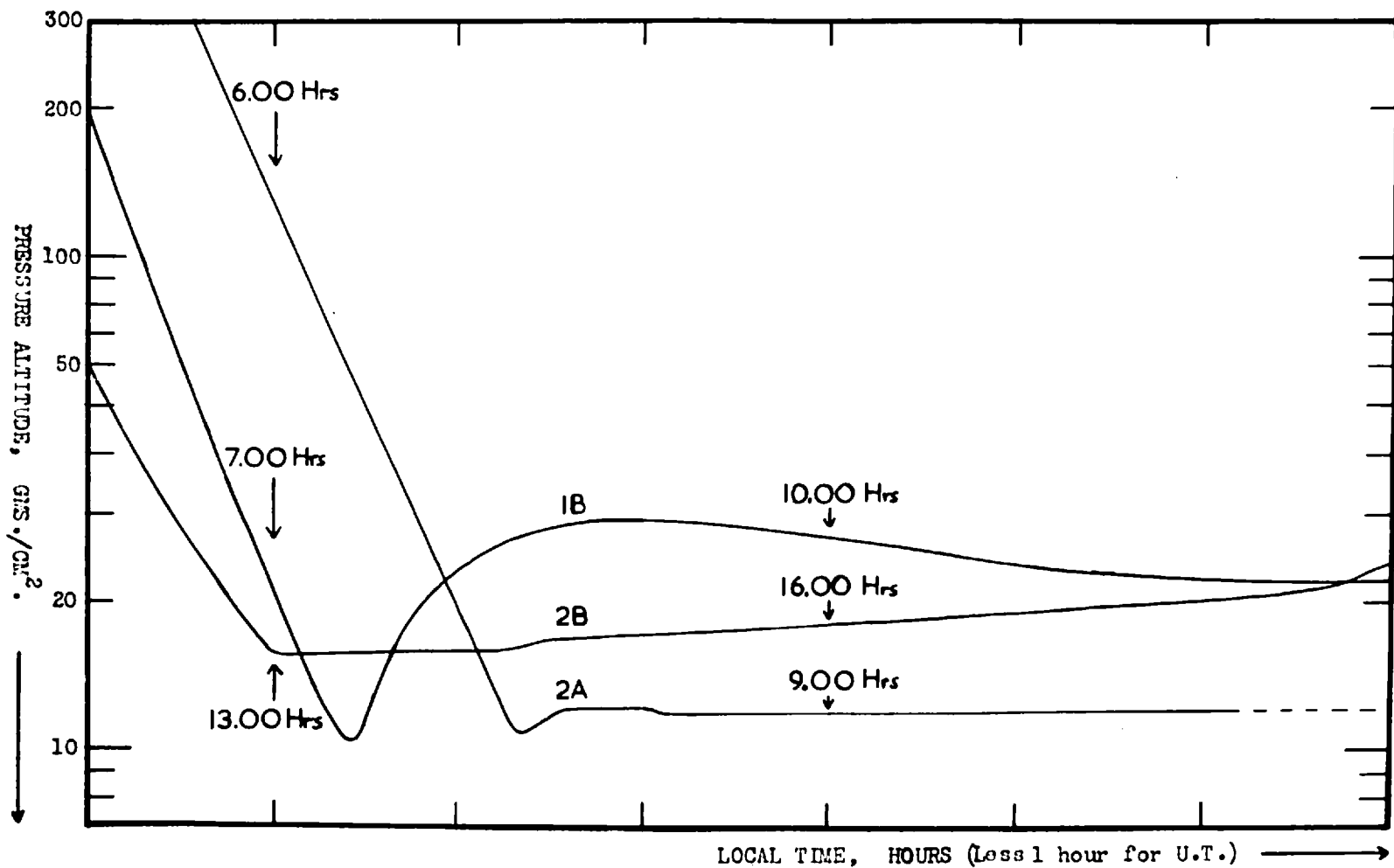
FIGURE 3.2   Pressure altitude against time for different flights.

latitude for the period of the flights during which data were

obtained.   Particulars of the balloon flights are given in the

following Table 3.1 .

<p align="center">TABLE 3.1</p>

Flight number	1B.	2A.	2B.
Date of flight	26.8.61	20.5.62	21.7.62
Launching site Geograph. coords. Geomag. coords. Threshold Rig.	Kiruna, Sweden. $67^{\circ}50'N,20^{\circ}26'E$ $64.6^{\circ}N, 115.9^{\circ}E$ 0.5 ± 0.05 Gv.	Bedford, Eng. $52.1^{\circ}N,4.5^{\circ}W$ $50^{\circ}N,79.2^{\circ}E$ 2.5 ± 0.1 Gv.	Kiruna, Sweden. $67^{\circ}50'N,20^{\circ}26'E$ $64.6^{\circ}N, 115.9^{\circ}E$ 0.5 ± 0.05 Gv.
No. of protons,	10,000	15,000	40,000
No. of alphas analysed at high altitude.	650	1,500	3,000

3.2   Raw data corrections - Introduction.

In the rest of this chapter the reduction of the raw data

will be discussed; this consists mainly of interpreting the

measured pulse height distribution for the two detectors in terms

of the energy spectrum of primary particles.

The Scintillator distribution is used to distinguish the

particle energies whereas the mixed C + S' detector enables some

resolution between α-particles and slow protons, the precise form of the response of this detector not being used in analysis as it is not so well defined. It is possible to normalize the theoretical pulse height distribution, based on the most probable response of the individual detectors, to the peaks in the experimentally observed pulse height distribution (Figure 2.2). In particular the positions of the lines of constant C + S' response give a check on the calibration of the electronics in flight, since for α-particles they are expected to be at pulse sizes four times those for protons. Each set of flight data is normalized to the theoretical distributions and thus the output corresponding to a minimum ionizing proton is determined which effectively calibrates the response in terms of energy or rigidity. Additionally to this calibration of most probable pulse size it is necessary to know the form of the statistical variations about this value for each particle rigidity in the scintillator.

The contributing factors have been summarized in Section 2.4 and those which depend most on the particle energy are the fluctuations in ionization loss and to a lesser extent the photo-electron statistics. As is well known a particle with a suitable impact parameter can lose a very large proportion of its kinetic energy to an electron and this gives rise to the 'Williams-Landau' tail of the energy loss distribution. The asymmetry is most pronounced for relativistic particles passing through a thin

absorber and was first treated theoretically by Landau (1944). A
fuller analysis covering a wide range of particle energies has
been carried out by Symon (1948) and his results have been used
to calculate the statistical variations at different energy losses
expected in the present detector, as well as the most probable
energy loss.

3.2a   Systematic corrections.

The raw data from tape playback must be corrected for the
following effects in order to obtain absolute intensities.

1)   Accidental coincidence between channels. This is given as
a percentage of the true coincidences by $\frac{2R_1 R_2 t}{R}$. 100 where
R_1 and R_2 are the individual counting rates of the two detectors,
'R' is the coincidence rate, and 't' is the resolving time of the
coincidence circuit, in this case 10 µsecs. Substituting typical
values gives less than 1% at the Pfotzer maximum.

2)   Accidental overlap in a single channel. This is given by
$100 R_1 t$ where R_1 is the individual channel rate and 't' is the gating
time, in this case 10 µsecs. It amounts to ⪅ 0.2% for the larger
detector.

3)   Due to the finite telemetry time, some coincident counts
are lost. However, because of the inhibiting gates in the circuitry,
the percentage losses are the same for all pulse sizes and the

correction factor can be accurately determined by counting the total number of subcarrier cycles transmitted in a fixed period.

4) Similarly, counts are lost in reducing the data to pulse height distributions during slow playback from the magnetic tape due to the printer dead time. These are estimated by measuring the total counting rate and the total number printed.

The first two effects can give rise to a small amount of background counts which have responses which do not necessarily lie within the theoretical distributions for single particles. Apart from being small however, where these counts do fall within the less densely populated part of the distribution corresponding to slow particles, they can be largely compensated for by the method used to correct for slow secondaries. (Section 3.2c)

It is preferable to apply the systematic correction factors 3) and 4) after determining the two dimensional distribution.

3.2b Statistical corrections.

Sea level μ-mesons provide a convenient source of relativistic singly charged particles that can be used to give a measure of the overall statistical variation in response at one particular energy loss. The pulse height distributions in the Scintillator at sea level have been normalized and plotted for the three detectors which produced most information at altitude in
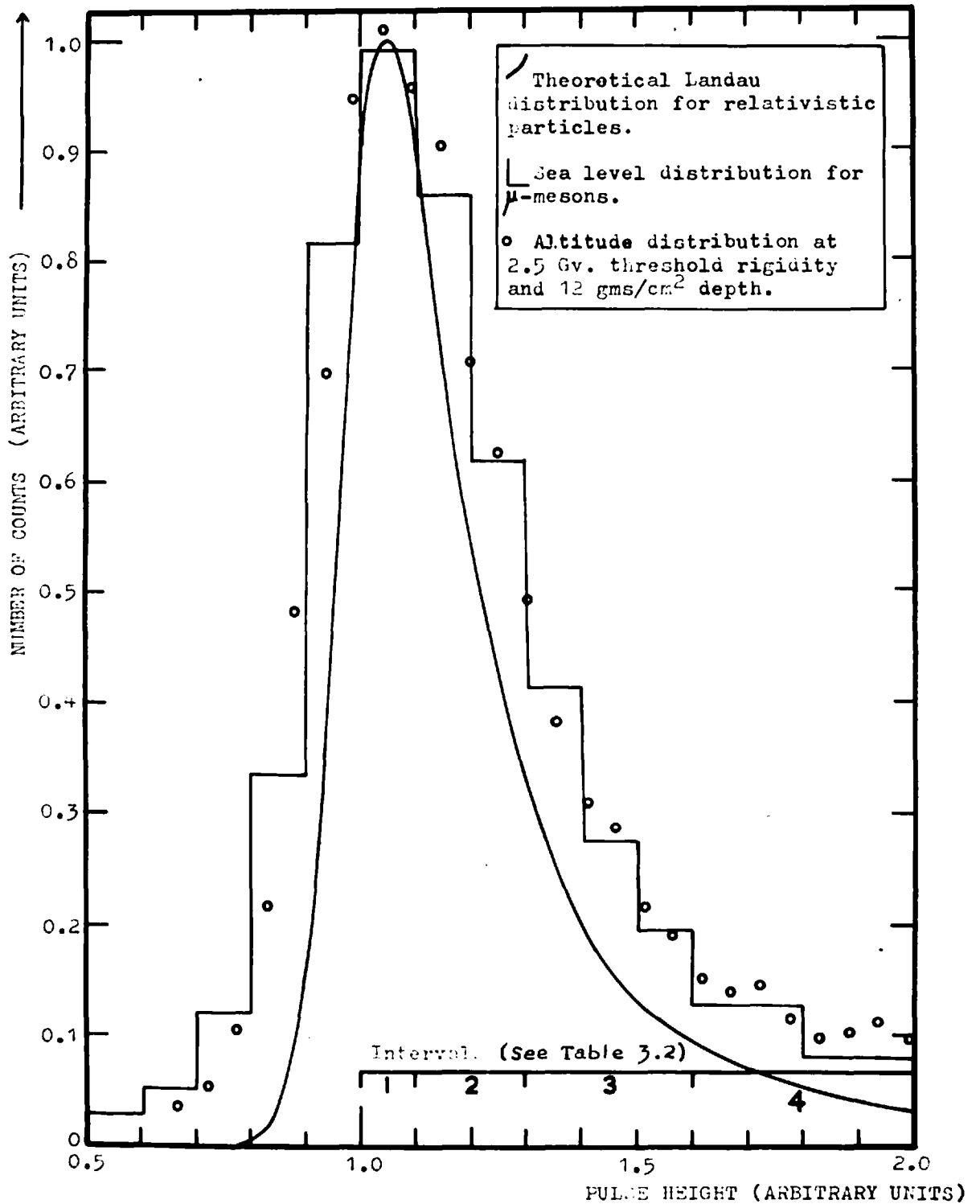
FIGURE 3.3   Scintillator pulse height distribution for relativistic singly charged particles.

figure 2.7 . The contribution to these curves from non-relativistic

protons is estimated to be less than 4% even at the larger energy

losses using the sea level proton spectrum of Mylroi and Wilson

(1951) and can therefore be neglected. Also the proportion of

electrons is made negligible by a suitable amount of absorber

above the telescope during laboratory calibrations.

These curves can be compared with both the theoretical

contributions due to the Landau effect and the distribution

obtained in a flight at altitude, where the threshold rigidity is

2.5 Gv. and the flux of particles is therefore predominantly

relativistic. These are shown in Figure 3.3 . The experimental

distributions are very similar, and considerably broader than the

Landau distribution due to the many additional contributing factors

mentioned in Section 2.4, these are however practically symmetrical

and will be independent of the value of the most probable response.

In order to facilitate the corrections for these

fluctuations, the relativistic meson distribution measured at sea

level has been converted to a block histogram by dividing it into

intervals of detector response which are fixed with respect to the

minimum ionizing response, **1.05 on this scale**, and correspond to

certain energy or rigidity intervals. Similar block histograms

were derived for particles with most probable responses lying in

the centre of other intervals by using theoretical distributions

derived from the results of Symon (1948), together with the further

empirically measured broadening. The figures which were derived

and are used in the statistical corrections are summarized in

Table 3.2 . These represent the percentage distributions of the

response for particles in each rigidity range, and when applied

to the true differential intensity spectrum they must give the

experimentally observed differential response distribution. Some

of the original intervals have been compounded in order to contain

comparable numbers of particles and minimize the statistical

uncertainties.

3.2c   Secondary particle corrections.

One of the main corrections to be applied other than

statistical fluctuations and geometry are due to secondaries.

These are of different types depending on their origin and in most

cases they are very hard to evaluate.

At balloon altitudes the earth's shadow effectively excludes

arrival of primaries or return albedo from beneath a vertical

telescope and the flux seen will contain a larger proportion of

primaries for narrower acceptance angles. The two main types of

secondaries in this case are a) first order splash albedo moving

upwards and b) those in the direction of the primaries, both first

order due to interactions, and second order which includes return

albedo from the opposite hemisphere and particles scattered from

TABLE 3.2

Interval.	< 1	1	2	3	4	5	6	7
Pulse height interval.	1.00	1.00-1.10	1.10-1.30	1.30-1.60	1.60-2.00	2.00-2.60	2.60-3.80	3.80-5.00
Rigidity interval at the detector, Gv.		>2.3	1.43-2.3	1.03-1.43	0.83-1.03	0.68-0.83	0.476-0.68	0.394-0.476
Energy interval at the detector Mev.		1540	800-1540	470-800	320-470	220-320	115-220	80-115
Rigidity interval above atmosphere for detector below 13gms/cm². Gv.		>2.3	1.46-2.3	1.07-1.46	0.88-1.07	0.75-0.88	0.61-0.75	0.57-0.61
Distribution of the true flux J(n) in n other intervals.	< 1	1	2	3	4	5	6	7
J(1)	24.2%	18.1%	26.9%	16.1%	7.5%	5.1%	2.1%	-
J(2)	7.5%	10.5%	30.7%	29.3%	13.2%	6.8%	2.0%	-
J(3)	0.6%	2.2%	12.6%	39.0%	30.0%	13.2%	2.4%	-
J(4)	-	0.1%	1.2%	11.6%	45.3%	34.0%	7.8%	-
J(5)	-	-	-	0.5%	10.9%	57.9%	30.7%	-
J(6)	-	-	-	-	-	7.6%	77.7%	14.7%
J(7)	-	-	-	-	-	-	7.0%	80.0%

trapped orbits. Interactions occur in both the atmosphere and in the detector to give rise to these secondaries. Type a) can be eliminated for various energies by a suitable design of detector having directional properties but other methods must be used to work out the contribution from b). The validity of the method adopted can be crucial to the evaluation of the primary flux and by introducing systematic errors possibly explains some of the disagreement in very low rigidity proton measurements, given in Figure 1.3 . The steeply rising secondary particle differential spectrum makes this problem more acute at low energies.

The first (S_1) or second (S_2) order secondaries can be broadly discriminated by their energies. At a specified latitude, in general the second order or return albedo secondaries will be below the geomagnetic threshold P, whereas the first order secondaries will be at all rigidities and will decrease with residual atmosphere towards zero at 0 gm./cm^2. Thus for two latitudes with thresholds P_1 and P_2 which are sufficiently close that the secondary production from primaries in the rigidity range $P_1 > P > P_2$ is negligible, the measured fluxes at a certain depth are: at P_1, $J(>P_1) + S_2(<P_1) + S_1$ 3.2
at P_2, $J(>P_2) + S_2(<P_2) + S_1$ 3.3

Here $J(>P)$ denotes the primary flux, galactic + solar, with rigidity greater than P. By extrapolation to 0 gm./cm^2. S_1 becomes zero, and for a rigidity resolving detector enables limits

to be set on $S_2(< P_2)$. By subtraction of the fluxes at the two latitudes, S_1 can be eliminated and the **primary flux in the region** $P_2 > P > P_1$ can be analysed. S_1, the secondary particle spectrum, can also be evaluated over the same rigidity limits. Primaries with rigidity $> P_2$ must be corrected for secondaries by extrapolation to the top of the atmosphere.

Another way of estimating the intensity of the return albedo secondaries (S_2) is by measuring the isotopic abundance of the hydrogen components at different depths and taking reasonable values for their relative occurrence among the first order secondaries, derived in turn from interactions of cosmic rays in emulsions or from controlled laboratory experiments. It is difficult to calculate the fluxes of first order secondaries from the results of other experiments due to the dependence on the material and configuration of the detector employed. This is apparent from the few instances shown in Figure 3.4 .

The intensity of return albedo has been estimated as negligible compared with the first order secondary flux at rigidities around 400 Mv. by measurements of the isotopic abundance of H_2 and H_3 (Brunstein, 1963). At higher rigidities, in the range from approximately 450 to 850 Mv. the flux of splash + return albedo at the top of the atmosphere has been measured as of the order 35 ± 10 particles / m^2. sec. steradian. Since the long term average of the return albedo near the vertical is

unlikely to be greater than the splash albedo at high latitudes;
this would suggest an upper limit of 0.04 particles / m^2. sec.
ster. Mv. in this range, based on the data of McDonald and Webber
(1959). The fast splash albedo with kinetic energy greater than
the rest energy has been measured by Anderson (1955) and McDonald
and Webber (1959) at balloon altitudes using cerenkov detectors
from which it may be concluded that at high latitude this flux at
0 gm./cm^2. is approximately 5 to 8% of the primary flux exceeding
the same energy. It was not possible to separate the fast splash
albedo peak in the present experiment in view of its relatively
low intensity at altitude, lying at 50% of the fast primary peak.
By using the subtraction procedure in making corrections, any
return albedo flux at the lower latitude will also be subtracted
from the high latitude intensity, and will therefore lead to a
positive systematic correction to the primary spectrum. In view
of the above figures however, it is not likely to be greater than
10% of the primary flux.

In order to obtain a measure of the intensities of
secondary particles produced in the residual atmosphere above the
telescope and in the telescope itself, control flights were made
at a latitude sufficiently low that the primary particles, other
than return albedo, were relativistic. It was convenient to make
these flights from R.A.F. Cardington, Bedford, where the limiting
primary rigidity 2.5 Gv. corresponded closely with the limit of

pulse height resolution of the detector, 2.3 ± 0.3 Gv. Thus, by

measuring the energy spectrum for such flights the secondary

particle spectrum at altitude can be determined below 2.3 Gv. and

will also include splash albedo particles as these were not

separated by the detector in this rigidity range. Such a spectrum

was derived from flight 2A. The pulse height distribution at

12 gm./cm^2. was converted into block histogram form, and by using

the statistical corrections in Table 3.2 and a succession of

approximations, the flux in the various rigidity intervals was

calculated in order to obtain the best solution for the relativistic

flux in interval 1). Since this is large compared with that in

the other intervals, the contributions to the responses appearing

in intervals 2) to 7) were subtracted out, then these intervals

were separately corrected for statistical fluctuations. The

intensities so derived, given in Table 3.3b, have been converted

to a differential energy spectrum at 12 gm./cm^2. depth using the

30 minute counting rates and assuming all the singly charged

particles to be protons. The spectrum is shown in Figure 3.4 .

This largely represents the secondary particle spectrum

but includes a small percentage of accidental background and

shower events which are characteristic of the detector used. Any

multiple particle events being detected with the telescope will

tend to give rise to an increase in the slope of the spectrum,

whereas the presence of mesons will enhance the counts at the high

TABLES 3.3a & 3.3b

Singly charged particle counts reduced to 30 minute rate.

Flight 2B	Observed raw counts corrected for those from interval 1)		Mean counts, and in brackets the uncorrected value	Counts corrected for fluctuations in pulse height
Depth gm./cm.^{2}	15.5	20.5	18	18
Interval				
1)	10440 ±190	10880 ±275		10660 ± 166
2)	702 ± 43	**718 ± 62**	710 ± 38 (705)	2000 ± 124
3)	908 ± 37	884 ± 51	896 ± 32 (907)	660 ± 107
4)	781 ± 28	730 ± 41	755 ± 25 (748)	550 ± 55
5)	685 ± 26	610 ± 35	647 ± 22 (672)	340 ± 38
6)	900 ± 24	1008 ± 36	954 ± 22 (922)	870 ± 28
7)	500 ± 19	620 ± 23	560 ± 16 (560)	505 ± 20
	Errors are statistical only.			

	Mean counts, and in brackets the uncorrected value		Counts corrected for statistics and Landau fluctuations		
Flight	1B		1B	2A	2B
Depth gm./cm.	12		12	12	12
Interval					
<1)	1780 ± 47	(1752)			
1)	1335 ± 41	(1359)	6970 ± 225	8000 ± 180	9680 ± 160
2)	2205 ± 53	(2192)	890 ± 175	178 ± 75	2020 ± 125
3)	1530 ± 44	(1550)	300 ± 115	112 ± 50	648 ± 110
4)	989 ± 35	(949)	440 ± 75	141 ± 50	507 ± 60
5)	731 ± 30	(747)	195 ± 50	93 ± 30	310 ± 40
6)	680 ± 29	(661)	510 ± 40	415 ± 25	704 ± 35
7)	322 ± 17	(322)	290 ± 20	303 ± 30	377 ± 25
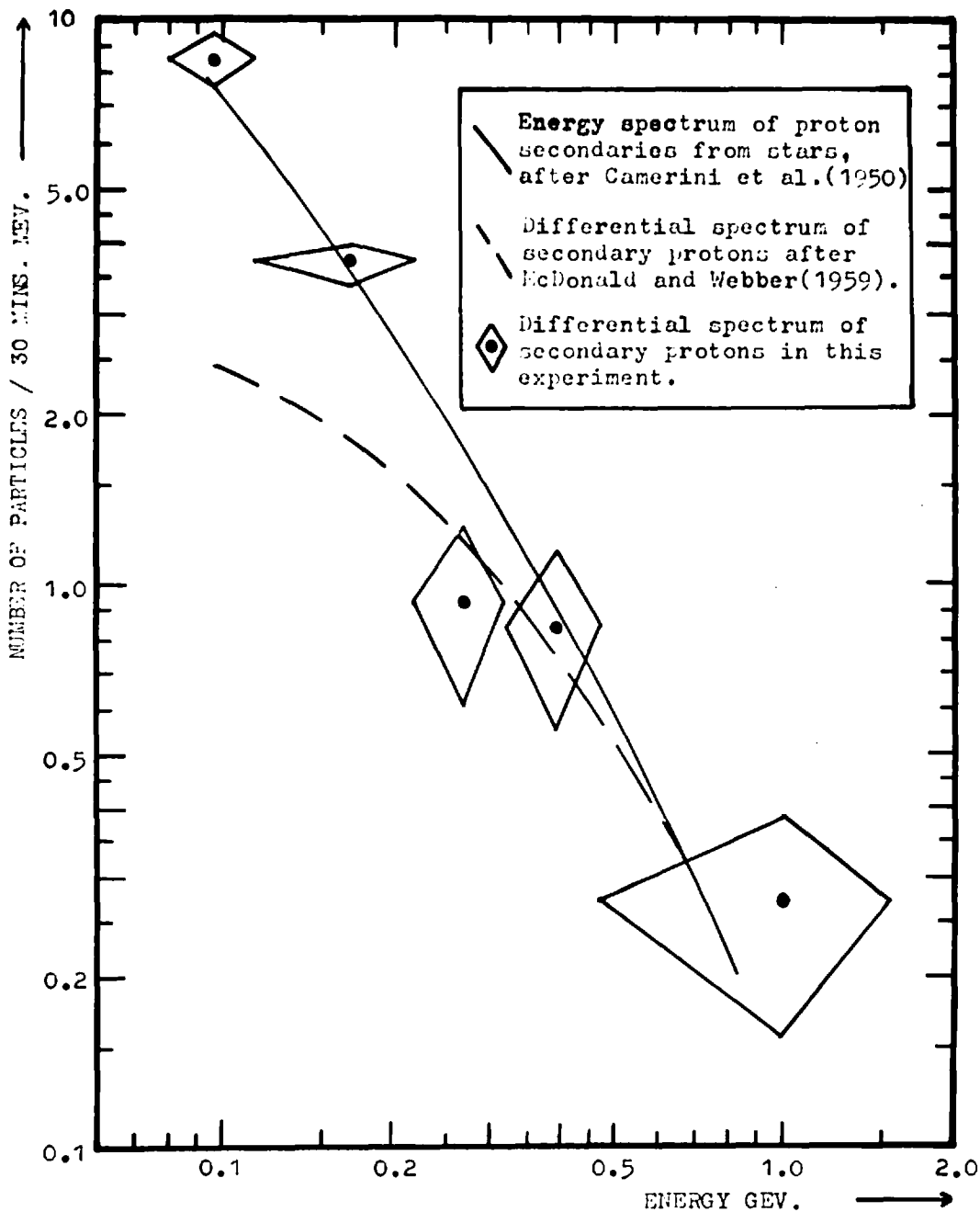
FIGURE 3.4   Differential spectrum of singly charged
secondary particles at 12 gms / cm² depth,
assumed to be protons. The curves have
been normalized at 0.7 Gev.

energy intervals. On the same plot is shown the secondary proton
spectrum from showers produced in emulsions as given by Camerini
et al. (1950). The close agreement is consistent with the
detection of secondary protons produced in the overlying atmosphere
which have become sufficiently scattered to be recorded as single
particle events in the telescope. A small proportion of multiple
events produced in the telescope material tends to increase the
apparent low energy flux since the response is enhanced compared
to a single particle. The differential energy spectrum of
secondary slow protons obtained in the balloon flights of McDonald
and Webber (1959) is also shown and both this and the spectrum of
Camerini are normalized to the present results at 700 Mev. It is
likely that with the greater amount of material, 8 gm./cm^2. in
McDonald and Webber's detector, the slower particles are not so
efficiently detected. In addition the slow particles are more
likely to have originated from a multiple star and therefore be
preferentially excluded by their multiple particle detector system.
These considerations probably account for the apparent difference
in slope at lower energies. The experimentally derived secondary
particle distribution is used as the basis for the corrections
for non-primary counts in the high latitude flights.

3.3   Derivation of the primary proton spectrum.

The secondary particle spectrum is expected to be similar
at a given altitude for flights at different latitudes from the
results of McDonald and Webber (1959). This is also a consequence
of the fact that the energy distribution of secondary particles
from stars is independent of the initiating particle energy down
to 1 Gev. and also that the multiplicity of stars decreases
appreciably for primary particle energies below this value
(Camerini et al., 1951). To a first approximation the secondary
particle spectrum can therefore be scaled up in proportion to the
number of primaries with energy greater than 1.5 Gev. The
validity of this treatment is supported by the following results.

The flux of slow protons below 80 Mev. down to the
instrument cut-off of 30 Mev. can be determined, although in view
of the slow proton and α-particle overlap the energies are not
sufficiently well defined to deduce a detailed spectrum in this
range. These particles can be considered to be entirely secondaries
even for flights with the low theoretical threshold rigidity
corresponding to 120 Mev. The ratios of this flux at 12 gm./cm^2.
to the relativistic primary flux for the different flights are
equal within the statistical errors of 6%. This result also
provides a check on the normalization of the rigidity intervals
applied to each flight, and on the slow proton separation from

α-particles carried out in the analysis.

Data were obtained in two flights at high latitude for which the altitude versus time curves are given in Figure 3.2 and the total particle intensity versus atmospheric depth curves in . Figure 3.6a. These are numbered 1B and 2B respectively for 1961 and 1962 and, although the later flight only reached a maximum altitude of 15 gm./cm^2., the flight profile can be used to give useful data at two different altitudes. The two lower latitude flights 1A and.2A for the same years gave the total raw intensities shown in Figure 3.6b, in which the earlier flight is limited owing to an electronic fault. It can be seen from Figures 3.6a and 3.6b that a significant increase in flux occurred between the two years. The two dimensional pulse height distributions are used to obtain the fluxes of particles occuring in the various intervals of pulse height defined in Table 3.2.. These fluxes are then solved by using the statistical variations in the Table, and the contribution to pulses in the various intervals due to relativistic particles in interval 1) are subtracted out. The raw data obtained in this way for the average altitudes 15.5 and 20.5 gm./cm^2. in flight 2B are given in Table 3.3a. Since the statistical errors do not justify a direct extrapolation to the normalizing depth of 12 gm./cm^2. the fluxes are averaged to obtain the raw data applicable at 18 gm./cm^2. The statistical and Landau corrections are then applied by the method of successive approximate solutions to obtain the

true fluxes in the various intervals. The experimental pulse
height distribution to be expected from these fluxes ~~are~~ is compared
with the actually observed distribution in the table as a check
on statistical corrections.

To evaluate the change in flux over the atmospheric depth,
12 to 18 gm./cm²., for the different intervals a semi-theoretical
method is considered more reliable than extrapolation of the
intensities obtained during the ascent of the balloon. Over a
small depth of atmosphere such that the change in particle range
is negligible, the change in flux can be represented by the
following equation if the splash albedo is neglected.

$$dJ(n)/dx \; = \; -J(n)/D + \overset{m \leqslant n}{\underset{}{\sum}} P_{mn} \cdot J(m)/D \qquad \ldots\ldots\ldots \; 3.4$$

J(n) is the flux in a rigidity interval n, x is the
atmospheric depth in gm./cm². and D is the absorption mean free path
taken as 120 gm./cm². over this rigidity range (Dymond, 1954).
$\overset{m \leqslant n}{\underset{}{\sum}} P_{mn} \cdot J(m)$ represents the production of flux in interval n by
interactions of flux J(m) and can be considered to be $P_{1n} \cdot J(1)$
as the multiplicity P_{mn} and the flux J(m) decrease rapidly with
rigidity. Over small depths such that $x < D$, the solution may be
approximated to:

$$J_{x2}(n) - J_{x1}(n) \; = \; P_{1n} \cdot J_{x1}(1) - J_{x1}(n) \cdot \cdot \frac{x2 - x1}{D} \qquad 3.5$$

$J_{x1}(n)$ can be calculated since $J_{x2}(n)$ is known, taking x1 = 12

and x2 = 18, also P_{1n} can be evaluated from the secondary particle measurements in intervals 'n' and the relativistic fluxes in interval 1). The results of such a calculated extrapolation for intervals 6) and 7) are shown as crosses on the intensity against depth curves for flight 1B in Figure 3.5 which are for similar rigidities. The good agreement over the depth 18 to 12 gm./cm.^{2} appears to justify such a method of extrapolation for a small change of depth. Therefore the counts for flight 2B have been corrected to 12 gm./cm.^{2} in this way. The results for all the flights at this depth are given in Table 3.3b and are corrected to the top of the atmosphere by the following procedures.

The raw intensities for the three flights are plotted as a function of pressure depth on a log.-linear scale in Figure 3.7 and they are well represented by straight lines at high altitude. The data for flight 2A (threshold 2.5 Gv.) are extrapolated from 12 gm./cm.^{2} to the top of the atmosphere including the telescope material of 1 gm./cm.^{2} air equivalent. Within 10% the production of secondary singly charged particles is counteracted by the absorption of α-particles and so this change in intensity is used as an extrapolation factor for the relativistic interval 1) > 2.3 Gv. The estimated fast splash albedo is then subtracted from the derived flux (Section 3.2c).

The lower rigidity intervals 2) to 7) are corrected first for secondary particles, interactions and splash albedo by

Intensity of protons in the range 120 - 200 Mev.
0.5 - 0.65 Mv.

Intensity of protons in the range 80 - 120 Mev.
0.4 - 0.5 Mv.

Integral intensity of α-particles as a function of atmospheric depth.

Theoretical depth dependence fitted to the experimental data. (See Appendix E).

PARTICLES / M² SEC. STERADIAN.

ATMOSPHERIC DEPTH GMS/CM²
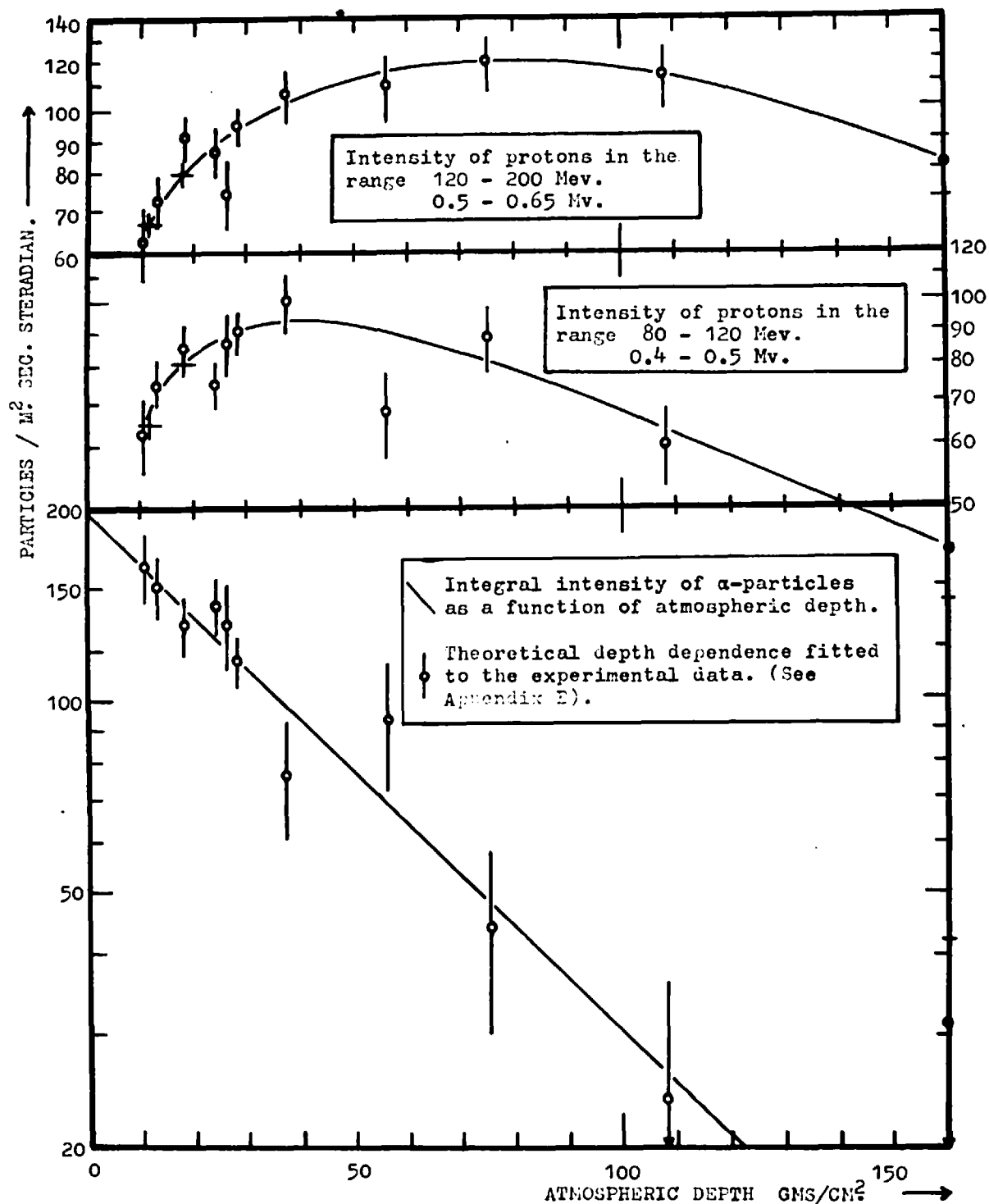
FIGURE 3.5   Particle fluxes during the ascent of flight 1B.
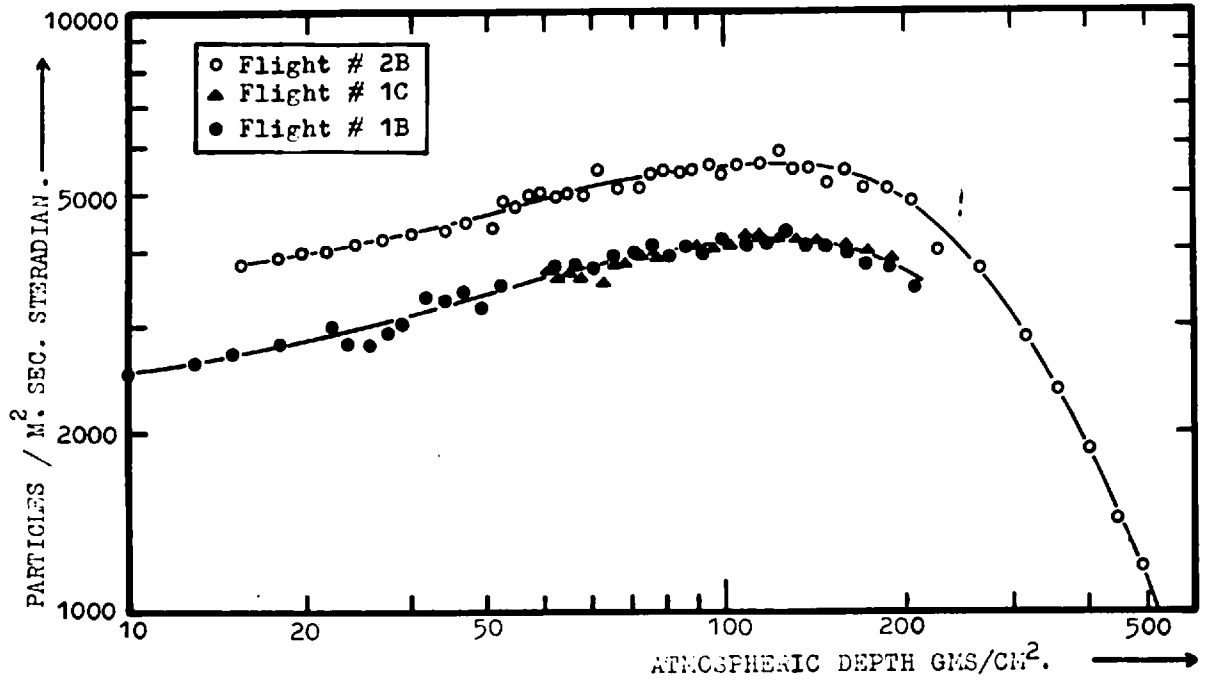
FIGURE 3.6a   Total raw intensity against atmospheric depth at 65° N.
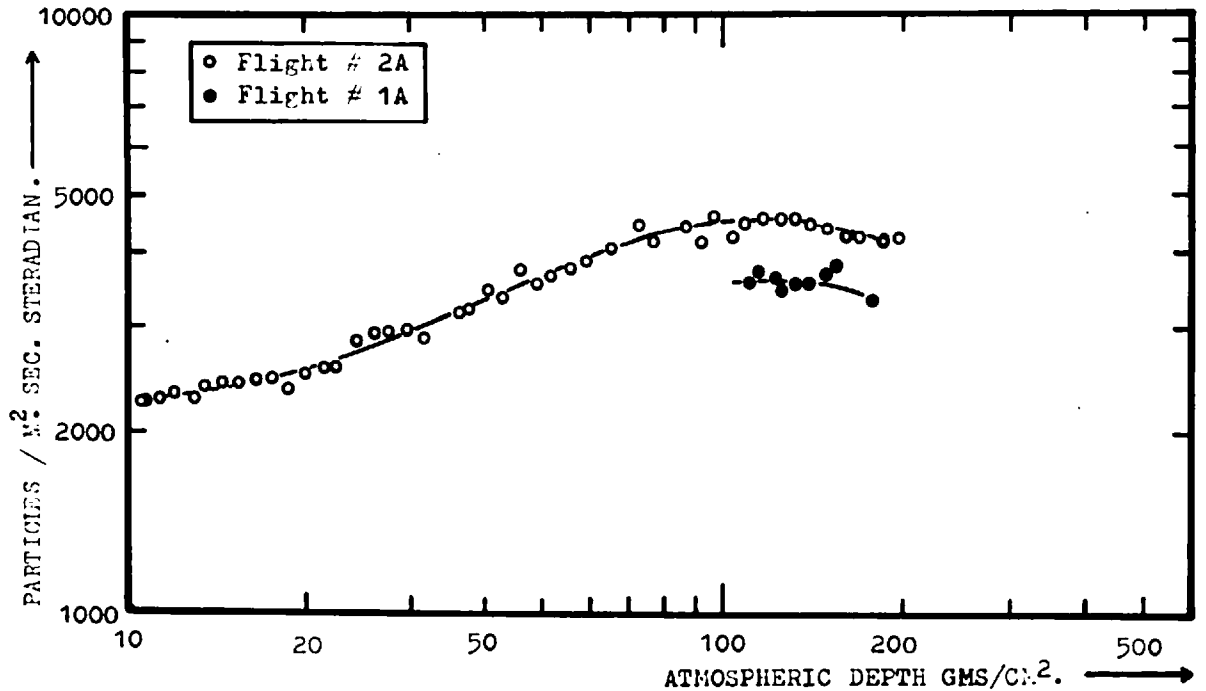
FIGURE 3.6b   Total raw intensity against atmospheric depth at 52° N.
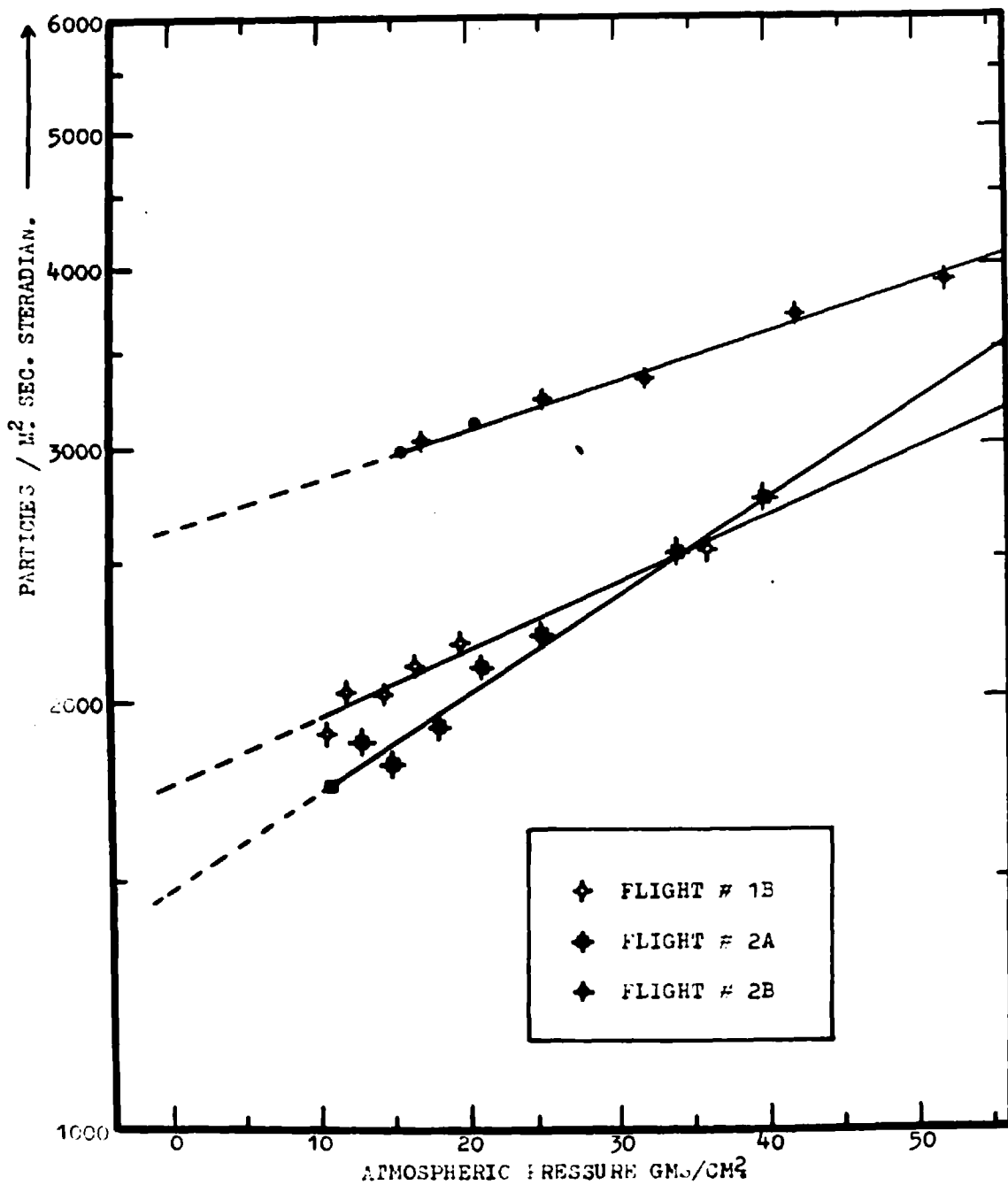
FIGURE 3.7   Total raw intensity against atmospheric depth for
different flights.

FIGURE 3.8   Pulse height distribution in the mixed detector for fixed scintillator response corresponding to different intervals of α-particle rigidity at 12 gms./cm^2 atmospheric depth.

α-Particles with rigidity between 1.85 and 2.8 Gv.

α-particles with rigidity between 1.5 and 1.85 Gv.

α-particles with rigidity > 2.8 Gv.

NUMBER OF COUNTS (ARBITRARY UNITS)

FIGURE 3.8

RESPONSE IN THE MIXED DETECTOR (ARBITRARY UNITS)
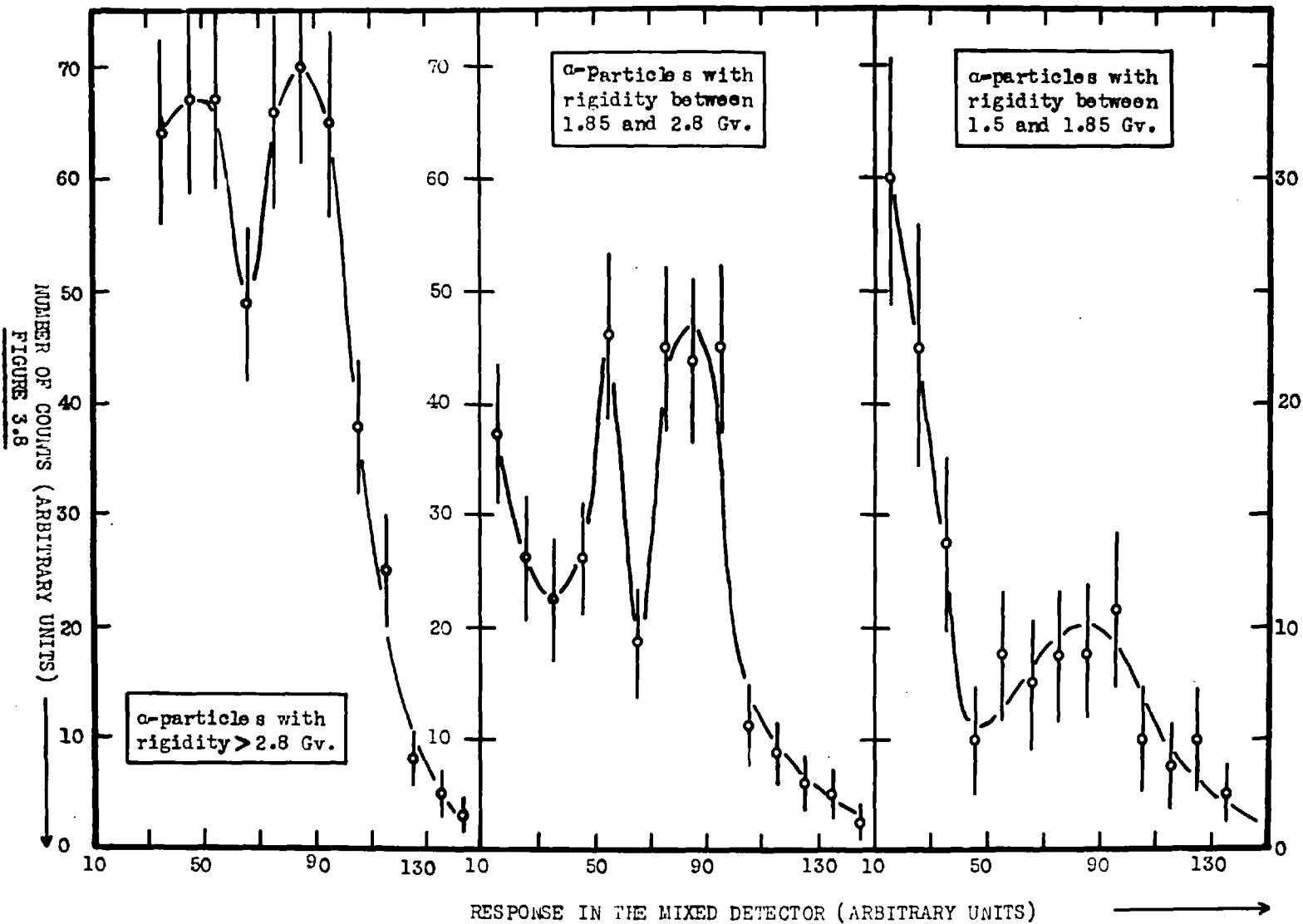
subtracting the contributions at 12 gm./cm^2 which are obtained by the scaling-up method previously discussed in this section. The theory of this procedure is treated in Section 3.2c. Finally the counts obtained (Table 3.4) are converted to a primary flux by using an absorption mean free path of 120 gm./cm^2 over the residual altitude (Dymond, 1954; Brooke, 1963), and using the isotropic geometry factor for the telescope (Appendix A). These final results for the singly charged particles are given in Table 3.5 together with the respective rigidity intervals at zero depth assuming that all the particles are protons. The errors in the rigidity intervals are those which result from a 2% uncertainty in the normalization of the minimum ionizing response.

3.4   Derivation of the α-particle fluxes.

Figure 3.8 shows pulse height distributions in the C + S' detector for selected intervals of scintillator response at the higher α-particle rigidities. The peak corresponding to fast α-particles is resolved, although the secondary slow protons are sufficiently numerous to limit any detailed measurement of the differential α-particle spectrum. Protons above 0.4 Gv. are free from this region of confusion and two intervals of low rigidity protons are plotted as a function of pressure depth in Figure 3.5 . Also shown is the integral α-particle intensity at different depths

Fully corrected primary proton counts in 30 minutes at 12 gr./cm²

Pulse height interval	Date of flight / Rigidity Gv.	1B 26.8.61	2A 20.5.62	2B 21.7.62
1)	>2.3	6970 ± 225	8000 ± 180	9680 ± 160
2)	1.43 -2.3	735 ± 190		1804 ± 155
3)	1.03 -1.43	203 ± 120		512 ± 125
4)	0.83 -1.03	317 ± 90		337 ± 85
5)	0.68 -0.83	114 ± 60		198 ± 60
6)	0.476-0.68	149 ± 45		202 ± 50
7)	0.394-0.476	26 ± 33		10 ± 45
			Errors are statistical only.	

TABLE 3.4

Summary of proton fluxes above the atmosphere.

Rigidity interval Gv.	Integral fluxes			Differential fluxes	
	26.8.61	20.5.62	21.7.62	26.8.61	21.7.62
>2.3	1120 ±160	1300 ±165	1500 ±175		
1.46-2.3	176 ± 46		416 ± 36	0.21 ±0.07	0.49 ±0.11
1.07-1.46	48 ± 29		118 ± 29	0.125 ±0.08	0.30 ±0.08
0.88-1.07	76 ± 21		78 ± 20	0.40 ±0.10	0.41 ±0.10
0.75-0.88	28 ± 14		45 ± 13	0.21 ±0.12	0.35 ±0.11
0.61-0.75	35 ± 11		48 ± 11	0.25 ±0.08	0.34 ±0.08
0.57-0.61	6 ± 8		3 ± 10	0.15 ±0.20	0.08 ±0.25
Errors are 20% >1.46 5% <1.46	Errors are statistical only except > 2.3 Gv. which has an extrapolation error ~ 10%.			Errors include rigidity interval uncertainties.	

TABLE 3.5

which was obtained during the balloon ascent. In order to allow
for the slow proton background in the α-particle region, this
background is taken to have the same depth dependence as the 0.4
to 0.5 Gv. proton interval. By normalizing the background intensity
at the 12 gm./cm^2 depth where it amounts to 20%, the contribution
is evaluated and subtracted for different depths. A theoretical
relation for the variation of α-particle intensity with depth has
been calculated in Appendix B and is normalized to the experimental
points in Figure 3.5 . This is derived from the solution to the
diffusion equation using available data for the fragmentation
parameters, absorption mean free paths, and primary fluxes for
particles with rigidities greater than 4.5 Gv. The values used
are given in Appendix B. The apparent mean free path obtained in
this way is a good fit to the experimental data although the
observed flux includes α-particles down to 1.0 Gv. This result is
in accordance with the observation that the interaction mean free
path of α-particles is independent of energy (Jain et al., 1959).
However the apparent mean free path is neither very sensitive to the
values of the fragmentation parameters nor ^{to} a slight energy dependence
of the interaction mean free path. Therefore, in spite of recent
conclusions contrary to Jain et al. (Evans and Hillier, 1961)
all the experimental α-particle fluxes have been extrapolated to
the top of the atmosphere using the apparent mean free path of
55 gm./cm^2. In addition, all Helium nuclei are taken to be

α-particles of mass 4. This is considered justified since the number of secondary Helium nuclei amounts to only about 10% at 12 gm./cm^2 although they probably include a high proportion of He$_3$ from the results of Yasin (1963). The generally accepted ratio of He$_3$ in the primary flux of He$_3$ + He$_4$ is of the order 10% and will therefore make very little difference to the evaluation of the integral α-particle flux. However, with 1.0 to 1.5 Gv., from Figure 1.1, He$_4$ in this interval produces the same response in a thin scintillator as He$_3$ in the interval 0.75 to 1.15 Gv., so for a rigorous measurement of the rigidity spectrum the isotopes must be resolved, although this has not been possible here.

In spite of the slow proton overlap in the fast α-particle region of the two dimensional pulse height distribution, the minimum response of the scintillator at 12 gm./cm^2 depth is nearly 2.5 times that of a minimum ionizing alpha for a primary α-particle in the rigidity range below 1.5 Gv. It is only protons in the region 240 to 270 Mv. which can give a confusing response and a very large proportion of these are expected to be secondaries at both latitudes of measurement. This can be seen from reference to the figures in Table 3.4 for interval 7) which show a very small flux of primaries at these low rigidities. If ionization losses by α-particles in the residual atmosphere and detector are allowed for, the region of response for primary α-particles between 1.0 and 1.5 Gv. can be determined. The fluxes in this interval

are evaluated for the three flights and the systematic corrections are applied.

There is good reason for assuming the rigidity spectrum of heavy nuclei to be the same as that of α-particles from the investigations referred to in Section 1.2 . Therefore under an evaporation process for the fragmentation of heavy particles (Kaplon, 1952) secondary α-particles will conserve the same energy per nucleon. In view of this, and since the proportion of fragmentation alphas is less than 10% at 12 gm./cm^2, the same altitude extrapolation is carried out as for the integral intensity using an apparent mean free path of 55 gm./cm^2. The number of α-particles reduced to 30 minute counts for the interval 1.0 to 1.5 Gv. are given in Table 3.6 together with the final fluxes. It can be seen that the background intensity is relatively small from the lower latitude flight where primaries were absent. This background is scaled up in proportion to the fast proton intensities, in a similar manner to that for the secondary proton corrections, and is subtracted from the high latitude fluxes prior to the final extrapolation to the top of the atmosphere. All the measured α-particle fluxes are summarized in Table 3.6 .

3.5 Derivation of the flux of Light, Medium and Heavy nuclei.

Although the experiment has been designed to measure

Alpha particle results from the present experiments.

Integral fluxes in units of particles/m^2 sec. steradian.				
Flight number.	1B	2A	2B	2B
Pressure, gm./cm^2.	12.0	12.0	15.5	20.5
Number of particles * per 30 minutes.	621 ± 25	480 ± 12	630 ± 15	612 ± 14
Isotropic geometry factor, cm^2 ster.	25.5	25.5	26.6	
Corrected integral primary flux.	199 ± 16	155 ± 10	253 ± 12	
Rigidity limit, Gv.	1.0	2.5	1.0	

* Errors are statistical only, excluding proton correction.

Low rigidity alpha flux, particles/m^2 sec. steradian				
Flight number.	1B	2A	2B	Rig. interval
Number of particles in 30 minutes at 12 gm./cm^2.	59 ± 14	18 ± 5	109 ± 20	0 to 1.38 Gv.
Number of alphas with background subtracted.	43 ± 15	0	86 ± 21	
Primary flux.	12 ± 4	0	23 ± 5	1.0 to 1.5Gv.

TABLE 3.6

Results from the present experiments on particles with Z > 2.

Total integral fluxes of Light, Medium and Heavy nuclei, particles/m^2 sec. steradian.				
Flight number.	1B	2A	2B	Rig. limit Gv.
Pressure, gm./cm^2.	12	12	15.5	
Number of particles in 30 minutes.	55 ± 8	48 ± 5	78 ± 12	0
Integral primary flux.	17.3 ± 2.6	14.3 ± 1.5	25.0 ± 4.0	1.0

TABLE 3.7

proton and α-particle fluxes, it has been possible to resolve the heavier particles on the non-linear region of the electronics, (Figure 2.9), although the statistics do not justify a subdivision into the groups, Light, Medium and Heavy. The two dimensional distribution is used to discriminate these particles and the data are corrected for systematic losses due to finite telemetry and printout time before converting to a flux at the depth of investigation.

It is rather difficult to make an extrapolation of such a large group of particles without knowledge of their relative abundances, in view of their different mean free paths. The results of Waddington (1960) are used to obtain an average mean free path as an approximation. The Light, Medium and Heavy interaction mean free paths are weighted by their relative abundances and averaged, giving 25 gm./cm^2., and the corresponding fragmentation parameter is 0.30 . Thus the apparent mean free path is taken as 36 gm./cm^2. The fluxes are extrapolated to the top of the atmosphere using this value and including the telescope material of 1 gm./cm^2. The results obtained in this way are summarized in Table 3.7 .

CHAPTER 4

DISCUSSION OF THE RESULTS

4.1   The integral flux of protons above the atmosphere.

All the flights reported here were made at times when sea
level neutron intensities were at comparatively steady values.
The two-hourly mean rates for the Mount Washington monitor are
plotted for the relevant months together with the daily numbers of
class 2 flares in Figure 4.1 . There were no class 3 flares within
at least 20 days prior to the flights and there was no evidence of

riometer events. It might be mentioned however that the period in
August 1961 was at the end of recovery from the large Forbush
decrease of July 1961. The general level of intensity was
equivalent to that midway between the solar minimum of 1954 and
the following solar maximum. This occurred as a rapid transition in
late 1957, and was a period during which no balloon flights have
been reported giving data on primary protons and α-particles.
The long term variation in neutron intensity is shown in Figure 4.4 .

The integral primary intensities of protons above 0.88 Gv.
which have been obtained in the present experiment are tabulated
together with other measurements above a similar low rigidity limit
in Table 4.1 . These have all been obtained with counters. The
values have been plotted in Figure 4.2 against the two-hourly mean
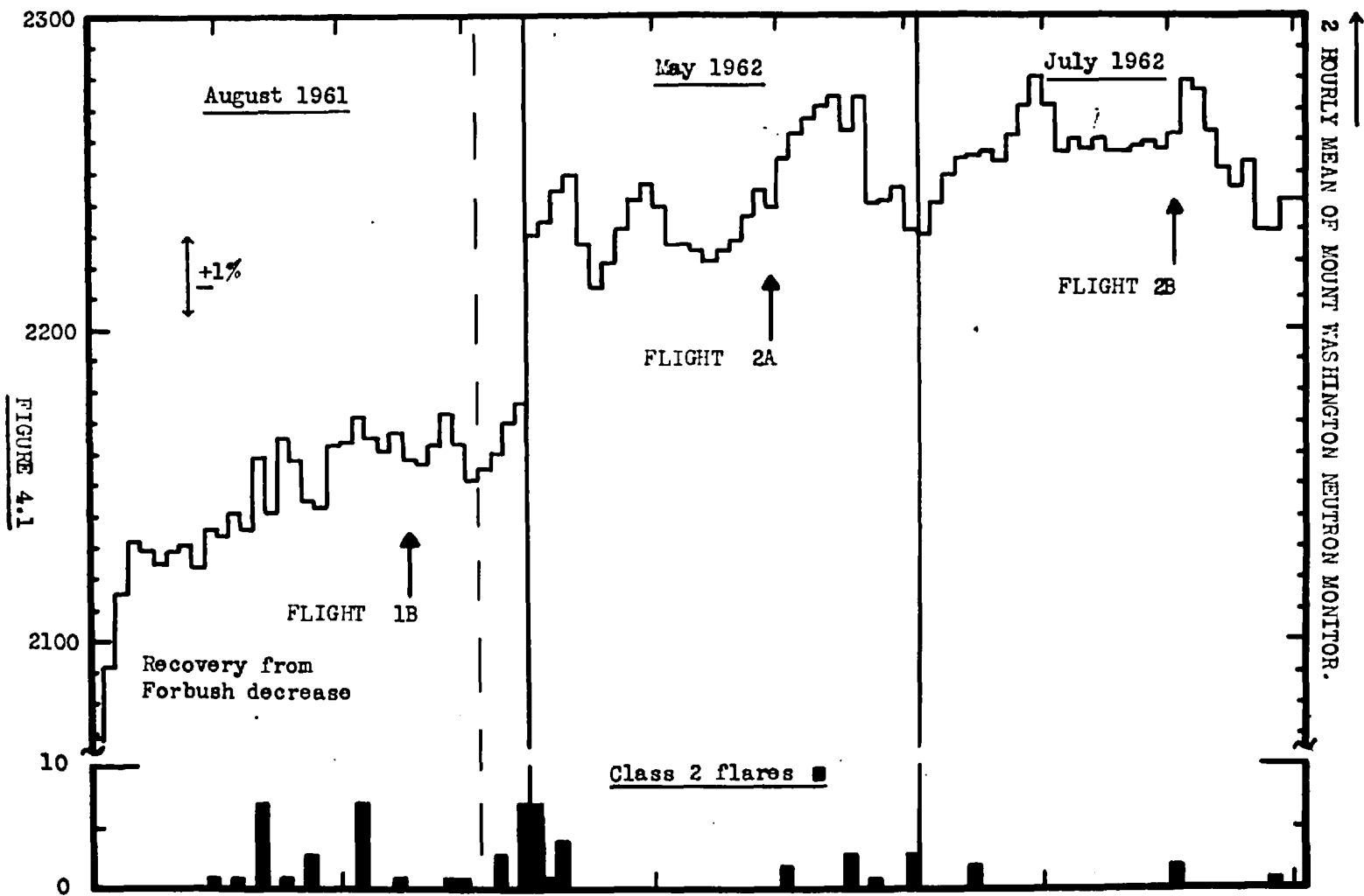
FIGURE 4.1   Two-hourly means of the Mount Washington neutron monitor during the months of the flights and daily numbers of flares of class 2 or greater.

Integral proton fluxes above low rigidity

Date of flight	Geomag lat.	Lower rig. limit Gv.	Integral flux parts./m^2 sec.ster.		Mount Wash.	Reference		
7.9.56	59°N	1.0	2146 ±	75	2340	Webber	(1962)	1
16.2.58	55°N	*	936 ±	40	1940	Webber	(1962)	2
2.7.58	55°	*	972 ±	40	1956	Webber	(1962)	3
12.4.59	55°	*	1145 ±	50	2083	Webber	(1962)	4
16.5.59	55°	*	925 ±	40	1936	Webber	(1962)	5
2.6.59	59°	1.0	1310 ±	60	2112	Webber	(1962)	6
22.8.60	73°	0.88	1076 ±	130	2125	Vogt	(1962)	7
† 8.9.60	73°	0.88	1129 ±	135	2017	Vogt	(1962)	8
15.9.60	73°	0.88	1138 ±	140	2101	Vogt	(1962)	9
†22.7.61	73°	0.88	1062 ±	120	2023	Meyer and Vogt (1963)		10
29.7.61	73°	0.88	1172 ±	140	2030	Meyer and Vogt (1963)		11
1.8.61	73°	0.88	1204 ±	145	2069	Meyer and Vogt (1963)		12
6.8.61	73°	0.88	1324 ±	185	2125	Meyer and Vogt (1963)		13
8.8.61	73°	0.88	1263 ±	150	2131	Meyer and Vogt (1963)		14
18.8.61	Explorer XII		1523 ±	200	2145	Bryant et al. (1962)		15
26.8.61	65°	0.88	1420 ±	160	2158	Present experiment		1B
21.7.62	65°	0.88	2120 ±	175	2262	Present experiment		2B

* Rigidity limited by the threshold rigidity.

† Low energy solar protons observed.
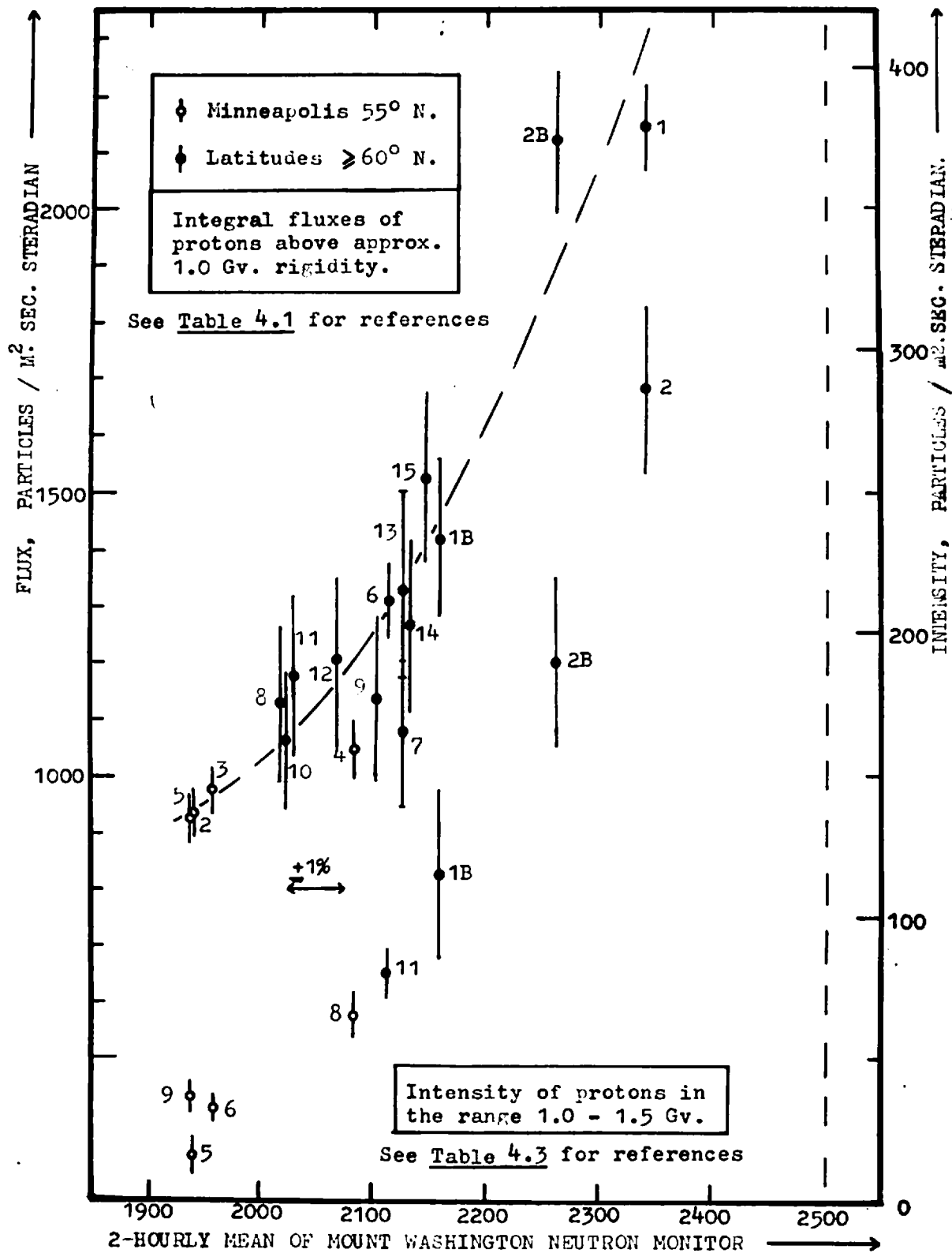
TABLE 4.1

FIGURE 4.2

rates of the Mount Washington neutron monitor on the days of

measurement. The correlation is clearly defined although there is

a fairly large spread in the points largely due to errors inherent

in the statistical counts and the secondary corrections required

for extrapolating to zero residual atmosphere. Some of the earlier

measurements have been made at Minneapolis and these are

distinguished as they probably represent a slightly higher rigidity

limit. ~~Measurements~~ *The fluxes* near solar minimum are progressively less

effective at producing a response at sea level and are therefore

less energetic. This implies that the rigidity dependence of the

modulating mechanism depends also on the state of the 11 year

cycle of activity.

A plot of this type is a useful way of comparing data

obtained at different times, in order to indicate any unusual

results. It is apparent that the flux obtained in 1962 may be

slightly higher than expected, especially as the increase is mainly

due to fast particles which appear as primary protons with rigidity

in excess of 1.5 Gv. (See Table 3.5). Such particles, if they were

all primary protons, would show a proportionate increase of

approximately 50% at lower depths in the atmosphere whereas a plot

of the overall intensity in 1961 against 1962 for different depths

shows a proportionate increase in 1962 of about 30% down to a

pressure of 40 gm./cm^2. Below this depth the increase becomes

gradually greater with altitude. This effect can be seen in the

altitude intensity graphs in Figure 3.6a though not so obviously
as in the former plot. This increase at high altitude is
interpreted as the arrival of lower rigidity particles which were
not present in 1961. However since the flux above 1.5 Gv. obtained
at altitude in 1962 is 45% over the 1961 value, it is suggested
that the 1962 data might not be sufficiently corrected for fast
splash albedo. This does not show much effect at depths below 40
gm./cm^2 as it is more rapidly absorbed but could increase the high
altitude relativistic flux. The suggestion that this albedo is
predominantly electrons (McDonald and Webber, 1959) is in
qualitative agreement with such effects. The results of other
investigators have been used to estimate the splash albedo which
could not be resolved at altitude as discussed in section 3.2c.
Although it is not really understood how this increase in fast
albedo was produced other than in an extra 1.3 gm./cm^2 in the lower
detector of gondola 2B, these considerations are taken to account
for the anomalously high fast particle intensity in 1962 in the
absence of any other interpretation.

4.2   The primary proton rigidity spectrum from 0.6 to 2.0 Gv.

The differential spectra of protons which have been
obtained from these experiments are shown in Figure 4.3 and apply
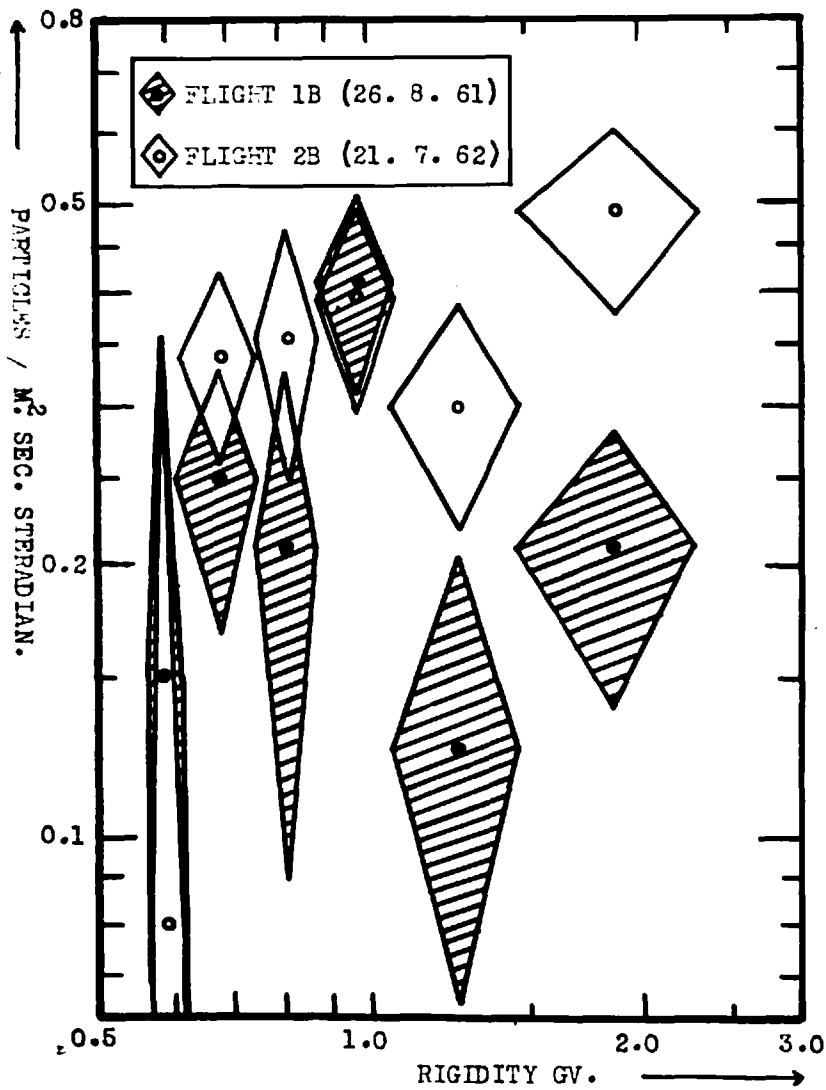to two flights made from Kiruna, Northern Sweden in August 1961

FIGURE 4.3a   Differential rigidity spectra of
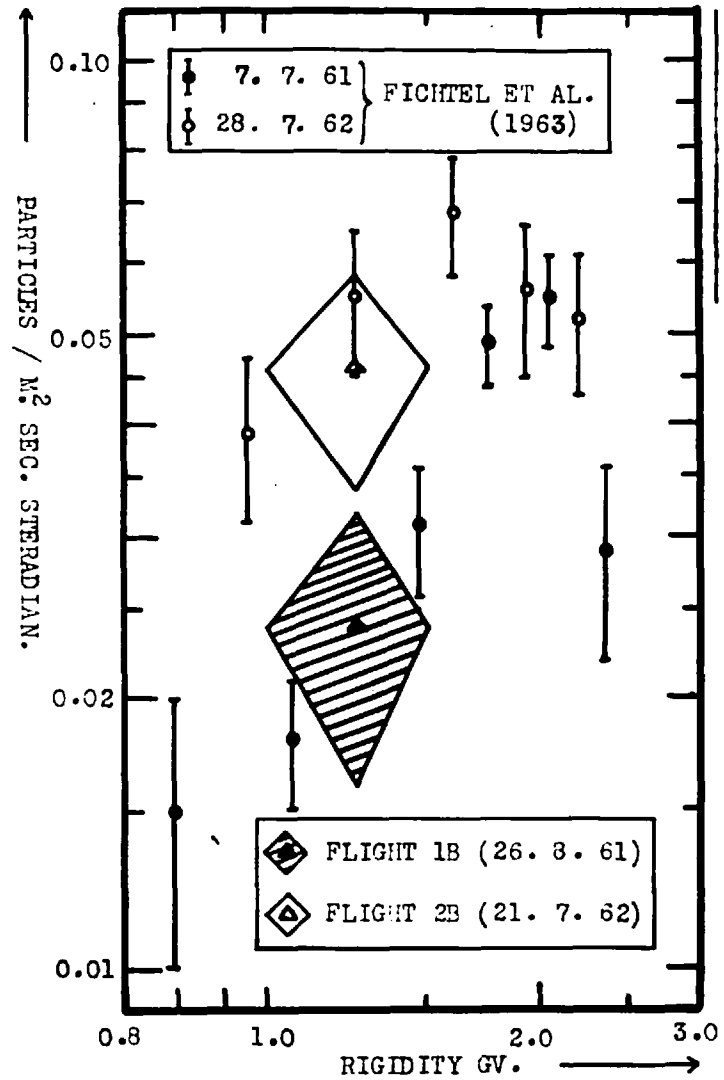protons obtained in 1961 & 1962.

FIGURE 4.3b   Differential α-particle
fluxes in 1961 & 1962.

and July 1962 at a geomagnetic latitude 65° N. The errors involved
are large, mainly owing to the fact that the average altitude
reached was 12 gm./cm.^{2} of residual atmosphere which required
systematic corrections for secondaries and background which were
greater than 40% below 1.0 Gv. At the higher rigidities the errors
are mostly due to uncertainty in the rigidity limits. It was not
possible to extend measurements below 0.6 Gv. as the uncertainties
due to corrections amounted to more than 100% of the corrected
flux. The theoretical threshold rigidity was 0.5 Gv. for both
flights (Quenby and Wenk, 1962). There appears to have been a
large increase of over 50% in the intensity of particles in the
range 1.0 to 2.0 Gv. while the flux below 1.0 Gv. has not changed
so greatly over the given period. In contradiction with some
earlier measurements, this lower rigidity flux is appreciable even
taking account of the errors and seems to be in agreement with the
results of other investigators for this stage of the 11 year cycle
as shown in Figure 1.3 . In particular, the variations in flux
obtained by Fichtel et al. (1963) with emulsions also show a small
change between 1961 and 1962 at around 0.6 Gv. Although the lowest
interval suggests a fall-off in intensity, this cannot be seriously
taken as suggesting a cut-off in view of the large errors. For
part of the region between 1.0 and 2.0 Gv. the differential
spectrum appears to have a positive slope in both years.

This is the only occasion on which direct differential

measurement of primary protons has been quoted over such a large

range of rigidities and the indication is that there is either

a) a minimum in the differential spectrum between 1.0 and 1.5 Gv.

or b) the spectrum remains fairly flat from 0.6 to 2.0 Gv. at this

time. The former case is difficult to interpret other than through

the existence of some independent mechanism which favours the

presence of particles below 1.0 Gv. and opposes the 11 year solar

modulation of the galactic intensity, which is fairly well

established as progressively removing particles more towards lower

rigidities. The smaller change in intensity from 1961 to 1962 at

lower rigidities is also suggestive of some mechanism additional

to the long term galactic modulation. This will be discussed

further in Section 4.3 . The errors involved in plotting small

intervals of a differential spectrum render it very difficult to

define the changes in shape from one year to another unless

statistics are improved by using results from a number of flights

at about the same time. In order to detect long term changes in

the differential spectrum it is preferable to minimise errors by

taking the flux in broad rigidity intervals and to investigate the

variations over different stages of the solar cycle. It is first

necessary to adopt an index with which to measure the state of the

solar modulation.

In view of the large phase lag of 6 to 12 months between

the long term variations in the cosmic ray intensity and any of

the parameters measuring solar activity such as magnetic indices, solar radio emission or average sunspot numbers, they are not very suitable for representing the state of the main modulating mechanism from one half cycle to the next. This phase lag is illustrated in Figure 4.4 . The cosmic ray flux itself is probably a better standard, provided that possible changes in shape of the spectrum between intensity decrease and recovery are minimised by taking as wide a range of energies as possible. The neutron monitor of Mount Washington covers these conditions and is the only high latitude station that has been operating since the last solar minimum, it is also relatively immune from solar particles and yet is more sensitive to the low end of the spectrum in view of its latitude. This station, together with Climax, has also been found to give more consistent long term variations than other stations, and will therefore be used as a standard here.

4.3 Changes in intensity of low rigidity protons over the solar cycle.

The present results are compared with previous measurements on the primary proton interval 1.0 to 1.5 Gv. by plotting the fluxes against the daily two-hourly means of the Mount Washington neutron monitor at the time of the measurement in Figure 4.2 . The proton intensities in this case have been derived from the smoothed integral spectrum and those results
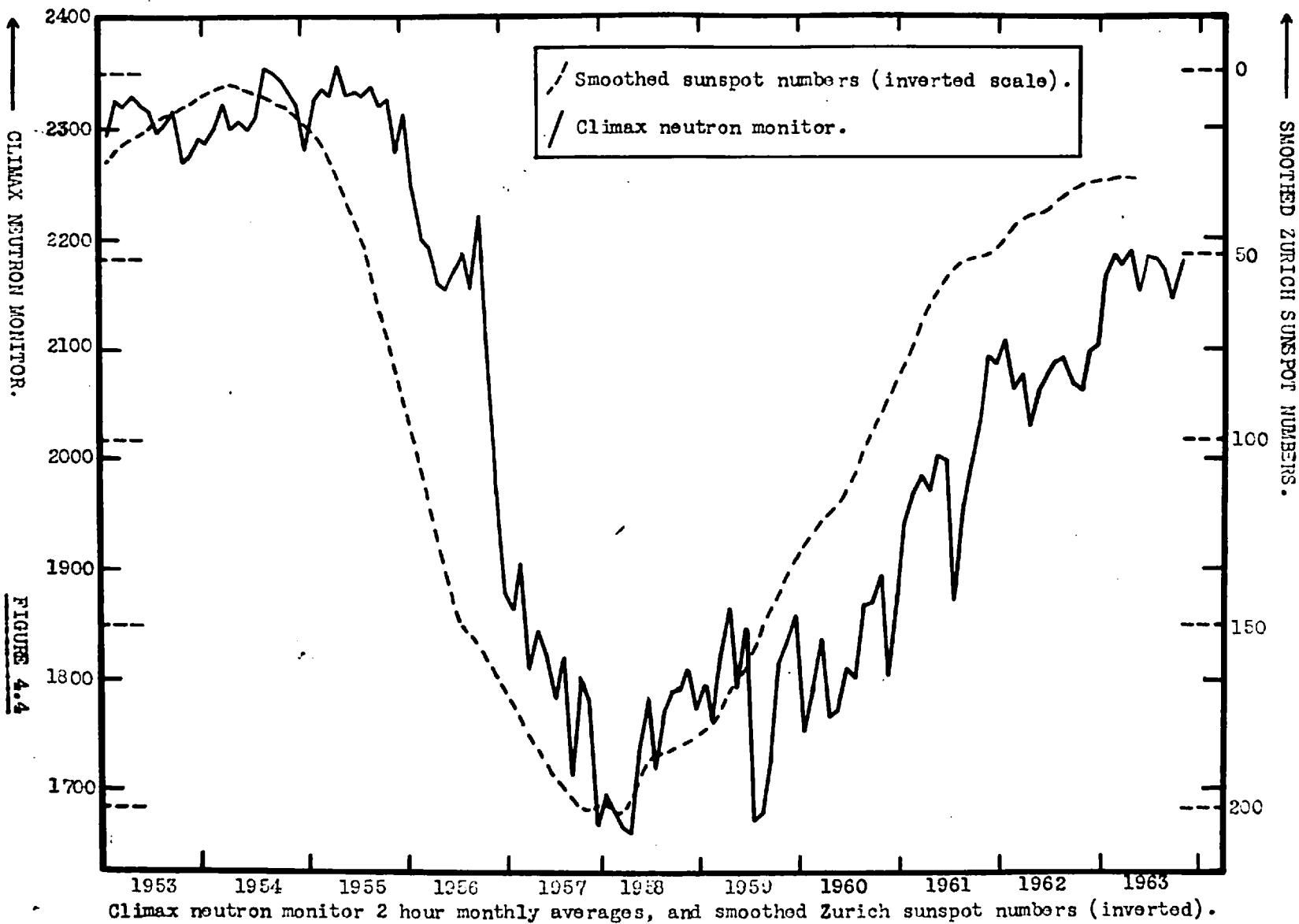
Climax neutron monitor 2 hour monthly averages, and smoothed Zurich sunspot numbers (inverted).

CLIMAX NEUTRON MONITOR.

FIGURE 4.4

SMOOTHED ZURICH SUNSPOT NUMBERS.

- 99 -

Smoothed sunspot numbers (inverted scale).

Climax neutron monitor.

obtained from Minneapolis have been distinguished in view of the possible threshold limitation of the flux. The modulation at this rigidity is seen to be well correlated with the overall flux and does not show any measurable difference between the rising and falling periods of the solar cycle. However this might be expected since the Mount Washington neutron monitor represents a fairly low average primary rigidity.

In contrast, Simpson (1963) has reported evidence for a fairly definite phase lag in recovery of low rigidity over high rigidity particles for the period of declining solar activity, compared to the period prior to solar maximum. This has been obtained with neutron monitors which represent an integrated range of energies, and it is a more sensitive verification of the effect to plot the low rigidity interval 1.0 to 1.5 Gv. against the daily mean rates of a low latitude neutron monitor. When this is done for the flight data available, and using the neutron monitors that were in operation for the whole period, it is found possible to obtain either a lag or lead of the interval depending on which monitor is used. This is a result of the irregular correlation of some monitors over a long period.

Latitude surveys, which have been summarized by Kondo et al. (1963) for the nucleonic component, show a change in the power law of the high rigidity particle spectrum over the last solar cycle which is not in phase with the change in the latitude "knee",

and this can also be interpreted as a phase difference over the
two half-cycles. However, using either the Mount Washington or
Climax monitors which show a close correlation since 1955 (Figure
4.6) and relying on the one measurement prior to solar maximum,
there is no phase lag of the rigidity interval 1.0 to 1.5 Gv. over
higher rigidities that differs for the two half-cycles. It will
probably not be possible to resolve this question until data are
obtained extending after the next solar minimum with equipment
that has a longer term stability than neutron monitors.

The fluxes in an interval 0.62 to 0.88 Gv. have also been
plotted against the average neutron intensity for the same period,
together with the figures given by Vogt (1962) and Meyer and Vogt
(1963) and a value deduced from the differential spectrum of
Bryant et al. (1962). (See figure 4.5). The positive correlation
is not very definite and in fact the variation within this interval
is consistent with no significant change in intensity over the whole
period 1960 to 1962. As mentioned in the introduction, the
measurement of protons in this region depends rather markedly on
the method used in correcting for secondaries, and in order to
compare other data it is worth surveying the methods used to derive
them

The results of Bryant et al. were obtained with Explorer XII
and are therefore free from atmospheric secondaries, they were
corrected for background secondaries in the detector by using

FIGURE 4.5

FIGURE 4.6

Percentage decrease of the monthly 2-hourly means of neutron monitor counting rates from the value at solar minimum taken in 1954 as:
Mount Washington   2470
Climax   3313
in terms of the 1962 values.

MOUNT WASHINGTON NEUTRON MONITOR. (1.34 GV.)
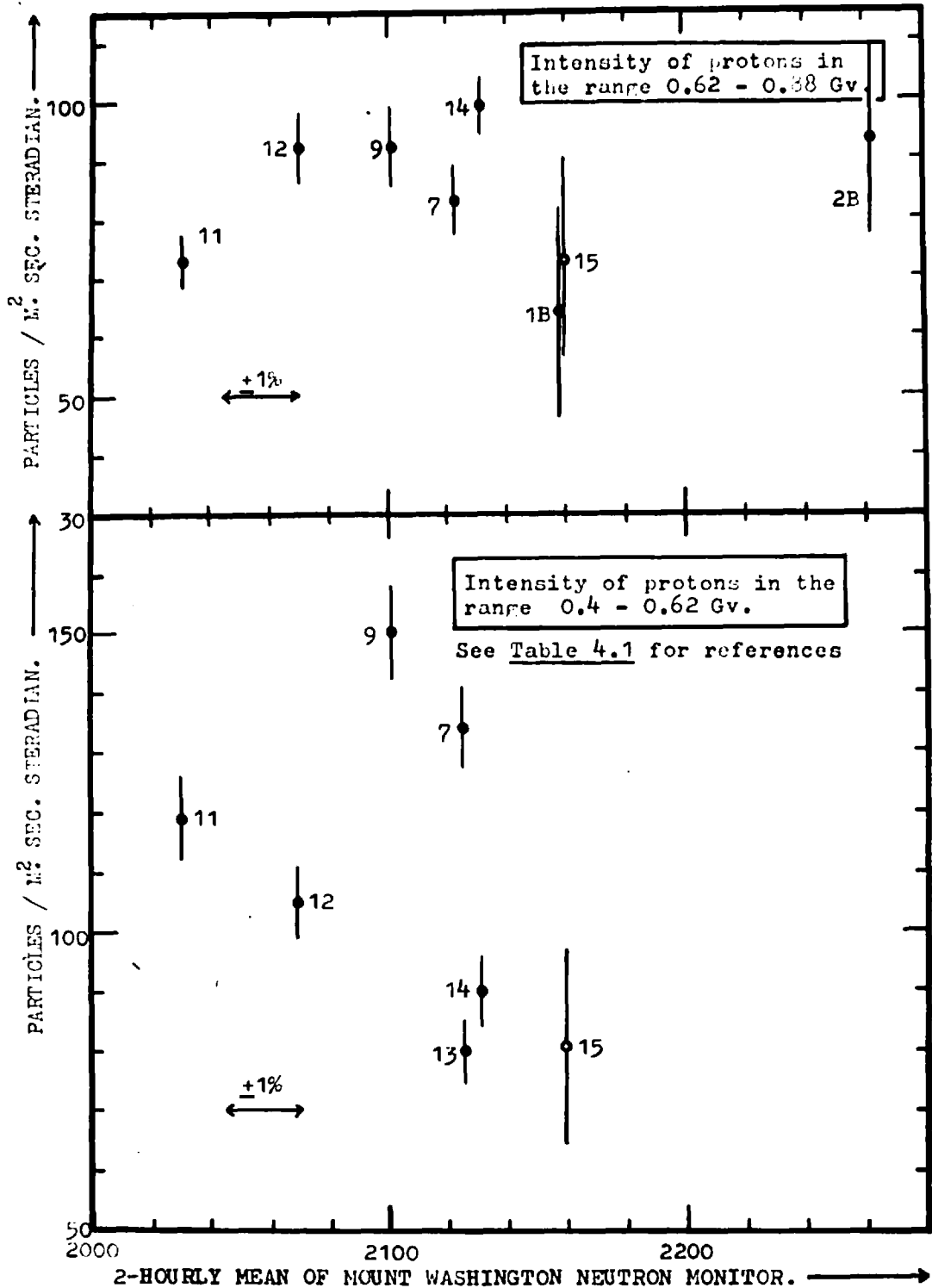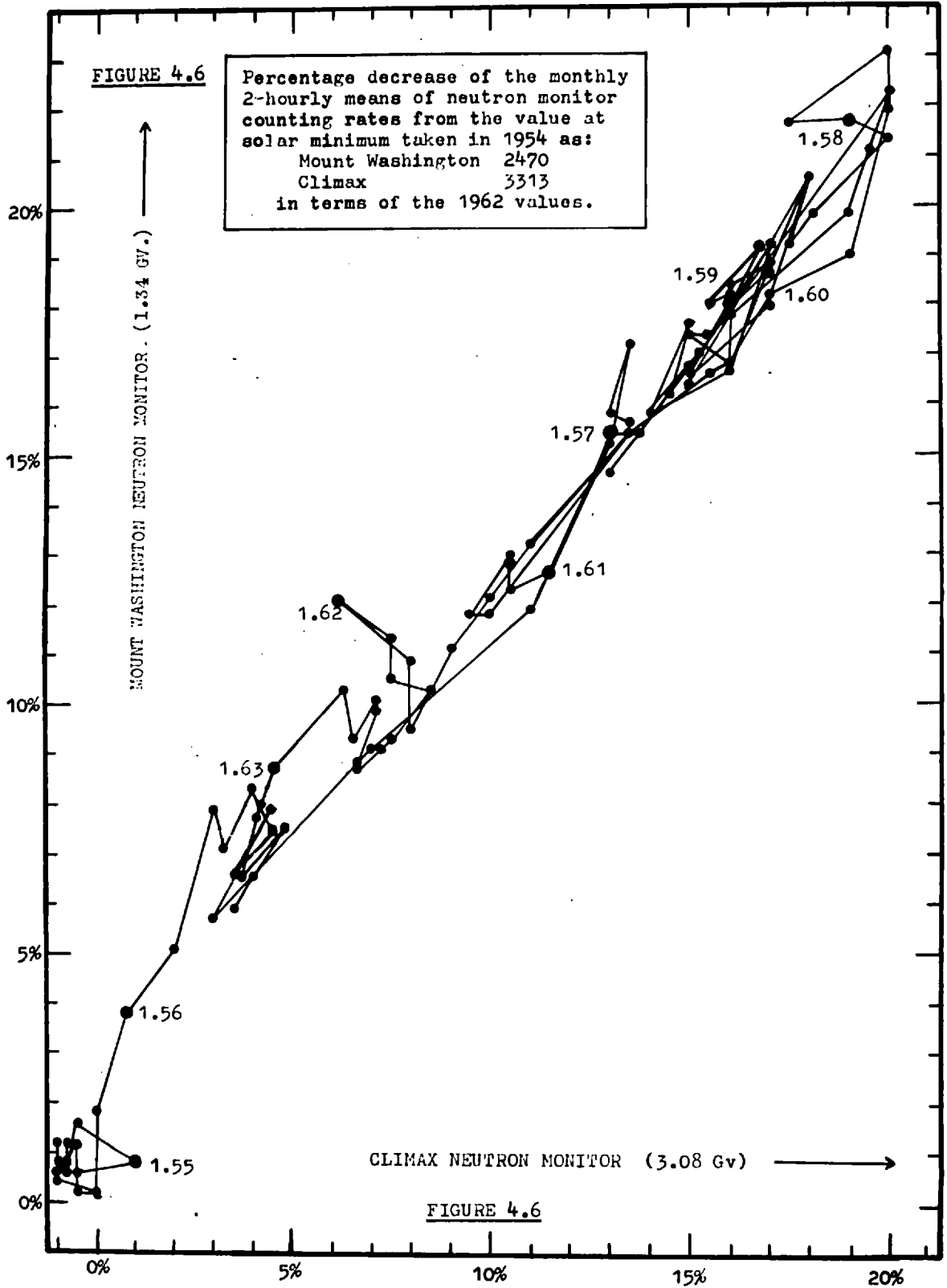
CLIMAX NEUTRON MONITOR   (3.08 Gv)

FIGURE 4.6

similar apparatus flown with balloons from Sioux Falls and Fort
Churchill. In these balloon measurements the return albedo was
estimated by making use of the isotropic abundances and also
calculations made by Ray (1962). Overall corrections amounted to
about 50%.

The results of Meyer and Vogt were corrected for
secondaries by calculations based on previous empirical data of
other workers and a comparison with their own altitude
extrapolations.

The results presented here were corrected by the
subtraction procedure described in Section 3.2c, using data from
different latitudes where the return albedo was estimated as
negligible compared with the first order secondary correction.
The presence of any return albedo would imply that the derived
intensities are a lower limit.

The rigidity interval 0.4 to 0.62 Gv. has been measured by
Meyer and Vogt and has also been plotted in Figure 4.5 . Even if
the absolute intensities might be open to criticism in view of the
corrections applied, the relative intensities are significant in
indicating irregular changes in intensity compared with the overall
flux. The variation shows less correlation than the 0.62 to 0.88
Gv. interval, although the enhanced fluxes of 8 Sept. 1960 and 22
July 1961, which could be definitely associated with preceding
class 3 flares, have been omitted here. This is further evidence

for an independent and intermittent source of low rigidity
protons at times of apparently quiet solar activity, and is
consistent with the conclusions of Meyer and Vogt, which they
based on the time variations, that there is either continuous or
frequent production of protons by the sun, or that the storage
times of particles produced with flares is large. In view of this
it is possible that the flux in the interval 0.62 to 0.88 Gv. is
influenced to some extent by solar particles at quiet times, during
the years following solar maximum.

A solar source of particles, with rigidities high enough
to produce effects in sea level neutron monitors, has been
suggested by Kodama (1959). These conclusions are reached from a
study of the correlation of the 27-day recurrence amplitudes of
monitors with the intensity of solar noise at 3750 Mc./sec. during
solar minimum. No quantitative estimate is made of the particle
intensities but there is an indication that they are enhanced at
lower rigidities. This is in accordance with the steep solar
flare particle spectra (Frier, 1963). Sea level latitude surveys
of the nucleonic component from 1956 to 1959 (Lockwood, 1960;
Sandstrom, 1963) indicate a fairly sharp and constant "knee" in
the latitude curve at 3.0 Gv., implying that the specific response
from lower rigidity patricles is exceedingly small. Therefore,
the results of Kodama indicate a significant low-rigidity flux of
solar particles that is expected to increase with solar activity.

A continuation of observations into the International
Years of the Quiet Sun is **necessary** in order to make a good
discrimination between the solar and galactic protons. This is a
first essential if the galactic proton spectrum is to be compared
with that of α-particles.

4.4   The galactic spectrum of low rigidity protons.

Since it is not yet possible to ascertain the form of the
unmodulated galactic spectrum of protons by direct measurement, it
must be deduced from the changes in intensity at different
rigidities, with particular emphasis on the solar minimum spectrum.
It seems likely from these variations that the galactic spectrum
is very close to the solar minimum spectrum at high rigidities
where it is well described by an exponential form. However at low
rigidities it is uncertain whether the flux at the earth recovers
to the full galactic intensity at solar minimum. The following
discussion would suggest that it does recover between 1.0 to 1.5 Gv.
and that the galactic spectrum changes in shape below 2.0 Gv.

It is evident from the positive correlation of the
rigidity interval 1.0 to 1.5 Gv. with the overall flux (Figure 4.2)
that this interval contains fewer solar particles than the lower
rigidity intervals, and it is possible to make a crude extrapolation
of the intensity to the last solar minimum when the two-hourly rate

of Mount Washington was 2500. If this intensity of 420 ± 20

particles/m^2 sec. ster. is taken to represent the solar minimum

value $J_{s.m.}$, then as a ratio of this flux, the measured fluxes J_e

at the earth are: $J_e/J_{s.m.} = 0.27 \pm 0.03$ for August 1961, and

$J_e/J_{s.m.} = 0.45 \pm 0.05$ for July 1962.

The results from Ariel I, obtained during May and June 1962

(Elliot, 1963) for the solar modulation of particles with charge

$Z \geqslant 6$, are found to be satisfactorily fitted by predictions based

on Parker's model of the interplanetary field (Parker, 1963), by a

suitable choice of the parameters used in the theory. In order to

derive the form of the modulation from the measured spectrum, the

integral galactic spectrum is taken to be represented by $J = J_0 P^{-1.5}$

over a range from 2 to 15 Gv. where J is the integral intensity

above a rigidity P. By taking the values of the parameters

applicable in this measured range, the modulation for a proton

rigidity 1.25 Gv can be calculated, giving $J_e/J_\infty = 0.53 \pm 0.04$,

where J_∞ is the unmodulated galactic intensity.

Since at high rigidities the spectra of heavy particles and

protons are very similar (Section 1.2), the integral proton spectrum

of flight 2B can be normalized to the measured Ariel spectrum and

the assumed galactic spectrum. By extrapolating the exponential

spectrum, a value for the galactic intensity is obtained for the

interval 1.0 to 1.5 Gv., $J_{exp} = 3500 \pm 500$ particles/m^2 sec. ster.

Using the measured value of J_e, we obtain the following ratios for

1962: $\qquad J_e/J_{s.m.} = 0.45 \pm 0.05$ (P = 1.25 Gv.)

$\qquad\qquad J_e/J_{exp} = 0.05 \pm 0.01$ (P = 1.25 Gv.)

These may be compared with the value predicted from the Parker
modulation at a similar time.

$\qquad\qquad J_e/J_{\infty} = 0.53 \pm 0.04$ (P = 1.25 Gv.)

Provided the Ariel modulation assumptions are valid, it
can be seen that the solar minimum value $J_{s.m.}$ is more consistent
a value for the unmodulated intensity J_{∞} than the exponential
value J_{exp}, $J_{s.m.}$ also appears to represent an upper limit to
this flux. It is therefore implied that the solar minimum spectra
is a better representation of the integral galactic spectrum than
one of the type $J = J_o P^{-1.5}$ below 2 Gv.

4.5   The integral flux of α-particles above the atmosphere.

The α-particle fluxes above 1.0 Gv. in the high latitude
flights are tabulated with other data available in Table 4.2, and
plotted in Figure 4.7 . In general the air cut-off has prevented
measurement of these particles below 1.0 Gv. until recently. The
fluxes obtained by McDonald are included as a large proportion of
measurements made near solar minimum, although they have a slightly
higher rigidity limit. The points in Figure 4.7 are more diverse
towards solar minimum which is possibly due to both differences
in the low rigidity limit and also the fact that neutron monitors

Integral α-particle fluxes above 1.0 Gv. rigidity.

Date of flight	Geomag. lat.	Lower rig. limit Gv.	Integral flux parts./m². sec.ster.	Mount Wash.	Reference	
18.6.54	60°N	1.0 *	302 ± 21	2458	Frier et al. (1959)	1
7.7.55	55°N	1.55	306 ± 25	2461	McDonald (1958)	2
17.5.56	54°N	†	255 ± 20	2240	Fowler et al.(1958)	3
21.8.56	55°N	1.15	298 ± 25	2370	McDonald (1958)	4
17.8.56	55°N	1.55	270 ± 25	2369	McDonald (1957)	5
7.9.56	59°N	0.8*	307 ± 20	2340	Webber (1962)	6
18.9.56	55°N	†	240 ± 26	2297	Duke (1960)	7
17.5.57	55°N	1.25*	157 ± 17	2080	Frier et al. (1958)	8
30.7.57	55°N	†	151 ± 9	2089	Engler (1961a)	9
30.7.57	55°N	†	164 ± 17	2089	Dahanayake (1963) et al.	10
1.9.57	55°N	†	136 ± 9[+]	1959	Frier et al. (1959)	11
11.9.57	61°N	1.0	137 ± 11	1971	Aizu et al. (1959)	12
16.2.58	55°N	†	135 ± 8	1956	Webber (1962)	13
2.7.58	55°N	†	130 ± 15	1940	Webber (1962)	14
3.8.58	61°N	1.0	135 ± 8	1998	Engler (1961b)	15
12.4.59	55°N	†	159 ± 9	2083	Webber (1962)	16
16.5.59	55°N	†	132 ± 8[+]	1936	Webber (1962)	17
1.6.59	55°N	†	172 ± 8	2110	Webber (1962)	18
2.6.59	59°N	0.8*	182 ± 9	2112	Webber (1962)	19
8.7.61	58°N	1.0*	197 ± 11	2161	Stephenson (1962)	20

†   Limit determined by the threshold rigidity.

*   Limit determined by the air cut-off.

+   Obtained during a large Forbush decrease.

TABLE 4.2

continued overleaf.

TABLE 4.2 (continued)

Date of flight	Geomag. lat.	Lower rig. limit	Integral flux parts./m^2 sec.ster.	Mount Wash.	Reference	
7.7.61	73°N	0.8*	219 ± 13	2147	Fichtel et al. (1963)	21
28.7.62	73°N	0.8*	253 ± 18	2231	Fichtel et al. (1963)	22
26.8.61	65°N	1.0*	199 ± 16	2158	Present experiment	1B
21.7.62	65°N	1.0*	253 ± 12	2262	Present experiment	2B
These references apply to the α-particles > 2.5 Gv. in Figure 4.8					McDonald and Webber (1962b)	M

TABLE 4.3

| Protons and α-particles in the interval 1.0 to 1.5 Gv. rigidity.					
Date of flight	α-particle flux	proton flux	Mount Wash.	Reference	No. on graphs
18.6.54	50 ± 10*	–	2458	Frier et al. (1959)	1
7.9.56	47 ± 5	286 ± 30	2340	Webber (1962)	2
18.9.56	10 ± 2†*	–	2297	Duke (1960)	3
11.9.57	8 ± 2*	–	1971	Aizu et al. (1959)	4
16.2.58	4.5 †	15 ± 6	1940	Webber (1962)	5
2.7.58	5.0 †	32 ± 5	1956	Webber (1962)	6
3.8.58	8 ± 2*	–	1998	Engler (1961b)	7
12.4.59	10.0 †	65 ± 8	2083	Webber (1962)	8
16.5.59	3.5 †	36 ± 5	1936	Webber (1962)	9
1.6.59	6 ± 1†	–	2110	Webber (1962)	10
2.6.59	9 ± 1.5	80 ± 9	2112	Webber (1962)	11
26.8.61	12 ± 4	115 ± 20*	2158	Present experiment	1B
21.7.62	23 ± 6	190 ± 20*	2262	Present experiment	2B
* Obtained from smoothed integral spectrum. † At 55° N.					
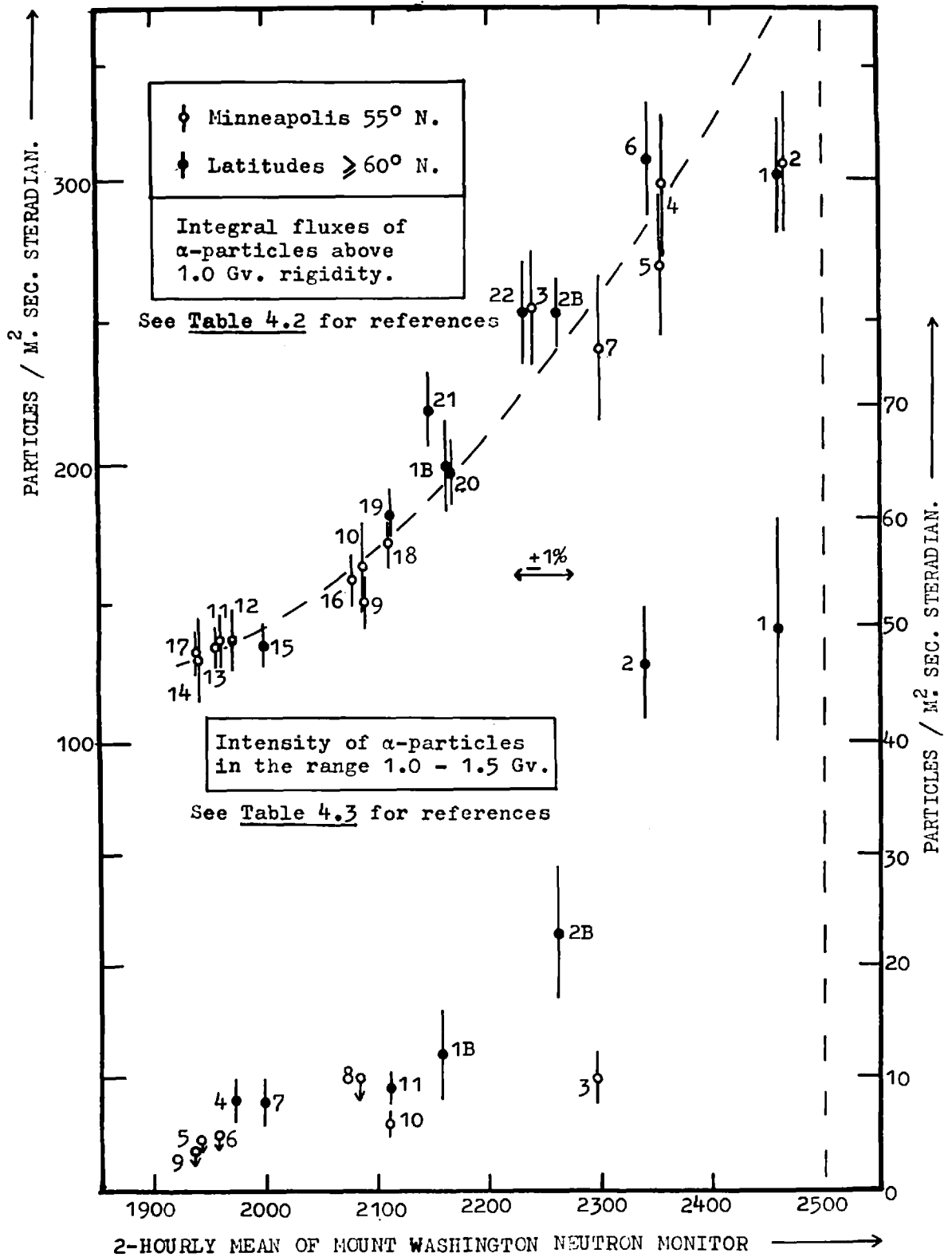
FIGURE 4.7

are very insensitive at rigidities below 3.0 Gv. New results from

the present solar minimum will be essential to define the changes

in intensity in this region. In comparison with protons from

Figure 4.2, the ratio of the integral fluxes of protons to those of

α-particles remains effectively constant over the half cycle from

maximum solar modulation to Mount Washington neutron rates of 2200

in two hours. Towards solar minimum there seems a tendency for the

ratio to increase when all the data are considered. However, there

are few proton data for this half cycle, and if only the higher

latitude α-particle measurements are considered, the ratio is

indistinguishable from that at solar maximum. It is concluded,

therefore, that the question of any change in the ratio of the

integral flux of protons to α-particles over the solar cycle is

unresolved other than the change being smaller than the

uncertainties in the measurements. Although the lowest possible

rigidity limit, for which a reasonable number of results are

available, has been taken, the large rigidity range necessarily

includes a preponderance of protons and α-particles whose

velocities β are indistinguishable. A comparison of the proton

to α-particle ratio must be made more sensitive if the possibility

of a modulating mechanism with **both β dependence** and **rigidity**

dependence is to be excluded. This is discussed in Section 4.7 .

The flux of α-particles at the top of the atmosphere for

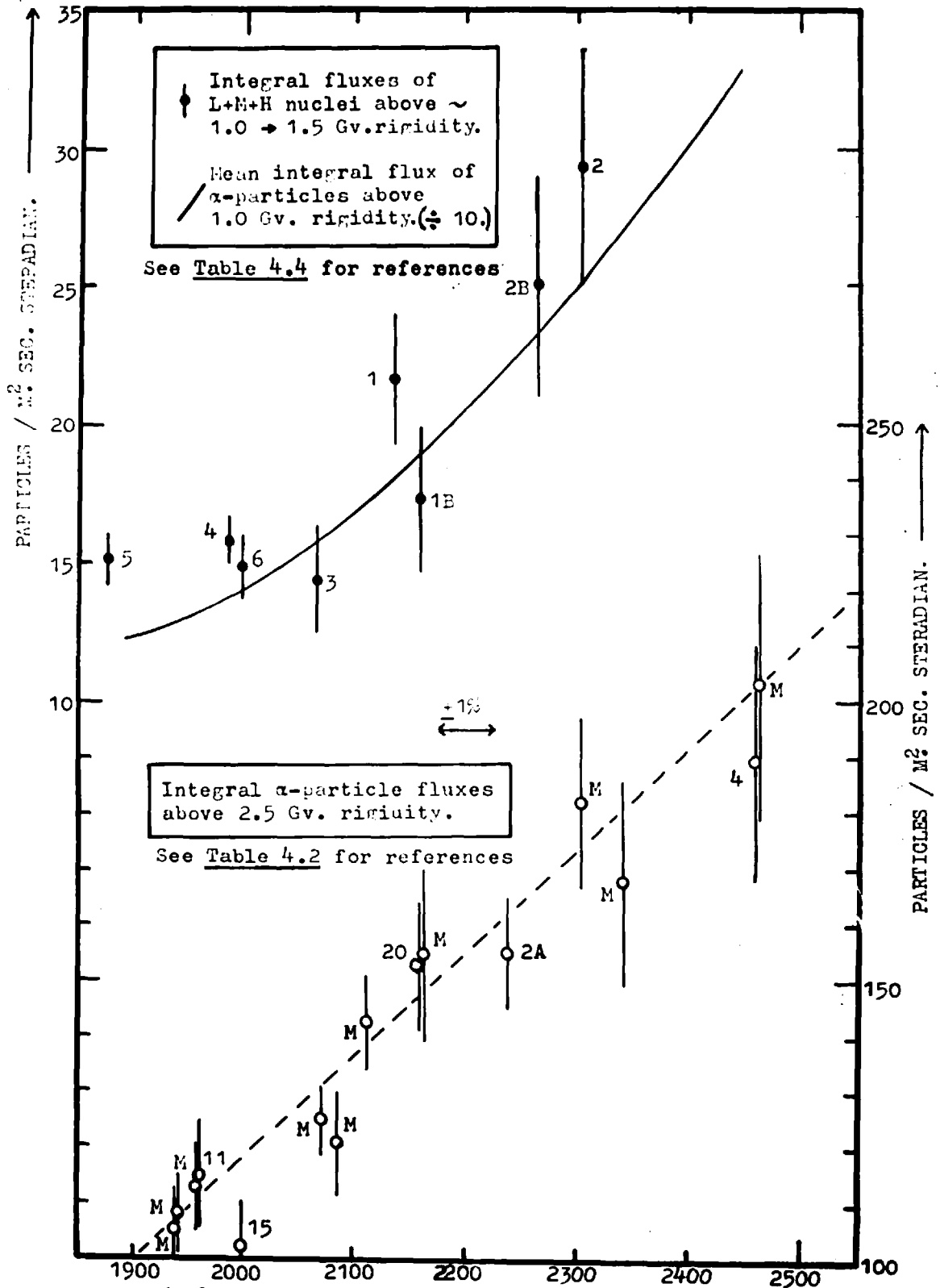the low latitude flight is compared in Figure 4.8 with previous

FIGURE 4.8   2-HOURLY MEAN OF MT. WASHINGTON NEUTRON MONITOR.

integral measurements above 2.5 Gv., which is approximately the geomagnetic threshold for this flight. The correlation of all these points is excellent and they give a very clear indication of the fast α-particle intensity variations over the solar cycle. Moreover the primary particles are linearly dependent on the Mount Washington neutron intensity over this range whereas the lower rigidity particles become enhanced at solar minimum. The presence of low rigidity particles at solar minimum is also well illustrated by the plot in Figure 4.4. This shows the percentage changes in the two-hourly mean intensity of the Mount Washington and Climax neutron monitors for each month since 1954 which is used as a base level. It can be seen that particles with rigidities intermediate between the thresholds 3.0 and 1.35 Gv. largely diminished in intensity during 1955.

4.6   The intensity variation of low rigidity α-particles.

In view of the slow proton overlap in the fast α-particle region of the two-dimensional pulse height distribution (Figure 3.8), it has not been possible to measure the rigidity spectrum of α-particles over the whole ionisation sensitive range. However the lower rigidity region is most interesting from the aspect of comparing the flux values with those of protons. The α-particle fluxes which have been obtained in the rigidity interval 1.0 to

1.5 Gv. are plotted in Figure 4.7, in a similar way as for the
protons as a function of the Mount Washington neutron monitor rate.
Also included are the results of other investigations for the same
interval. Those which have been obtained at Minneapolis are
distinguished, and it is evident that these latter fluxes are
lower than those for higher latitudes where there is little doubt
of their being free from geomagnetic thresholds. These α-particles
also show a positive correlation with the overall flux and again,
as with the protons, there is insufficient data to detect any
phase change over the decrease and recovery of the flux. Some of
these data have corresponding measurements for protons in the same
rigidity interval which were made on the same balloon flights, and
these will now be discussed.

4.7   Changes in intensity of the primary protons and α-particles
                       in the rigidity interval 1.0 to 1.5 Gv.

        Figure 4.9 shows the results of simultaneous direct
measurements of protons and α-particles in the rigidity interval
1.0 to 1.5 Gv., plotting proton flux against α-particle flux.
Those results obtained from Minneapolis have been distinguished
and the only higher latitude results, other than those which are
presented here, have been for the flights made from International
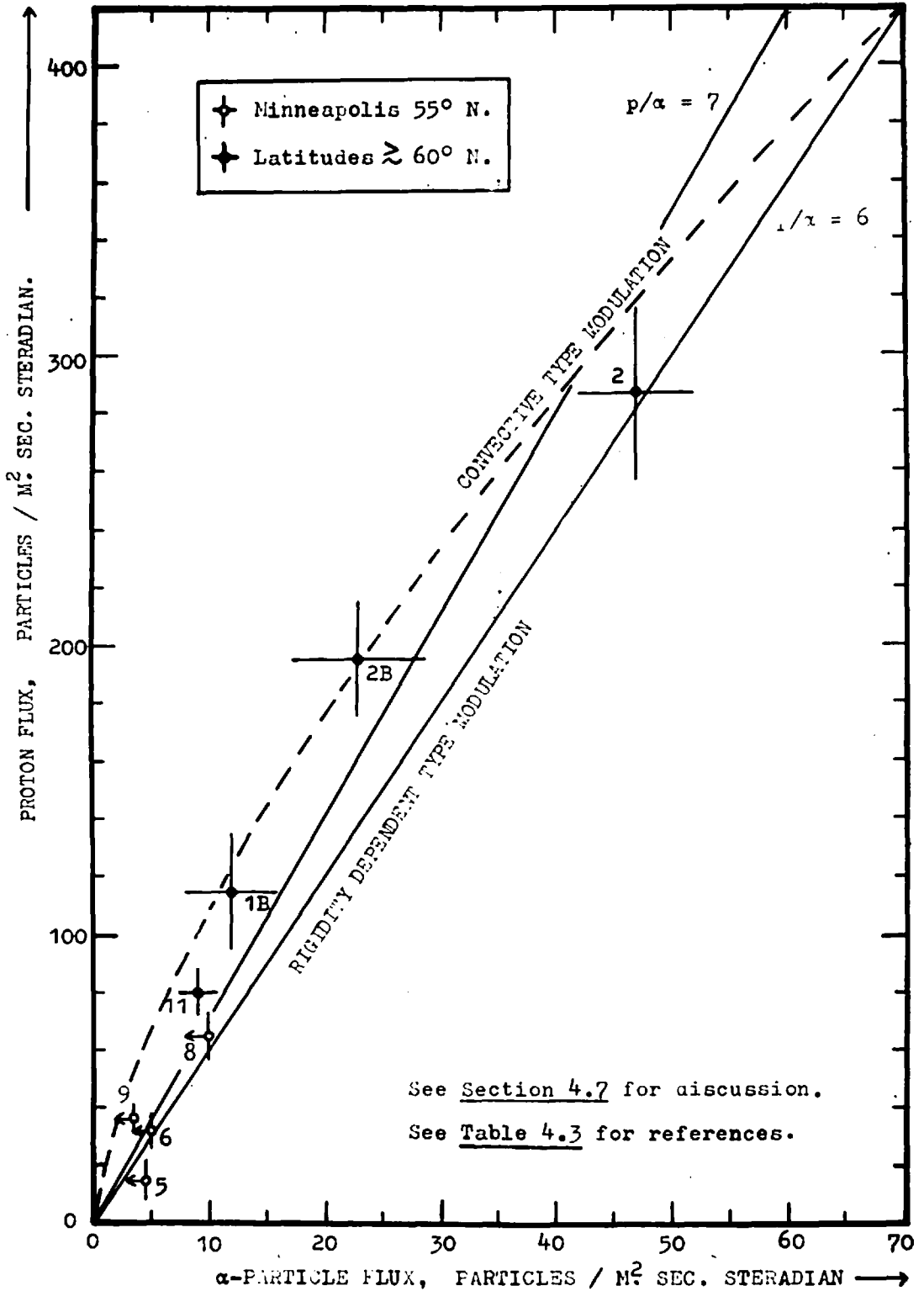Falls in 1956 (Webber, 1962) and 1959 (McDonald and Webber, 1960).

FIGURE 4.9   Proton and τ-particle fluxes in the rigidity
range 1.0 → 1.5 Gv. measured simultaneously.

Such a plot does not need to presuppose that the galactic spectra

of protons and α-particles are similar in order to compare their

modulation, but only assumes some ratio for their intensities

which remains virtually constant over periods up to a decade or

more at distances beyond the influence of the sun. For a solar

modulating mechanism that is purely rigidity dependent these

values are expected to be fitted by a straight line through the

origin, whereas, the existence of any additional factor in the

modulation which differentiates between protons and α-particles

will cause a deviation to some extent from this proportional

relationship. In order to give an indication of this effect, and

assuming a certain but arbitrary value for the unmodulated galactic

intensity of both particles, the theoretical dependence of the

ratio has been drawn for two opposing idealized models of the

modulating mechanism.

Firstly a case is considered where rigidity is the only

controlling parameter associated with the particle. This has been

suggested in the literature on earlier measurements, and to describe

such an effect the solar dipole model was constructed by Elliot

(1960). This line is drawn for a galactic ratio of 7.0 and 6.0,

which remains unchanged throughout modulation. Although a better

fit is obtained for a line of slope 7.0 the points do not lie very

close to it and are rather suggestive of a curve. It can be noted

that the origin (0, 0) will represent an experimental point if the

data do not include any solar produced particles. The second

theoretical case is taken as one where the modulation is dependent

solely on the velocity of the particle β, in a way that is predicted

by the modification made to the theory of Parker (1958) by Dorman

(1960). Values have been arbitrarily taken for the galactic

intensities in order to derive this as follows: protons, 420

particles/m^2 sec. ster.; α-particles, 70 particles/m^2 sec. ster.,

and these represent a fair approximation to the sunspot minimum

values obtained by extrapolation. The curve is drawn for a rigidity

of 1.25 Gv., and for a slightly higher mean rigidity the

corresponding curve is not quite so bowed. The distinction, which

may be applicable if the spectra are falling towards lower rigidities

as in the Minneapolis measurements, is negligible however. The

experimental points appear to show some deviation from linearity,

and indicate a ratio for the intensity of protons to α-particles

which clearly differs from that for the total integral fluxes.

This remains close to 7.0 over the solar cycle from Figures 4.2

and 4.7 . It will be extremely interesting to obtain further

measurements in order to approach the galactic intensities at these

low rigidities and define the modulation better.

The many modulating mechanisms which have been devised to

describe long term cosmic ray intensity variations have been

essentially simple in their original formulation and some have

been gradually modified in order to fit more experimental data as

they become available. A summary of most of these theories is presented by Dorman (1963), and some have already proved to be less acceptable because they are too restrictive in the number of phenomena which they explain, e.g. Davis, (1955); Morrison (1956); Ehmert, (1960), although some features of these theories are not excluded. Until more extensive results are available, of the type presented here, it is only considered worth using them to make a broad comparison of the validity of either a static or $_\wedge^{\alpha}$convective field at large distances from the sun beyond the earth's orbit. This will now be treated in more detail.

4.8   Relative modulation of protons and α-particles.

Of the models which take account of the solar wind, the hypothesis of Parker is very general and has recently shown a reasonable description of the 11 year modulation from the results of Ariel I (Elliot, 1963). Its predictions are now compared in more detail with the present results. The original theory (Parker, 1958) was first modified by Dorman (1960) to fit the low rigidity modulation and has since been reviewed by Parker (1963).

Cosmic rays from the galaxy are regarded as diffusing through a spherical heliocentric region of plasma moving outward from the sun, constituting the solar wind and containing 'frozen in' inhomogeneous fields. The time scale of diffusion is shorter

than the long term changes in the irregularities or wind velocity
so that an average steady state is maintained in the absence of
spasmodic solar outbursts. The diffusion equation may be written:

$$dj/dt = -\nabla.(uj) + D\nabla^2(j) \qquad \ldots\ldots\ldots\ldots \quad 4.1$$

where 'j' is the differential spectrum of particles as a function
of radial distance 'r' from the sun. D is the coefficient of
diffusion and 'u' is the solar wind velocity, taken as independent
of position in this instance. Assuming that D is also independent
of position and that the steady state is reached so that $dj/dt \rightarrow 0$,
a solution is given by Parker of the form,

$$j_o(r) = j(r).\exp(r_2 - r_1)u/D \qquad \ldots\ldots\ldots\ldots \quad 4.2$$

where r_2 and r_1 determine the radial limits within which the solar
wind occurs. Introducing the number of scattering inhomogeneities
'n' as $(r_2 - r_1)/s$ where 's' is a typical scale size of the
scattering centres, and using the transport diffusion equation to
give $D = (1/3)\lambda v$ where 'v' is the particle velocity and 'λ' is the
mean free path, then,

$$j_o(r) = j(r).\exp \frac{-3uns}{\beta c\lambda} \qquad \ldots\ldots\ldots\ldots\ldots \quad 4.3$$

It remains to determine the parameters 's' and 'λ'. For particles
with a low rigidity and therefore small radius of gyration 'ρ',
which is less than the typical dimension of the scattering centres,

the mean free path will be of the same order as that scale size, i.e. λ = s. For larger radii of gyration the mean free path is determined by the degree of scattering. The value 'λ' is of the order Ns where N is the number of collisions required to deflect the particle by approximately $\sqrt{2}$ radians. Each collision with a scattering centre of dimensions 's' will cause a deflection s/ρ and if occurring randomly, after N collisions the deflection is $\sqrt{2N}s/\rho$. Therefore $\lambda \sim Ns \sim \frac{\rho^2}{s^2}.s \sim \rho^2/s$. We thus have the idealized cases,

$$j_o(r) = j(r).\exp \frac{-3un}{\beta c} \qquad \text{for } \rho < s \qquad \ldots\ldots \quad 4.4$$

$$j_o(r) = j(r).\exp \frac{-3un}{\beta c}.\frac{s^2}{\rho^2} \quad \text{for } \rho > s \qquad \ldots\ldots \quad 4.5$$

These are of the form given by Parker (1963) and they are found to fit the Ariel data by a suitable choice of the parameters. By assuming a certain value for the field strength in order to relate rigidity to the radius of gyration, the scattering scale size 's' is about four times the radius of gyration corresponding to the rigidity interval measured in the present experiment. Equation 4.4 is therefore taken to determine the modulation.

Using this relation for the rigidity 1.25 Gv. the curves given in Figure 4.10 are obtained. These show the predicted ratio of protons to α-particles for this model, for different ratios of the galactic fluxes, plotted as a function of the factor
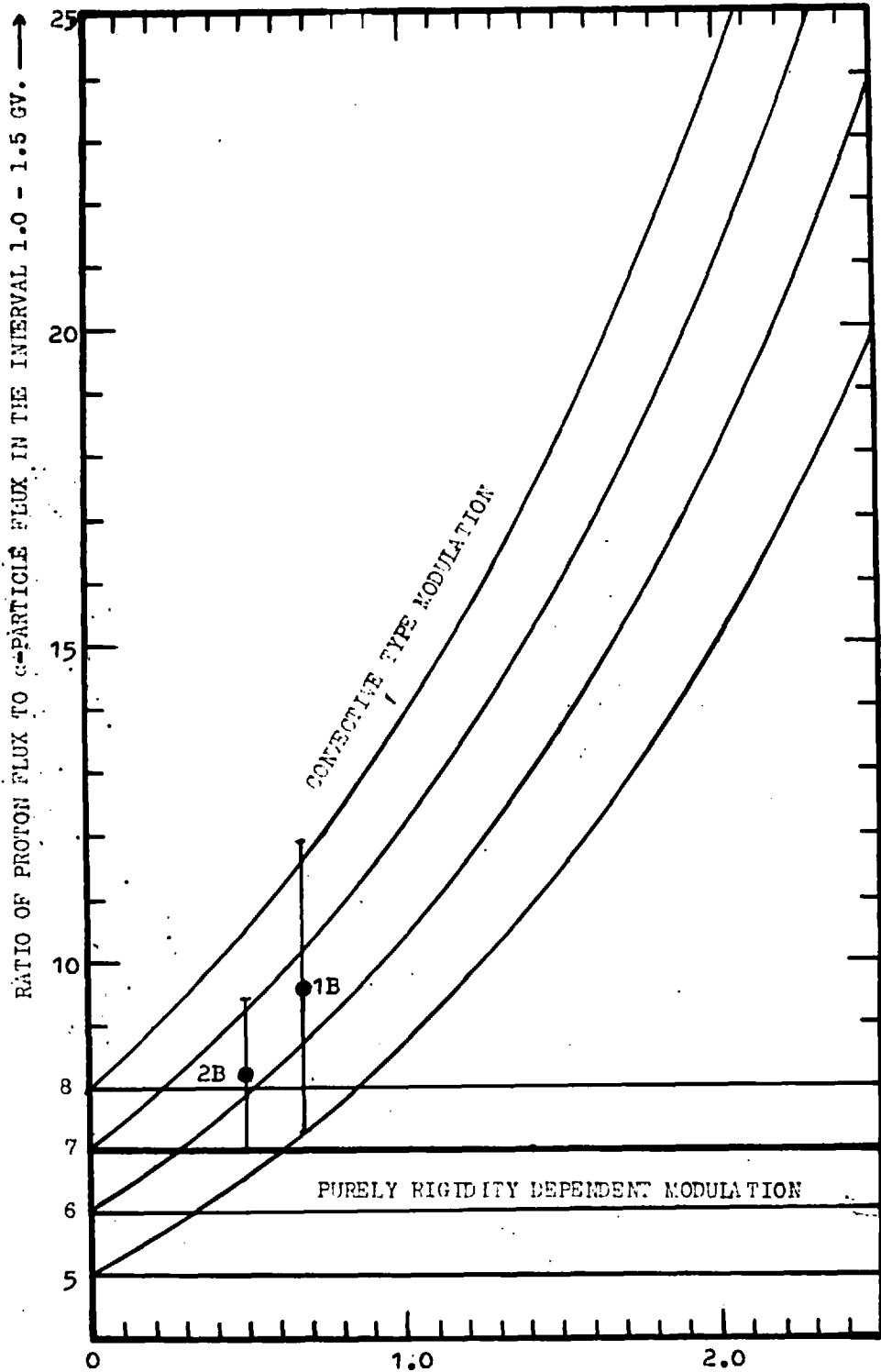
FIGURE 4.10

SOLAR ACTIVITY K(t)
See Section 4.8 .

representing solar activity, $\beta un/c$, which has been abbreviated to

K(t). The straight lines representing constant ratios are typical

of a purely rigidity dependent modulation. The ratio obtained

from the flight 2B made in July 1962 is plotted against the value

of K(t) applicable to May and June 1962 derived from the results

of Ariel I (Elliot, 1963).

Unfortunately, there are no reliable primary spectra that

have been published for the earlier measurement in August 1961 and

so an approximate value of K(t) has been deduced by using the

change in response of neutron monitors over the period, and

assuming the convective model to be operative. This method relies

on the latitude survey of the nucleonic component made by Kondo et

al. (1963) for normalizing the monitors, but is independent of the

specific yield functions and differential response curves. Since

there were no comparable latitude surveys at the times of interest,

the percentage deviations of the monthly means of sea level neutron

monitor rates from solar maximum, taken as the average of the first

three months of 1958, are calculated for August 1961 and May + June

1962. Then, taking the sea level latitude survey for 1958 to 1959

made by Kondo et al. as corresponding to the base level, the

latitude curves of neutron monitor rate against geomagnetic

threshold are drawn using the thresholds of Quenby and Wenk (1962).

The relative slopes of these curves at any given rigidity are in

the ratio of the differential primary intensities at that rigidity. Thus the differential spectrum can be derived for 1961 relative to 1962 and be fitted by a certain modulation factor K(t) for the low rigidity particles in a similar way to the Ariel data. Although this value is not expected to be very reliable in view of the shortage of monitors between 3 and 6 Gv. it gives the only possible estimate for the change in the modulation.

The two available experimental points show a ratio greater than 7.0 which applies for the high rigidity flux and, although by no means conclusive, they show a variation that is in better agreement with that expected for the solar wind model than that from a static, purely rigidity dependent modulation.

In view of the air cut-off for α-particles the investigation of a much lower rigidity than 1.0 Gv. is difficult other than with satellites. However, if a modulation of the form in Equation 4.4 is responsible for the divergence of protons and α-particles over the solar cycle, the variations will be more sensitive towards lower rigidities in accordance with the curves given in Figure 4.11 . Here the predicted ratio of protons to α-particles, compared with the unmodulated intensities, has been plotted as a function of rigidity for different stages of the solar cycle. It must be emphasised that this is an idealized case, and although it is probably more applicable to low rigidities, it is only shown as a semi-quantitative guide to the effects at lower rigidities.
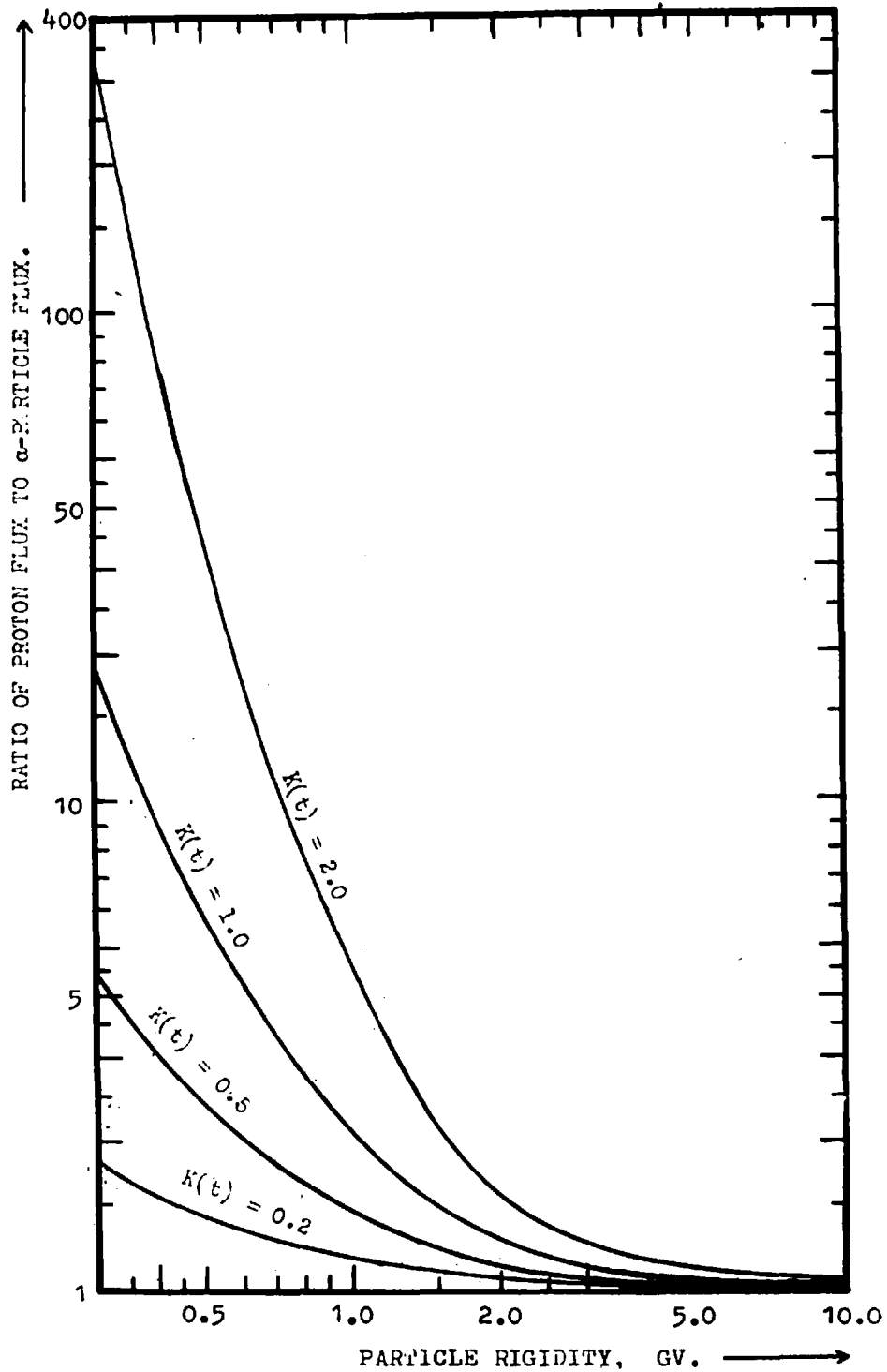
FIGURE 4.11 Proton to α-particle ratio of fluxes as a
function of rigidity for different stages
of the solar cycle w.r.t. the unmodulated
ratio for a convective model. (Section 4.8)

The practicability of measuring the variations at a lower rigidity than that used here will depend greatly on how fast the unmodulated galactic spectrum falls away in this region, and also on the quiet time intensity of solar protons. For a certain change in the ratio of protons to α-particles, provided that it is attainable over the solar cycle for the rigidity measured, a greater statistical accuracy will be obtained for the higher rigidity intervals, although at lower values the variation will be observed over a shorter period close to solar minimum. Such experiments are being designed at Imperial College to measure the intensities at a mean rigidity of approximately 0.6 Gv. with satellites during and after the next solar minimum.

It is of great interest to extend the simultaneous measurements of protons and α-particles in order to obtain a rigidity dependence for the ratio of their differential intensities, and thus impose more stringent restrictions on the possible modulating mechanisms.

4.9   The Light, Medium and Heavy nuclei.

The main significance of these results is in demonstrating that the change in integral intensity over the solar cycle has broadly followed the same variation as the α-particles above a similar rigidity limit.   A summary of fluxes which have been obtained for particles with charge $Z > 2$ is given in Table 4.4 and these values, which all have a low threshold rigidity, are plotted in Figure 4.8 against their respective Mount Washington neutron monitor two-hourly rates for the days of measurement.

Total Light + Medium + Heavy nuclei fluxes above low rigidity.

Date of flight	Geomag. lat.	Lower rig. limit Gv.	Integral flux parts./m^2 sec.ster.	Mount Wash.	Reference	
13.3.56	53°N	1.4	21.6 ± 2.3	2134	Biswas et al. (1960)	1
18.9.56	55°N	1.3	29.3 ± 4.2	2297	Evans (1963)	2
30.7.57	55°N	1.75	14.4 ± 1.9	2068	Fichtel (1961)	3
11.9.57	61°N	1.3	15.8 ± 0.7	1985	Aizu et al. (1962)	4
4.9.59	53.5°N	1.3	15.2 ± 0.9	1875	Koshiba et al. (1963)	5
3.8.58	61°N	0.9	14.8 ± 1.2	1998	Foster and Debenedetti (1963)	6
26.8.61	65°N	1.0	17.3 ± 2.6	2158	Present experiment	1B
21.7.62	65°N	1.0	25.0 ± 4.0	2262	Present experiment	2B

TABLE 4.4

In Figure 4.8 the 'best line' representing the α-particle variation from Figure 4.7 has been drawn and scaled down in intensity by a factor of 10 for comparison. The statistical errors are fairly large, but nevertheless there is a close similarity in the modulation of these different particles. This is consistent with a common controlling environment. However, near solar maximum, there is a tendency for the heavy particle flux to remain constant although the neutron counts change by about 10%. If this is a real phenomenon, a tentative explanation could be the production of a small flux of heavy solar particles at about this time. As an unusual rise in the heavy flux has been detected which was not accompanied with a comparable increase of particles of lower charge (Kurnosova et al., 1961), it seems possible that heavy particles can be preferentially accelerated by the sun, at least for short periods. If there is a background flux of solar produced protons that persists for periods of several months, as has been suggested in Section 4.3, it is likely that most of the particles which are enhanced in intensity with large solar flares are also present at a low level during the years of maximum solar activity.

COROLLARY

Improvements for continuation of the measurements.

The flights which have been made so far are only intended as part of a longer term survey as the significance of the results will be of much more value when they can be related to reliable sunspot minimum fluxes. It is proposed to continue in 1964 and 1965 similar investigations as have been reported here. As a result of the work to date it has been possible to determine certain modifications to the telescope, with a view to improving the particle charge and energy resolution, and still maintaining the same technique for particle identification and telemetry of pulse heights.

The expansible rubber balloons which were used for these flights, apart from not proving very reliable, were not capable of taking the load higher than 10 gm./cm.^{2} without risk of bursting. This altitude limitation was one of the major factors in restricting the accuracy with which the spectra could be determined due to the relatively large number of secondaries at this depth and the complete absorption of α-particles below 1.0 Gv. Flights are now being made with larger polyethylene balloons to obtain a higher altitude.

By a suitable mixture of Cerenkov and residual scintillation light, a slightly better fast splash albedo

resolution can be achieved together with the effect of taking the slow proton and α-particle overlapping region to lower proton rigidities. Some confusion of this type is unavoidable, so in order to eliminate these slow particles, all of which are secondaries even at 65° N. geomagnetic latitude, a third scintillator detector has been introduced, separated by a few grams of absorber beneath the original elements, and operating in coincidence with these. This configuration necessitates some alteration in the geometry since the Cerenkov detector must still be viewed from below to achieve good directional properties. In this system the scintillators are viewed from the side using perspex light pipes, thus reducing the amount of material above the detector. The pulse height distribution for relativistic μ-mesons has a comparable width at half maximum to that obtained with the darvic cone method of light collection. As the amount of absorber is such that protons below 0.35 Gv. will not be detected, it follows that α-particles below 0.7 Gv. will not penetrate to the third detector. To enable these particles to be seen the electronics have been modified so that the telescope will operate in two-fold coincidence from the upper two detectors when the light output in the first scintillator exceeds approximately 20 times that from a minimum ionizing proton. This means that for particles producing such effects, which includes heavy particles, the geometry will be larger and this will to some extent compensate for the low

flux of these particles. It is arranged that the half-width
contribution from path length variations under these conditions is
not greater than 20% by a suitable finite separation of the two
upper detectors.

It is expected that the proportion of background will be
greatly diminished as a result of a threefold system. In laboratory
tests it has been possible to improve the Cerenkov response
distribution by minimizing the edge effects, using the upper and
lower detector elements to define the geometry. Calibrations of
the detector response are being augmented by using artificially
accelerated particles, and several general modifications are also
being made with a view to economising further of power consumption
in the gondola and making it lighter in weight.

APPENDIX A

Calculation of the geometry of a truncated conical telescope.

Consider two disk shaped elements of radius R_1 and R_2 lying parallel and separated by a distance 'd' along the vertical axis through their centres. See Figure A. The effective coincidence area of the telescope for particles arriving at an angle θ to the vertical is that which is shaded, $S(\theta)$. Let the cosmic ray flux at an angle θ be represented by $I_o.F(\theta)$ particles/m^2 sec. steradian where I_o is the vertical flux. The contribution to the counting rate from particles arriving at an angle θ within a solid angle $d\omega$ is then:

$$dN = I_o.F(\theta)S(\theta)\cos\theta \, d\omega \quad \text{particles/sec}$$

$S(\theta)$ is given by $R_1^2(\phi - \tfrac{1}{2}\sin2\phi) + R^2(\chi - \tfrac{1}{2}\sin2\chi)$

where $\cos\chi = \dfrac{(R_2^2 - R_1^2) + D^2\tan^2\theta}{2R_2 D\tan\theta}$

$\cos\phi = \dfrac{(R_1^2 - R_2^2) + D^2\tan^2\theta}{2R_1 D\tan\theta}$

When $\theta < \arctan\dfrac{(R_1 - R_2)}{D}$ S is constant $= \pi R_2^2$

and when $\theta = \arctan\dfrac{(R_1 + R_2)}{D} = \theta_{max}$ S is zero.

Let the arrival direction in azimuth be α, then integrating over all $d\omega$, the counting rate from particles in the upper hemisphere,

$$N = I_o \int_0^{2\pi} d\alpha \int_{\theta=0}^{\theta=\theta_{max}} F(\theta) S(\theta) \cos\theta \, \sin\theta \, d\theta \quad \text{particles/sec.}$$

The geometry factor is defined as N/I_o metre^2 steradian and has to be evaluated by numerical integration in view of the complexity of the function $S(\theta)$.

For the opening angle of the telescopes used, which were approximately 15° either side of the zenith, the flux is practically isotropic at balloon altitudes. i.e. $F(\theta) = 1$. At sea level the variation in the intensity with zenith angle is fitted closely by the form $F(\theta) = \cos^2\theta$.

The corresponding geometries for the standard configuration used in the telescopes were:

$$\text{Isotropic geometry} = 25.8 \pm 0.1 \text{ cm}^2 \text{ steradian}$$

$$\text{Cos}^2 \text{ geometry} = 24.4 \pm 0.1 \text{ cm}^2 \text{ steradian}$$

$$\frac{\pi^2 R_1^2 \cdot R_2^2}{D^2} \text{ geometry} = 29.5 \pm 0.1 \text{ cm}^2 \text{ steradian}$$

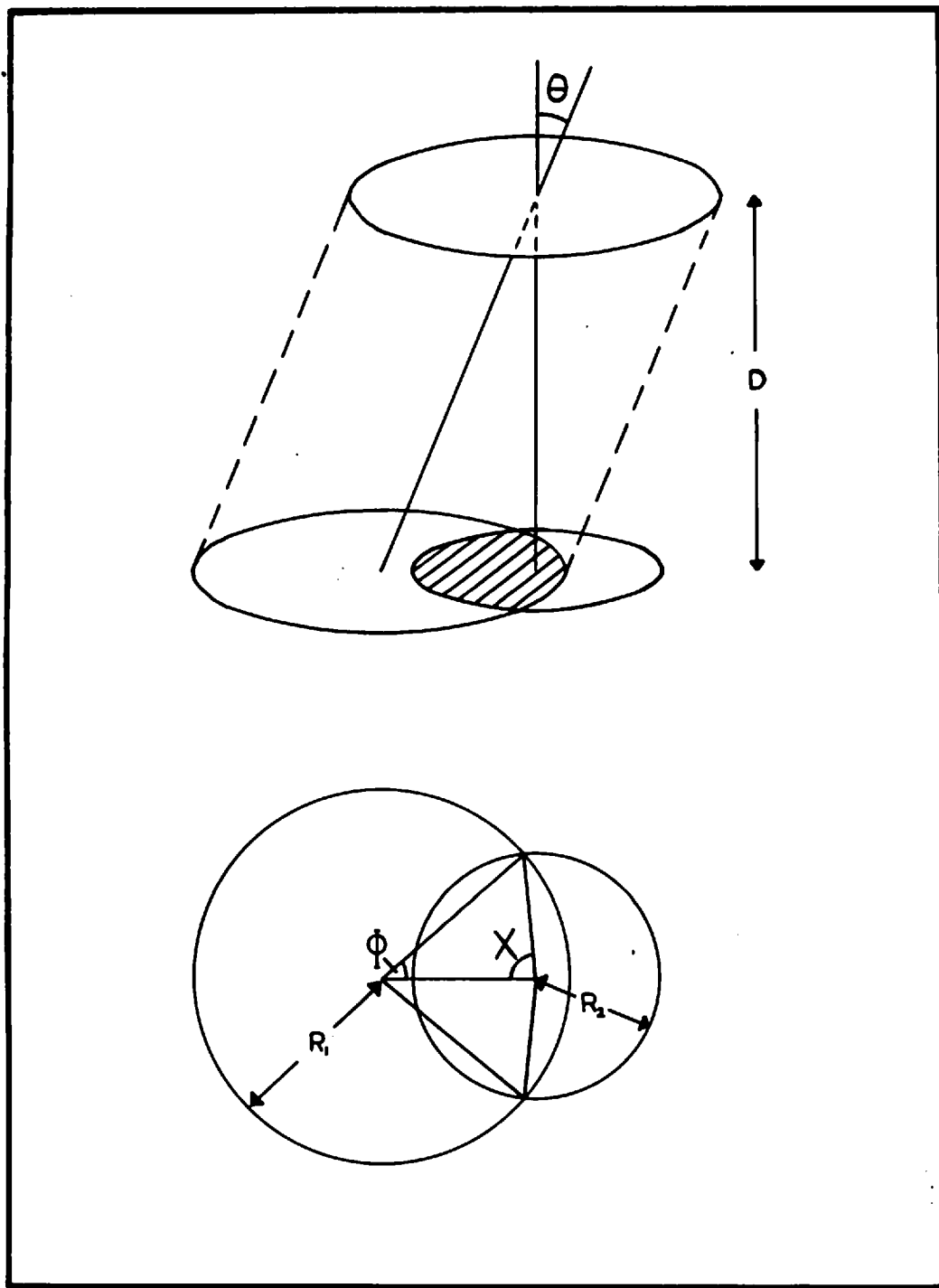The isotropic geometry factor was taken for calculating particle fluxes at altitude.

FIGURE A   Diagram used for calculation of the geometry of a non-cylindrical telescope. (Appendix A)

APPENDIX B

Values of parameters used in extrapolation of α-particle fluxes.

The general equation for vertical diffusion may be written in the following form if ionization loss and energy degradation are neglected.

$$dJ_j/dx = -J_j/\lambda_j + \sum_{i \geq j} P_{ij} \cdot J_i/\lambda_i$$

where J_j is the intensity of particles of type 'j' at a depth 'x'.

P_{ij} is the fragmentation parameter or the average number of particles of type 'j' resulting from a collision of a particle of type 'i'.

λ_j is the absorption mean free path of type-'j' particles.

The absorption mean free path λ is related to the interaction mean free path λ' by $\lambda_j = \lambda'_j/(1 - P_{jj})$

For convenience the primary cosmic ray particles are divided into the standard grouping for which the relevant parameters are given below after Waddington (1960).

j	Z	λ'_j Gm./cm.^{2}	λ_j Gm./cm.^{2}	Relative intensity ≥ 4.5 Gv.
α	2	44	45	90 ± 2
L	$3 \leq Z \leq 5$	32.0	36.4	1.96 ± 0.2
M	$6 \leq Z \leq 9$	26.8	32.3	5.6 ± 0.2
H	$Z \geq 10$	19.6	27.6	2.58 ± 0.2

Figure 3.5 shows the experimental extrapolation and Webber (1956)

derives the solution to the diffusion equation for α-particles
using the above grouping and at a depth x gm./cm^2 as:

$$J_\alpha(x) = J_\alpha^o \exp(-x/\lambda_\alpha) + \frac{A_{L\alpha} P_{L\alpha}}{\lambda_L'} \left[J_L^o + \frac{A_{ML} P_{ML}}{\lambda_M'} J_M^o + \right.$$

$$\left. \frac{A_{ML}}{\lambda_H'} J_H^o \left(P_{HL} + \frac{A_{ML} P_{HM} P_{ML}}{\lambda_M'} \right) \right] \left[\exp(-x/\lambda_\alpha) - \exp(-x/\lambda_L) \right]$$

$$+ \frac{A_{M\alpha}}{\lambda_M'} \left(P_{M\alpha} - \frac{A_{ML} P_{ML} P_{L\alpha}}{\lambda_L'} \right) \left(J_M^o + \frac{A_{HM} P_{HM} J_H^o}{\lambda_H'} \right) \left[\exp(-x/\lambda_\alpha) \right.$$

$$\left. - \exp(-x/\lambda_M) \right]$$

$$+ \frac{A_{H\alpha}}{\lambda_H'} \left[P_{H\alpha} - \frac{P_{HM} P_{M\alpha} A_{HM}}{\lambda_M'} - \frac{P_{HL} P_{L\alpha} A_{HL}}{\lambda_L'} + \frac{P_{HM} P_{ML} P_{L\alpha}}{\lambda_M' \lambda_L'} \times \right.$$

$$\left. \left(A_{HM} A_{ML} - A_{HL} A_{ML} \right) \right] \left[\exp(-x/\lambda_\alpha) - \exp(-x/\lambda_H) \right]$$

$$A_{ij} = \frac{\lambda_i \lambda_j}{\lambda_j - \lambda_i} > 0 \; ; \quad \lambda_i = \lambda_i'/(1 - P_{ii})$$

J_j^o denotes the primary flux of type-'j' particles.

The fragmentation parameters in air after Waddington (1960)
are taken as follows for evaluating the above solution:

$P_{HH} = 0.29 \pm 0.11$ $P_{HM} = 0.46 \pm 0.05$ $P_{HL} = 0.21 \pm 0.09$

$P_{MM} = 0.17 \pm 0.06$ $P_{ML} = 0.23 \pm 0.07$ $P_{M\alpha} = 1.27 \pm 0.28$

$P_{LL} = 0.12 \pm 0.07$ $P_{L\alpha} = 0.79 \pm 0.26$ $P_{H\alpha} = 1.23 \pm 0.40$

REFERENCES

Aizu, H., Y. Fujimoto, S. Hasegawa, M. Koshiba, I. Mito, J. Nishimura, K. Yokoi, and M. Schein, 1959, Phys. Rev. 116, 436.

Aizu, H., Y. Fujimoto, S. Hasegawa, M. Koshiba, I. Mito, J. Nishimura, K. Yokoi, and M. Schein, 1961, Phys. Rev. 121, 1206

Aizu, H., I. Mito, Y. Fujimoto, S. Hasegawa, M. Koshiba, J. Nishimura, and K. Yokoi, 1962, J. Phys. Soc. Japan, 17, Suppl. A3, 38.

Anderson, K. A., 1955, Tech. Report, Dept. Phys., Univ. of Minnesota.

Bethe, H., 1930, Annal der Physik, 5, 325.

Bhavsar, P. D., 1962, J. Geophys. Res. 67, 2627.

Biswas, S., P. J. Lavakare, N.A. Neelakantan, and G. Shukla, 1960, Il Nuovo Cim. 16, 644.

Bradt, H. L., and B. Peters, 1948, Phys. Rev. 74, 1828.

Brooke, G., 1962, J. Phys. Soc. Japan, 17, Suppl. A3, 311.

Brooks, F. D., 1956, Prog. Nuc. Phys., London and New York Pergamon Press, 5, 252.

Brunstein, K. A., 1963, Preprint, Univ. of California.

Bryant, D., T. L. Cline, U. D. Desai, and F. B. McDonald, 1962, J. Geophys. Res. 67, 4963.

Camerini, U., P. H. Fowler, W. O. Lock, and H. Muirhead, 1950, Phil. Mag. 41, 413.

Camerini, U., J. H. Davies, P. H. Fowler, C. Franzinetti, H. Muirhead, W. O. Lock, D. H. Perkins, and G. Yekuteili, 1951, Phil. Mag. 42, 1241.

Charkhchyan, A. N., and Charkhchyan T. N., 1961, Soviet Phys. J.E.T.P. 13, 1126.

Clark, M. A., 1952, Phys. Rev, 87, 87.

Dahanayake, C., P .C. B. Fernando, and M. L. T. Kannangara, 1963, Proc. Phys. Soc. 82, 107.

Davis, L., 1955, Phys. Rev. <u>100</u>, 1440.

Dorman, L. I., 1960, Proc. Moscow Cosmic Ray Conf. (IUPAP), <u>4</u>, 320.

Dorman, L. I., 1963, Progress in Elementary Particle and Cosmic Ray
     Physics, <u>7</u>, North Holland Publishing Co.

Duke, P. J., 1960, Proc. Moscow Cosmic Ray Conf. (IUPAP), <u>3</u>, 89.

Dymond, E. G., 1954, Progress in Elementary Particle and Cosmic Ray
     Physics, <u>2</u>, North Holland Publishing Co.

Earl, J. A., 1961, Phys. Rev. Letters, <u>6</u>, 125.

Earl, J. A., 1962, J. Geophys. Res. <u>67</u>, 2107.

Ehmert, A., 1960, Proc. Moscow Cosmic Ray Conf. (IUPAP), <u>4</u>, 142.

Elliot, H., 1958, Annals of I.G.Y. 374.

Elliot, H., 1960, Phil. Mag. <u>5</u>, 601.

Elliot, H., 1962, J. Phys. Soc. Japan, <u>17</u>, Suppl. A2, 588.

Elliot, H., 1963, Survey paper presented at the Jaipur Cosmic Ray
     conference. (IUPAP).

Engler, A., 1961a, Il Nuovo Cim. <u>19</u>, 1090.

Engler, A., F. Foster, T. L. Green, and J. H. Mulvey, 1961b, Il
     Nuovo Cim. <u>20</u>, 1157.

Evans, D. E., 1960, Proc. Moscow Cosmic Ray Conf. (IUPAP), <u>3</u>, 92.

Evans, D. E., and R. R. Hillier, 1961, Il Nuovo Cim. <u>22</u>, 1300.

Evans, D. E., 1963, Il Nuovo Cim. <u>27</u>, 394.

Fichtel, C. E., 1961, Il Nuovo Cim. <u>19</u>, 1100.

Fichtel, C. E., P. E. Guss, D. A. Kniffen, and Neelakantan, 1963,
     Abstracts, Jaipur Cosmic Ray Conference. (IUPAP).

Forbush, S. E., 1954, J. Geophys. Res. <u>59</u>, 525.

Foster, F., and A. Debenedette, 1963, Il Nuovo Cim. <u>28</u>, 1190.

Fowler, P. H., C. J. Waddington, P. S. Frier, J. Naugle, and E. P. Ney, 1957, Phil. Mag. 2, 157.

Fowler, P. H., P. S. Frier, and E. P. Ney, 1958, Il Nuovo Cim. Suppl. 8, 492.

Frank, I. M., and I. G. Tamm, 1937, Dokl. Akad. Nauk. U.S.S.R., 14, 109.

Fiedlander, M. W., and C. T. Spring, 1962, Il Nuovo Cim. 26, 1292.

Frier, P. S., E. J. Lofgren, E. P. Ney, F. Oppenheimer, H. L. Bradt, and B. Peters, 1948, Phys. Rev. 74, 213.

Frier, P. S., E. P. Ney, and P. H. Fowler, 1958, Nature, 181, 1319.

Frier, P. S., E. P. Ney, and C. J. Waddington, 1959, Phys. Rev. 114, 365.

Frier, P. S., 1962, J. Geophys. Res. 67, 2617.

Frier, P. S., and W. R. Webber, 1963, J. Geophys. Res. 68, 1605.

Frier, P. S., 1963, J. Geophys. Res. 68, 1805

Gooding, T. J., and H. G. Pugh, 1960, Nuc. Inst. Meth. 7, 189.

Hedgecock, P. C., 1962, Proposal presented at the S.P.A.R.M.O. Conference, Lindau.

Horwitz, N., 1955, Phys. Rev. 98, 165.

Jain, P. L., E. Lohrmann, and M. W. Teucher, 1959, Phys. Rev. 115, 636.

Kaplon, M. F., B. Peters, H. L. Reynolds, and D. M. Ritson, 1952, Phys. Rev. 85, 295.

Kidd, J. M., 1963, Il Nuovo Cim. 27, 57.

Kodama, M., 1959, J, Geomag. Geoelect. 11, 6.

Kondo, I., M. Kodama, and T. Makino, 1963, Abstracts, Jaipur Cosmic Ray Conference, (IUPAP).

Koshiba, M., E. Lohrmann, H. Aizu, and E. Tamai, 1963, Phys. Rev. 131, 2629.

Kurnosova, L. V., L. A. Razorenov, and M. I. Fradkin, 1961, Nature, (Priroda), 1, 94.

Laby, J. E., Y. K. Lim, and V. D. Hopper, 1957, Il Nuovo Cim. 5, 249.

Landau, L., 1944, Journal Phys. U.S.S.R. 81, 201.

Linsley, J., 1955, Phys. Rev. 97, 1292.

Lockwood, J. A., 1960, J. Geophys. Res. 65, 3859.

McDonald, F. B., 1957, Phys. Rev. 107, 1386.

McDonald, F. B., 1958, Il Nuovo Cim. Suppl. 8, 500.

McDonald, F. B., and W. R. Webber, 1959, Phys. Rev. 115, 194.

McDonald, F. B., and W. R. Webber, 1960, J. Geophys. Res. 65, 767.

McDonald, F. B., and W. R. Webber, 1962a, J. Geophys. Res. 67, 2119.

McDonald, F. B., and W. R. Webber, 1962b, J. Phys. Soc. Japan, 17, Suppl. A2, 428.

Meyer, P., and J. A. Simpson, 1957, Phys. Rev. 106, 568.

Meyer, P., and R. Vogt, 1961, Phys. Rev. Letters, 6, 193.

Meyer, P., and R. Vogt, 1963, Phys. Rev. 129, 2275.

Millar, C. H., and E. P. Hinks, 1957, Canadian J. Phys. 35, 363.

Morrison, P., 1956, Phys. Rev. 101, 1397.

Mylroi, M. G., and J. G. Wilson, 1951, Proc. Phys. Soc. A 64, 404.

Neher, H. V., 1956, Phys. Rev. 103, 228.

Ney, E. P., and D. N. Thon, 1951, Phys. Rev. 81, 1069.

Nicoll, D. R., 1963, Private Communication.

Parker, E. N., 1958, Phys. Rev. 110, 1445.

—

Parker, E. N., 1963, Interplanetary Dynamic Processes, Interscience
     Publishers, New York.

Pringle, R. W., 1961, Private Communication.

Quenby, J. J., and W. R. Webber, 1959, Phil. Mag. 4, 90.

Quenby, J. J., and G. Wenk, 1962, Phil. Mag. 7, 1457.

Ray, E. C., 1962, J. Geophys. Res. 67, 3289.

Sandstrom, A. E., M. A. Pomerantz, and B. O. Gronkvist, 1963,
     Tellus, 15, 184.

Sauer, H. H., 1963, J. Geophys. Res. 68, 957.

Simpson, J. A., 1955, 'Cosmic Radiation Neutron intensity Monitor',
     Institute for Nuclear Studies, Univ. Chicago.
          1963, Preprint, Institute for Nuclear Studies, Univ. Chicago.

Singer, S. F., 1958, Il Nuovo Cim. Suppl. 8, 334.

Stephenson, G. R., and C. J. Waddington, 1961, Phil. Mag. 6, 517.

Stephenson, G. R., 1962, Ph.D. Thesis, Univ. Bristol.

Sternheimer, R. M., 1959, Phys. Rev. 115, 137.

Symon, K. R., 1948, Ph.D. Thesis, Univ. Harvard.

Vogt, R., 1962, Phys. Rev. 125, 366.

Waddington, C. J., 1960, Progress in Nuclear Physics, 8, 1, Pergamon
     Press, London.

Webber, W. R., and F. B. McDonald, 1955, Phys. Rev. 100, 1460.

Webber, W. R., 1956, Il Nuovo Cim. 4, 1285.

Webber, W. R., and J. J. Quenby, 1959, Phil. Mag. 4, 654.

Webber, W. R., 1962, Progress in Elementary Particle and Cosmic Ray
     Physics, 6, 75, North Holland Publishing Co.

Webber, W. R., 1962a, J. Geophys. Res. 67, 5347.

Williams, E. J., 1931, Proc. Roy. Soc. London, 130, 328.

Winkler, J. R., E. N. Mitchell, K. A. Anderson, and L. Peterson, 1955,
       Phys. Rev. 98, 1411.

Winkler, J. R., and K. A. Anderson, 1957, Phys. Rev. 108, 148.

Wright, G. T., 1953, Phys. Rev. 91, 1282.

Yasin, M., 1963, Il Nuovo Cim. 28, 935.